CRANKTRAIN MODELING AND ANALYSIS OF CONNECTING ROD VIBRATIONAL EFFECTS ON THE OVERALL PERFORMANCE OF OTTO CYCLE ENGINES

A Thesis by

Jennifer M. Herring

Bachelor of Science, Wichita State University, 2012

Submitted to the Department of Mechanical Engineering
and the faculty of the Graduate School of
Wichita State University
in partial fulfillment of
the requirements for the degree of
Master of Science

May 2014

CRANKTRAIN MODELING AND ANALYSIS OF CONNECTING ROD VIBRATIONAL EFFECTS ON THE OVERALL PERFORMANCE OF OTTO CYCLE ENGINES

The following faculty members have examined the final copy of this thesis for form and content, and recommend that it be accepted in partial fulfillment of the requirement for the degree of Master of Science with a major in Mechanical Engineering.

_____
Hamid M. Lankarani, Committee Chair

_____
Krishna Krishnan, Committee Member

_____
Davood Askari, Committee Member

ABSTRACT

Since connecting rods are a major component in the smooth and efficient running of an engine, how they affect the overall performance is important. The durability of connecting rods in repeated and cyclic operations is significant to the health and performance of an engine. The purpose of this research is to determine what effects the vibrations of connecting rods have on the overall performance of Otto cycle engines. Some studies have been conducted on the static vibration of connecting rods as well as connecting rods in dynamic systems, but those studies only considered the connecting rod design.

Modeling, dynamic analysis, and vibrational analysis are conducted using two different software programs, MSC Adams/View and FEV Virtual Engine. Two different engine configurations are modeled: inline and vee; the results from the two programs are then compared. The data is also checked against vibrational analysis from literature sources as well as having the general performance of the pistons cross-checked against real engine data. The MSC Adams/View models are composed of simplified cranktrains and forces; while those of FEV Virtual Engine are modeled after actual dimensions and workings. It is determined that the vibrations of connecting rods, under typical operating conditions and material/geometrical properties, do not greatly affect the overall performance of an engine.

TABLE OF CONTENTS

TABLE OF CONTENTS (continued)

LIST OF TABLES

LIST OF FIGURES

LIST OF FIGURES (continued)

LIST OF FIGURES (continued)

LIST OF ABBRIVIATIONS

deg	degrees
E	power ten
flex	flexible
Hz	Hertz
in	inches
L	liters
lb	pounds
lb_{force}	pound-force
MN	modal neutral
rpm	revolutions per minute
sec	seconds

CHAPTER 1

INTRODUCTION

An Otto cycle engine is a four-stroke internal combustion engine; this type of engine is what powers most cars in the United States. It is a four-stroke engine because the piston strokes four times to complete one cycle: intake, compression, expansion (power), and exhaust strokes; the stroke length is constant. (A stroke is the movement of the piston from the top of the cylinder to the bottom or vice versa.) Otto cycle engines are internal combustion engines because the combustion of the fuel is internal to the system. The fuel is injected into the system on the intake stroke but is not ignited until the beginning of the power stroke.

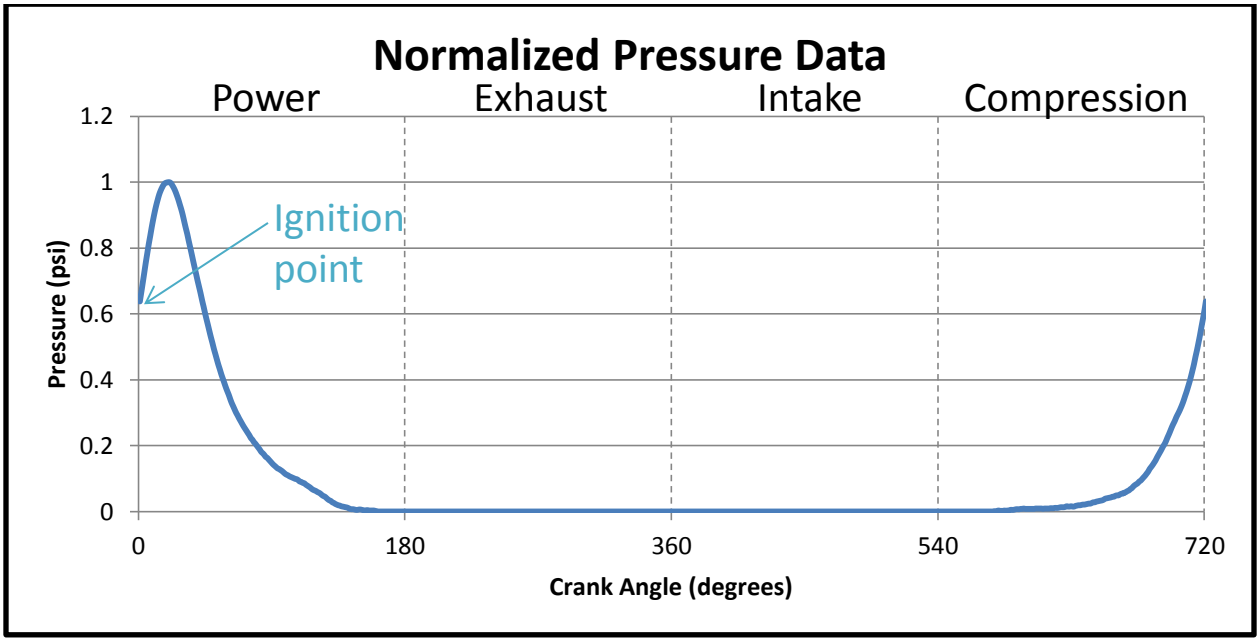

Figure 1.1: Normalized Pressure Data for One Cycle

The workings of an internal combustion engine are essentially that of multiple slider-crank mechanisms connected to each other by one long crankshaft and which operate simultaneously. The pistons are the sliders, the connecting rods are the links which connect the pistons to the crankshaft, and the crankshaft is what transmits power to the transmission. The

entire system is driven by the combustion of fuel which produces a driving (gas) force on the top of a piston. Though the connecting rod is a relatively simple part of the cranktrain, its function is highly important.

1.1 Background

Vibration in a system is usually unwanted and can cause early failure. This means the part that failed and any part which it damaged must be fixed or replaced, resulting in an expensive and time consuming repair; thus, all major moving parts of a system must be analyzed to make sure they do not reach resonant frequency [1]. Some machines must pass through at least one critical speed to reach their operational run speed in the supercritical range; therefore, the parts must be designed to be able to withstand passing through the first and possibly other natural frequencies. They must be able to do this twice each run, once when the machine starts up and once when it shuts down [2].

For internal combustion engines, the connecting rods should never reach their first flexible body natural frequency; but if for some reason they did, they should be able to withstand it long enough for the system to settle. If a connecting rod failed, it could bend causing the piston to jam on the cylinder wall or break resulting in the cylinder wall being gouged or cracked from the impact of the destroyed connecting rod. Both of these failures would result in costly repairs or completely destroy the engine, requiring it to be replaced; therefore, it can easily be seen that the connecting rod is a vital part which requires it to be well designed.

Many different variables cause connecting rod vibrations, though limited to those found within the engine. The deformation of the crankshaft causes vibration in the system; it also causes friction between the piston skirts and the cylinder walls. The firing of the cylinders as well as the angles and loads which the connecting rods experience all cause vibrations. These

vibrations can be reduced by strengthening the crankshaft and increasing the width of its bearings, lengthening the connecting rods so they experiences smaller angles and side-forces, redesigning the piston skirts so there is less friction between them and the cylinder walls, and stiffening the block so the crankshaft experiences less torsion [3]. Vibrations can also result from the inertias of the system's different moving parts as well as from gas forces; system vibrations can be reduced by using material which has inherently high damping characteristics [4].

Resonant frequencies are highly destructive and are avoided as much as possible or passed through as quickly as possible. They are highly dangerous because one part reaches the exciting frequency of another part causing the frequencies of both parts to become locked together and, by exciting each other, to grow exponentially until something within the system fails thereby breaking the cycle. Resonant frequencies do not always cause failure, but they always produce undesirable results. For systems with rotational parts, the structure becomes very important because the structural resonant frequencies must be kept isolated as much as possible from the rotational frequencies or else the structure has to be made more rigid thereby pushing the structural resonant frequencies higher [1, 3, 5].

1.2 Literature Review

Engines can be successfully modeled by computer programs and/or equations so their vibrations can be determined allowing those vibrations to be reduced through modifications to the design [6]. The dynamics of an internal combustion engine are affected by many different items; some of which are the internal forces caused by friction or ignition, part dimensions, part interaction, and ignition timing. One example of frictional forces is those which result from piston friction which is mainly caused by the lubricating oil temperature [7]. Gas pressures as

well as vertical imbalances caused by inertial forces affect the instantaneous angular speed of an engine [8]. Even the advancement of the spark angle affects an engine by causing oscillations which can last anywhere from one to hundreds of cycles [9].

During analysis, a part can be left as a rigid body or can be converted into a flexible body; the part is converted into a flexible body by using the finite element method. A rigid body analysis treats the body as if it cannot deform which also means that the part will not break. This is fine for basic analysis and for short stocky parts which are very unlikely to deform or break; but for detailed analysis of long thin parts, it only results in a solution near that of the actual solution. Due to the complex nature of dynamic systems, flexible and rigid parts are commonly used together to improve the realism of the system while at the same time keeping computational requirements to a minimum to help prevent the analysis software from crashing [10].

Flexible body vibrational analysis follows the same principles as that of rigid body analysis; there is just more work required for flexible bodies due to their many nodes. For a study of the main bearings of an engine, the crankshaft was converted into a flexible body so that finite element analysis could be used with the Newton-Raphson method to perform a numerical analysis [11]. A connecting rod could be converted into a flexible body so that the stresses which it experienced during an actual run could be analyzed to determine whether or not the connecting rod design was adequate for the engine it was to be used in [12].

Some work which has been done on the vibration analysis of a connecting rod is that of static analysis. Chegini et al. [13] analyzed the connecting rod of a Nissan Z24 to determine its natural frequencies. The connecting rod was modeled in SolidWorks, and then modal analysis of the design using MSC/Patran and MSC/Nastran was performed. It was analyzed as a solid piece with no boundary conditions and the first through sixth modes of vibration were determined.

The first critical frequency was found to be the seventh mode shape; but since the previous modes were of much lower frequencies, it was determined that the connecting rods would not reach resonance.

Quinghui et al. [14] analyzed the vibrations and stresses of a connecting rod for a diesel engine. First the generalized equation of motion was determined so that the inherent frequency equation could be found. Next, a computer aided design program was used to design a piston, connecting rod, crankshaft, and flywheel which were then assembled to form the cranktrain. The connecting rod was converted into a flexible body using HyperWorks which was then connected to MSC/Nastran to get the connecting rod's natural frequencies. MSC Adams/View was used to animate the system; the durability module of Adams/View was used to analyze the stresses. It was determined that this analysis method could be used to optimize connecting rod designs.

1.3 Motivation

Internal combustion engines are used by millions of people every day as they drive places. Engines themselves are mounted on dampers which are bolted to the vehicle's frame this is to help reduce the external vibrations which are caused by the internal workings. The internal workings are that of multiple slider-crank mechanisms which experience forces, frictions, and vibrations. Since no part is truly rigid, the part under observation can be modeled as a flexible body so as to produce a more realistic model and one appropriate for vibrational analysis; hence, it would be of importance to study how the vibration of connecting rods effect the overall function of an engine. By using two different software programs, models and dynamic analysis as well as vibrational analysis of engines are explored in this research.

CHAPTER 2

OBJECTIVE AND METHODOLOGY

2.1 Objective

The purpose of this research was to determine the vibration of connecting rods in motion and how the vibration affects engine performance. Since the vibratory response of a dynamic system is very complex, modeling software was used. In MSC Adams/View, an inline-1 model was analyzed first and then a vee-2 model; the results were compared to the much more accurate inline-1 and a vee-6 FEV Virtual Engine models. All attempts were made to accurately model the motions and gas forces of the MSC Adams/View systems as if they were part of real engines though no frictions or clearances were included; the FEV Virtual Engine models had friction, clearances, and forces. Different parameters were changed to see the effects they had on the performance of the systems. A flowchart showing the generalized modeling procedures for both the rigid and flexible models can be seen in Figure 2.1.

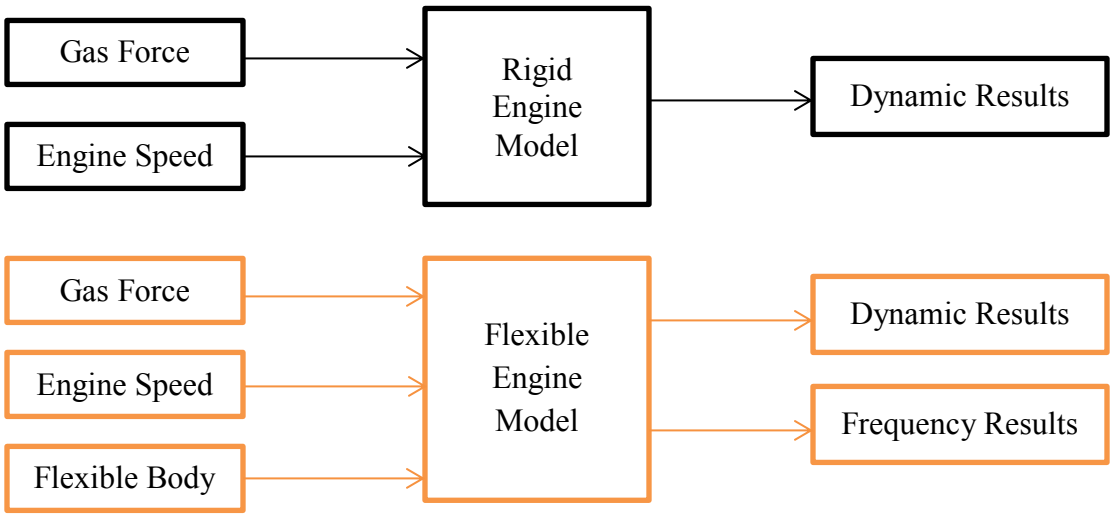

Figure 2.1: Rigid and Flexible Model Flowcharts

2.2 Methodology

For modeling and analysis, the programs MSC Adams/View Student Version 2013.2 and FEV Virtual Engine S 20 were both used. Simplistic engine models were created in Adams/ View while complex engine models were created in Virtual Engine. To verify that the Adams/ View models were accurate, their piston positions, velocities, and accelerations were compared to analytical data as well as real engine data [15, 16, 17, 18]; they were also compared the Virtual Engine piston results. For all of the engine types, the connecting rods were converted into flexible bodies so that the natural frequencies could be found and to determine how their vibrations affected the system. The connecting rod natural modes of vibration were checked against Chegini et al. [13] and Quinghui et al. [14]. For the Adams/View models, the gas force data had to be created using normalized pressure data received from Robert L. Norton; the Virtual Engine gas force data was already built into the database and just had to be applied to the pistons. All of the programs were run at steady state with a constant angular velocity of 3400 revolutions per minute (rpm).

CHAPTER 3

MSC ADAMS/VIEW MODELING AND SIMULATION

An entire engine model did not have to be created due to some inherent properties of an engine, this was the route taken with the Adams/View models as seen in Figure 3.1. For example, even though a crankshaft transfers its torsional vibration to all moving components attached to it, the shearing oil film forces which the moving parts in a real engine create actually cancel out the torsional vibration of the crankshaft [4].

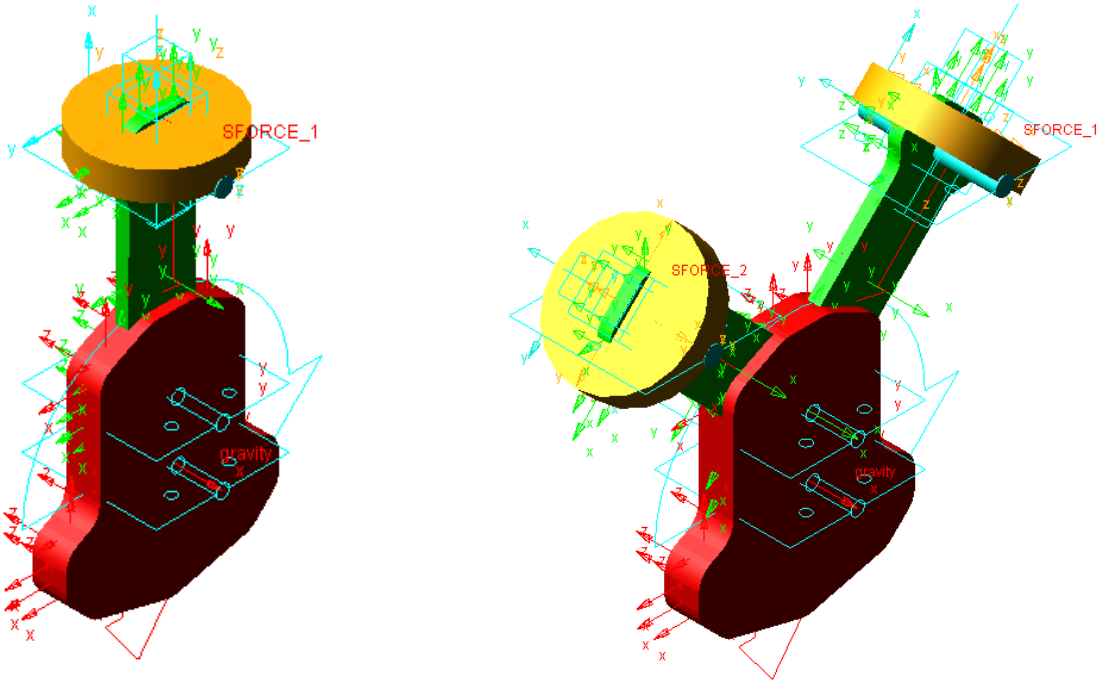

Figure 3.1: Adams/View Complete Inline-1 and Vee-2 Models

General dimensions and weights (Table 3.1) were measured by the author from a dis-assembled 1986 Toyota 22R-E engine, a straight four-cylinder (inline-4) engine; this data was then used as a guideline for the Adams/View models. For the Adams/View models only, two different materials were used for the connecting rods: cast iron and aluminum. (The material properties used for all of the models were the default properties which came with the program.)

TABLE 3.1

TOYOTA 22R-E ENGINE DATA

22R-E Engine Data			
Stroke (in)	**Bore Diameter (in)**	**Axial Cylinder Distance (in)**	**Effective Connecting Rod Length (in)**
3.25	3.625	3.45	6.00
Piston Pin Diameter (in)		**Piston Pin Length (in)**	**Piston Boss Spacing (in)**
outside	**inside**		
0.875	0.50	2.75	1.50
Piston Height (in)	**Bearing Position (in)**	**Crank-Connecting Rod Ratio**	**Connecting Rod-Stroke Ratio**
2.125	2.0625	0.27	1.85
Crank Pin (in)		**Crank Main Pin (in)**	
diameter	**length**	**diameter**	**length**
2.00	1.125	2.25	1.25
Piston Weight (lb)	**Connecting Rod Weight (lb)**	**Piston Pin Weight (lb)**	**Crankshaft Weight (lb)**
1.0625	1.75	0.25	40.00
Total Displacement (L):		2.20	

This chapter covers the modeling and simulation of the Adams/View models. The inline-1 model was covered first, followed by the vee-2 model. Due to the connecting rods having to be converted into flexible (flex) bodies, different mesh configurations were discussed; and the final configuration was chosen. How the gas forces for the models were created and applied was covered last.

3.1 Inline-1 Engine

Due to the majority of the mass of the piston being located in the top 5/8 inch, the piston was modeled as a solid cylinder (Figure 3.2). The piston pin was modeled as a solid rod (Figure 3.3). The general shape of the connecting rod (Figure 3.4) and the general shape of the crank-shaft (Figure 3.5) for one cylinder were also modeled.

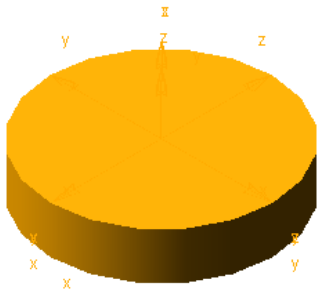

Figure 3.2: Adams/View Piston Final Model

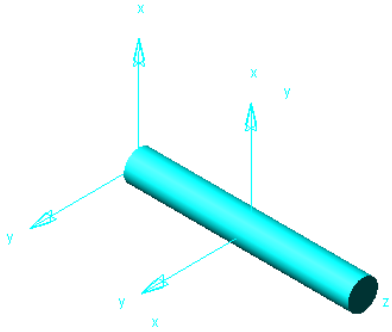

Figure 3.3: Adams/View Piston Pin Final Model

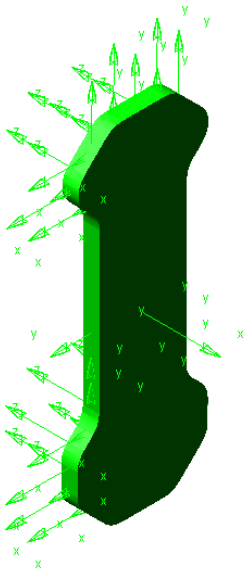

Figure 3.4: Adams/View Connecting Rod Final Model

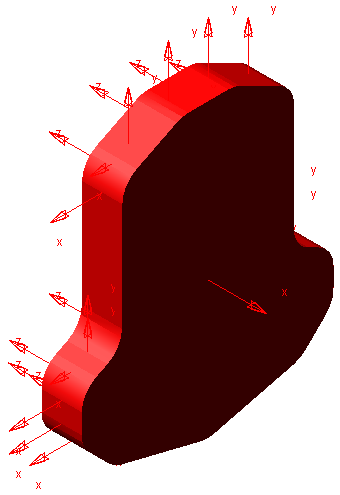

Figure 3.5: Adams/View Crankshaft Final Model

The Adams/View Rigid Body Plate command was used to model the crankshaft and the connecting rod; the grid spacing was set at 0.5 by 0.5 inches. With the Plate command, the general shape of an object was created but was rounded out according to the radius given; also, the thickness of the part was specified. The sketches in Figures 3.6-3.7 are the basic part outlines for the connecting rod and crankshaft respectively while the colored models in those same figures are the final models. The exact dimensions of the sketches can be found from the grid spacing.

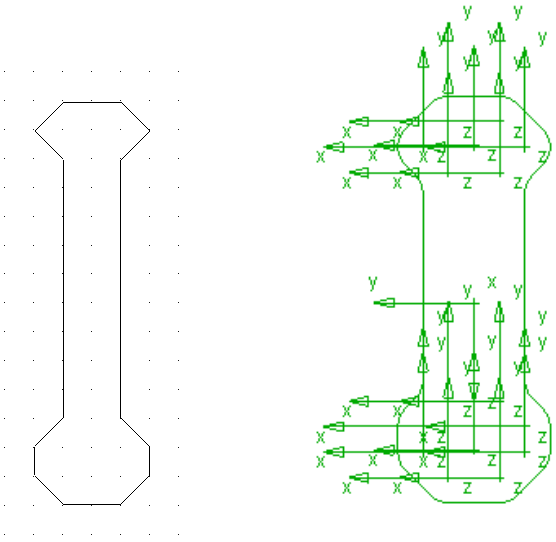

Figure 3.6: Adams/View Connecting Rod Sketch and Final Model

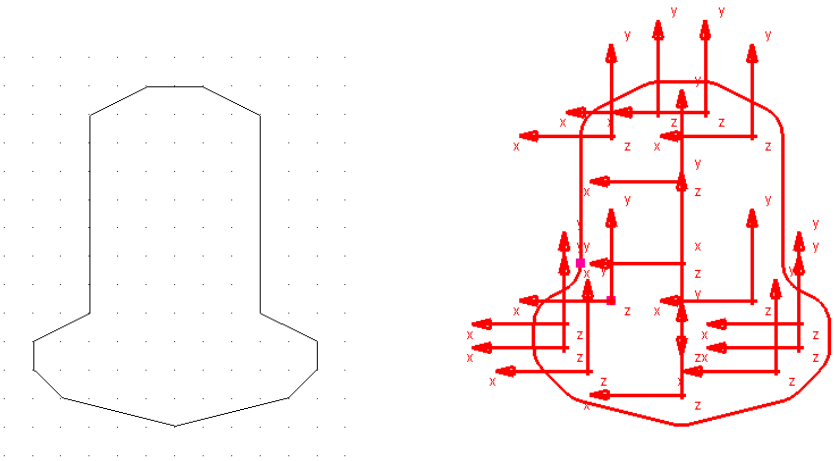

Figure 3.7: Adams/View Crankshaft Sketch and Final Model

Since the weight of one section of the 22R-E crankshaft could not be directly measured without cutting, the total weight was acquired and was then divided by 4.75, four cylinders and the rest of the mass was assessed to be three quarters of a cylinder thus the 4.75. The crank-connecting rod ratio of 0.29 was close to the practical upper limit of 1/3; for smooth operation of a slider-crank mechanism, the ratio should be between 1/5 and 1/3 [15]. The model data for the Adams/View parts can be found in Table 3.2.

TABLE 3.2

MSC ADAMS/VIEW MODEL DATA

Adams/View Data					
	Crankshaft	**Connecting Rod**		**Piston Pin**	**Piston**
Thickness (in)	1	0.375		-----	-----
Height (in)	6	6.5		-----	0.875
Radius (in)	0.65	0.5		0.27	2
Length (in)	1.75 (stroke/2)	6 (effective)		4	-----
Material	Cast Iron	Cast Iron	Aluminum	Steel	Aluminum
Weight (lb)	8.42	1.74	0.67	0.258	1.06
Crank-Connecting Rod Ratio			**Connecting Rod-Stroke Ratio**		
0.29			1.71		

The piston pin was fixed to the bottom of the piston. The center of the top portion of the connecting rod was attached to the piston pin midpoint while the center of the bottom portion of the connecting rod was attached to the crankshaft where the crank pin would be located if there was a crank pin. The joints between the ground and the crankshaft, the crankshaft and the connecting rod, and the connecting rod and the piston pin were modeled as revolute joints. A sliding joint was used between the piston and the ground. No piston offset was used; the final model can be seen in Figure 3.8. A sample of positions for the inline-1 model can be seen in Figure 3.9.

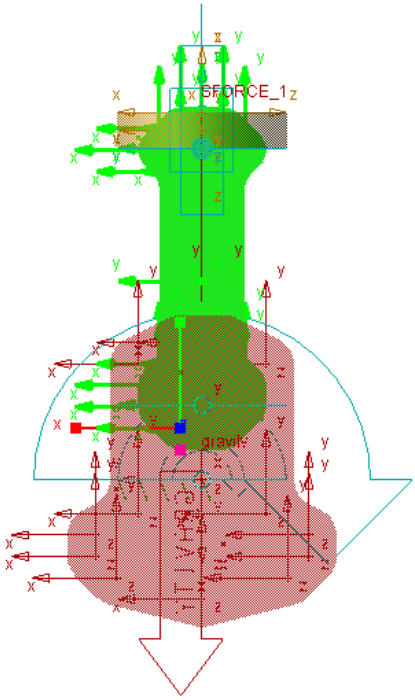

Figure 3.8: Adams/View Complete Inline-1 Model

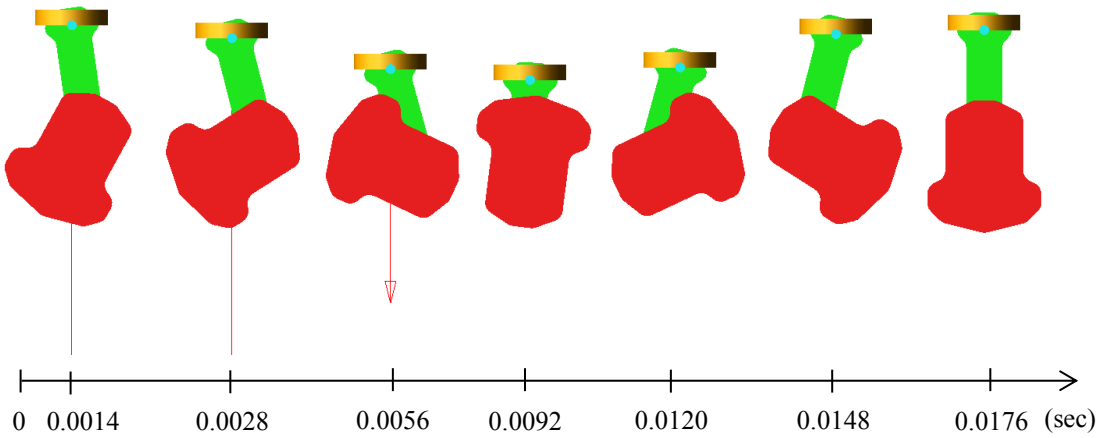

Figure 3.9: Adams/View Inline-1 Positions

3.2 Vee-2 Engine

The model of the two-cylinder vee (vee-2) engine (Figure 3.10) used the same parts as that of the single cylinder model and followed the same modeling principles. The only difference was that it had two cylinders with a bank angle of 45 degrees (deg). All of the parts were in the same plane; in other words, the connecting rods were not side-by-side as they would be in a real engine but actually occupied the same space where they connected to the crankshaft. It was decided that for this vibrational analysis the arrangement would not adversely affect the final results though for further research it was recommended that the vee-2 model be made more realistic. A sampling of positions for the vee-2 engine can be seen in Figure 3.11.

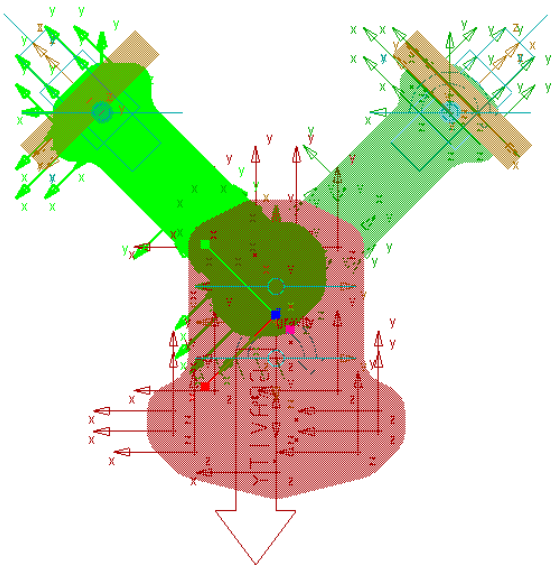

Figure 3.10: Adams/View Complete Vee-2 Model

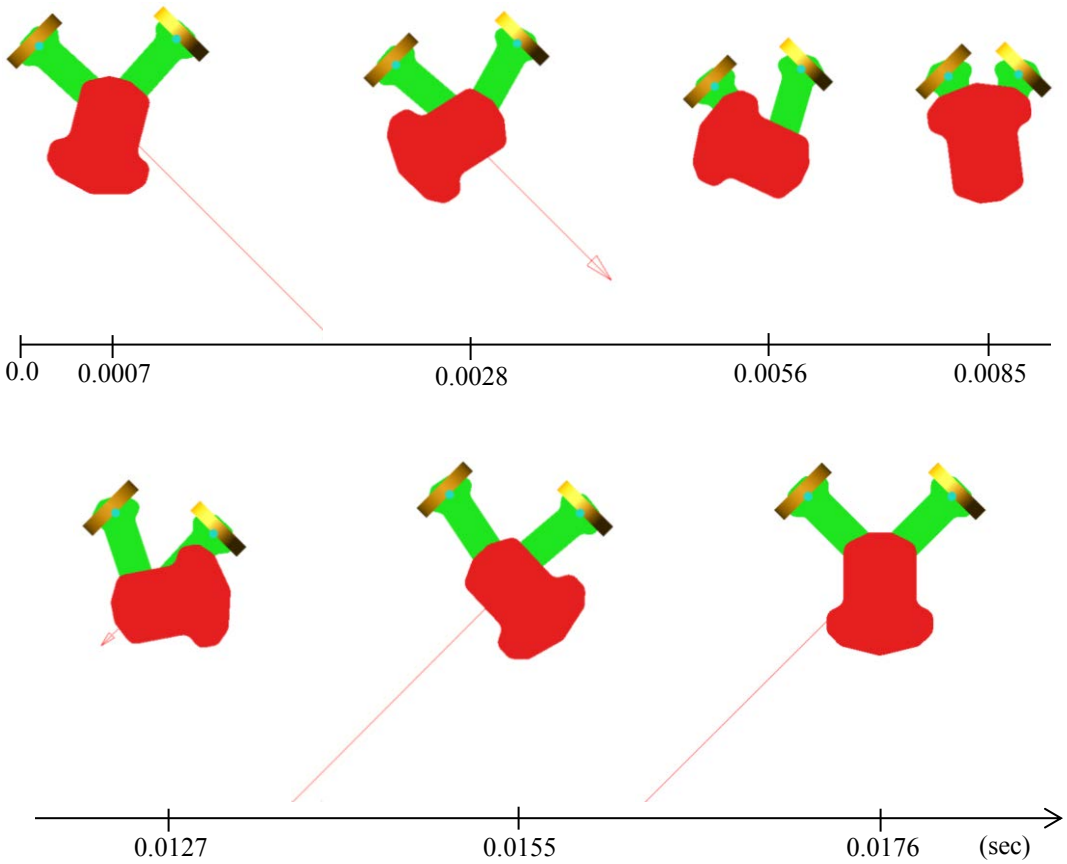

Figure 3.11: Adams/View Vee-2 Positions

3.3 Flexibility Modeling

The rigid connecting rods were converted into flex bodies so that frequency results as well as more accurate dynamic results could be generated. The flex bodies were created within Adams/View using ViewFlex, this option did not require a modal neutral (MN) file import because it created its own MN file. Three different meshing schemes (Tables 3.3 and 3.4) were tried, and it was decided to use the results from the moderately populated mesh (Table 3.4). The results from the different mesh configurations did not vary much; but it was decided that the sparsely populated mesh was too rigid and that the heavily populated mesh was overpopulated, possibly allowing errors to occur in the results. The final meshed models can be seen in Figure 3.12.

TABLE 3.3

REJECTED MESH CONFIGURATION DATA

Sparsely Populated Mesh			
Number of Modes	**Edge Shape**		**Attachment Method**
6	Straight		Rigid (RBE2)
Growth Rate	**Angle Per Element (deg)**	**MSN Based Refinement**	**Curvature Based Scaling**
1.5	45	OFF	OFF
Heavily Populated Mesh			
Number of Modes	**Edge Shape**		**Attachment Method**
6	Mixed		Rigid (RBE2)
Growth Rate	**Angle Per Element (deg)**	**MSN Based Refinement**	**Curvature Based Scaling**
1.2	25	ON	ON

TABLE 3.4

USED MESH CONFIGURATION DATA

Moderately Populated Mesh			
Number of Modes	**FlexBody Type**	**Element Type**	**Element Shape**
6	Geometry	Solid	Tetrahedral
Element Order	**Element Specification**	**Edge Shape**	**Attachment Method**
Linear	Auto	Mixed	Compliant (RBE3)
Growth Rate	**Angle Per Element (deg)**	**MSN Based Refinement**	**Curvature Based Scaling**
1.5	25	ON	ON

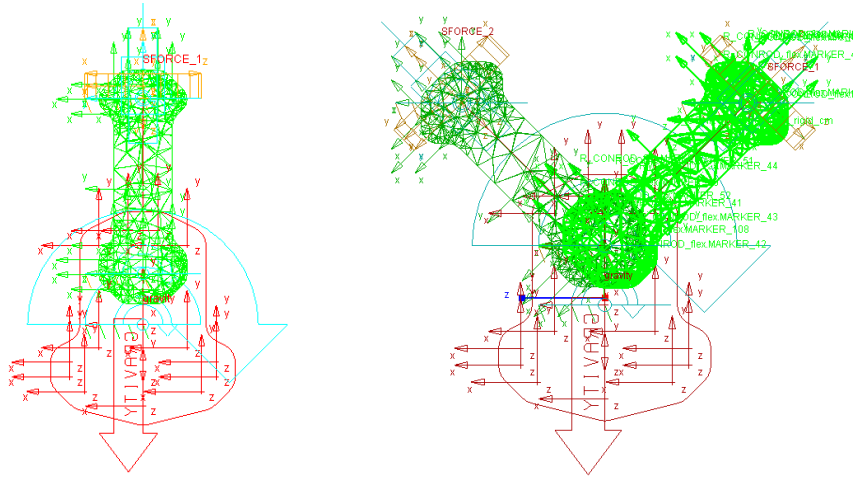

Figure 3.12: Adams/View Meshed Inline-1 and Vee-2 Models

3.4 Inclusion of Gas Forces

As mentioned in the beginning of this paper, even though all systems do experience damping, all models in Adams/View were designed as perfect systems (i.e. no damping was included) [5]. Also, neither cylinder wall side forces nor cylinder wall oil shearing forces were included in the Adams/View models; only gas forces were used [4].

The gas force data of a four-stroke Otto cycle internal combustion engine was received from Robert L. Norton in the form of normalized pressure data (Appendix A) for a crank angle of 0 to 720 degrees. A peak pressure of 600 pounds per square inch (psi) [4, 15] was chosen and

multiplied against the normalized pressure data. This peak pressure data was then multiplied by the piston area to get the gas force, units of pound-force (lb_{force}). The gas force for the inline-1 models starting at top-dead-center can be seen in Figure 3.13.

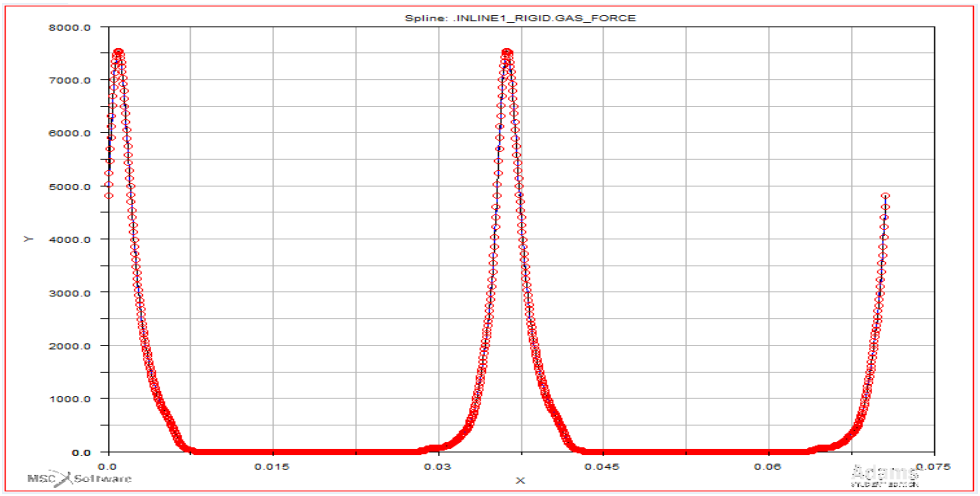

Figure 3.13: Inline-1 Engine Gas Force (y-axis: lb_{force} & x-axis: seconds)

A test data file containing time and gas force was imported into Adams/View and was then converted into a spline. In the spline file, linear extrapolation was not selected because it was not needed and because it adversely affected the data. The gas force spline was used by an applied force which moved with the part it was applied to: the top, central portion of the piston. The force run-time function expression which read the spline data was set up to use the Akima fitting method. The first independent variable was time; there was no other independent variable used. The equation derivative order was set to zero. (The time for the test data file was created from the time it took to run the system at 3400 rpm for 1440 degrees of crankshaft rotation, two cycles; the gas force was matched to its respective time.) Although in a real engine the gas force is the driving force; due to the models being run at steady state, a revolute motion attached to the crankshaft's main pin location and set at 3400 rpm was required to drive the system at a constant angular velocity.

The vee-2 engine was set to fire the left side first then the right with 360 degrees between them. The left and right gas forces for the vee-2 engine can be seen in Figures 3.14 and 3.15 respectively; both were set for the crankshaft in a vertical starting position. Figure 3.16 shows the gas forces for the vee engine as they were during an actual run.

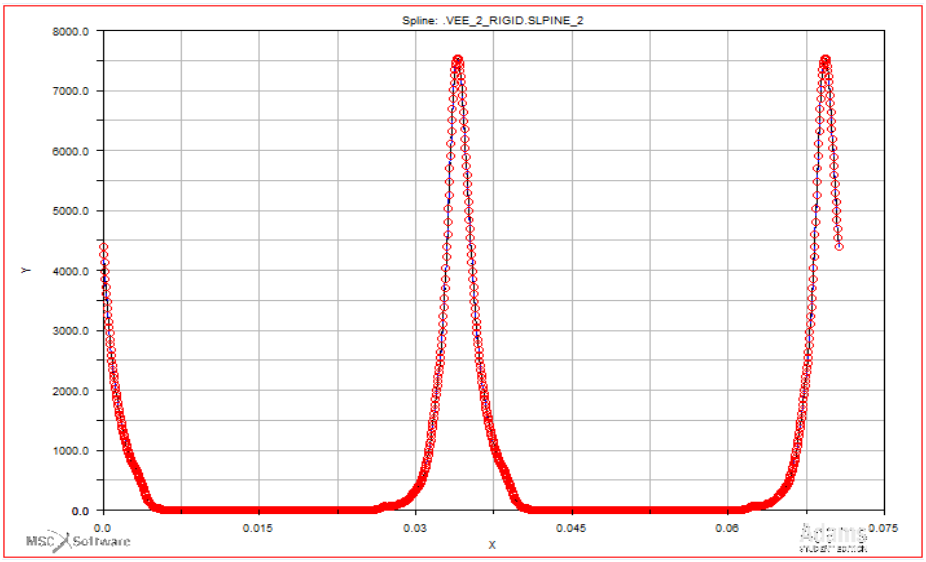

Figure 3.14: Left Piston Vee-2 Engine Gas Force (y-axis: lb_{force} & x-axis: seconds)

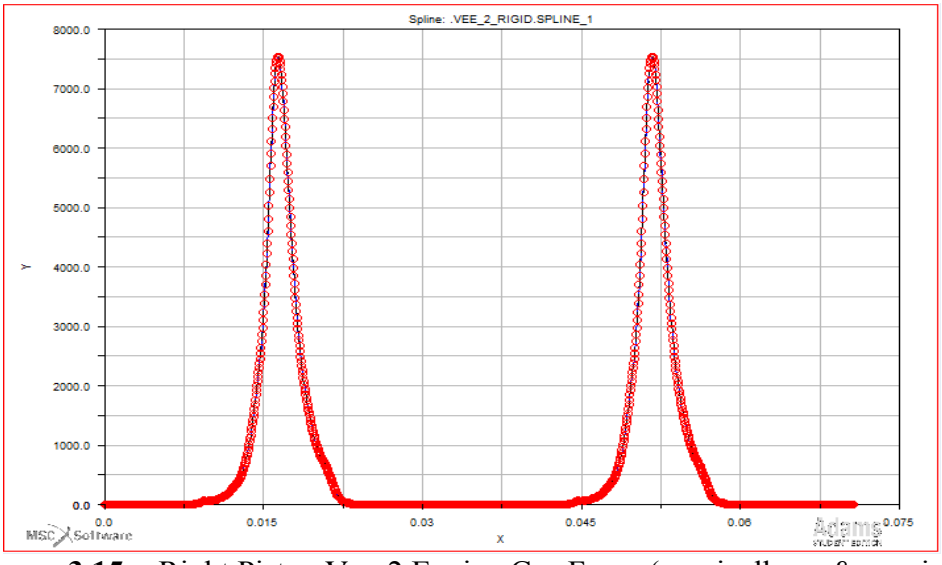

Figure 3.15: Right Piston Vee-2 Engine Gas Force (y-axis: lb_{force} & x-axis: seconds)

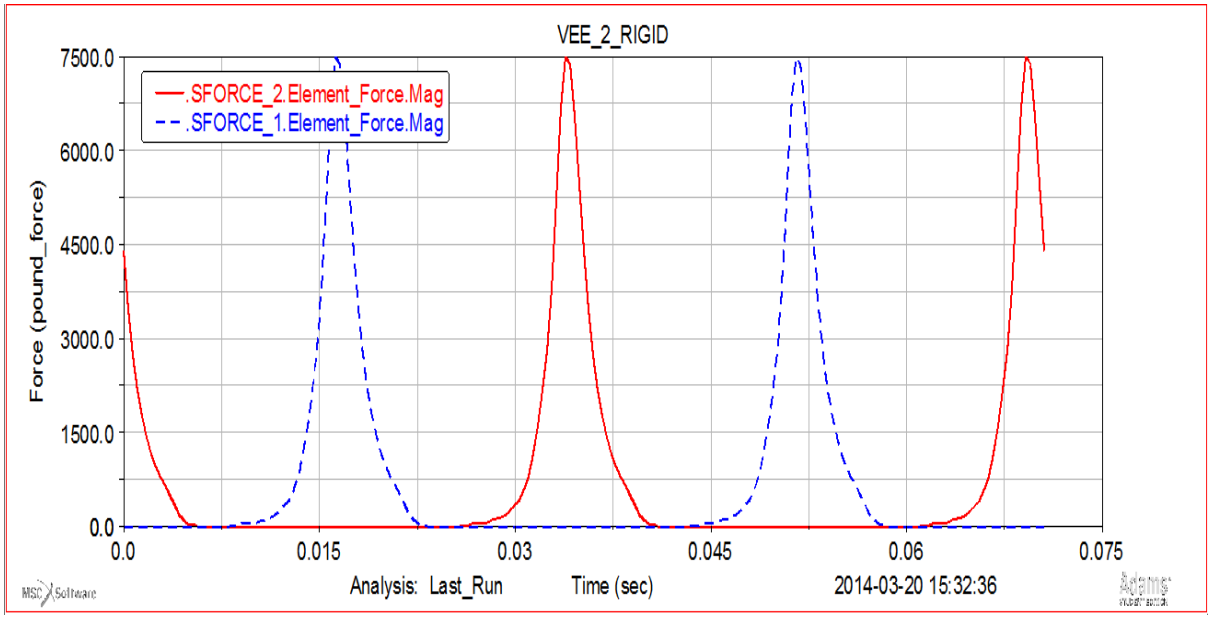

Figure 3.16: Vee-2 Engine Gas Forces: Left (red) & Right (blue)

CHAPTER 4

FEV VIRTUAL ENGINE MODELING AND SIMULATION

This chapter covers the modeling and simulation for the Virtual Engine models. The inline-1 model was covered first, followed by the vee-6 model. The rigid connecting rods were converted into flex bodies by applying modal neutral (MN) files; gas forces were applied from an internal database file. All of the material properties were left as they were originally defined in the template files. Figure 4.1 shows the inline-1 model while Figure 4.2 shows the vee-6 model. (The difference in appearance between the models with the flexible connecting rods and those with the rigid connecting rods were virtually indistinguishable; therefore, only the models with the flexible connecting rods were shown.)

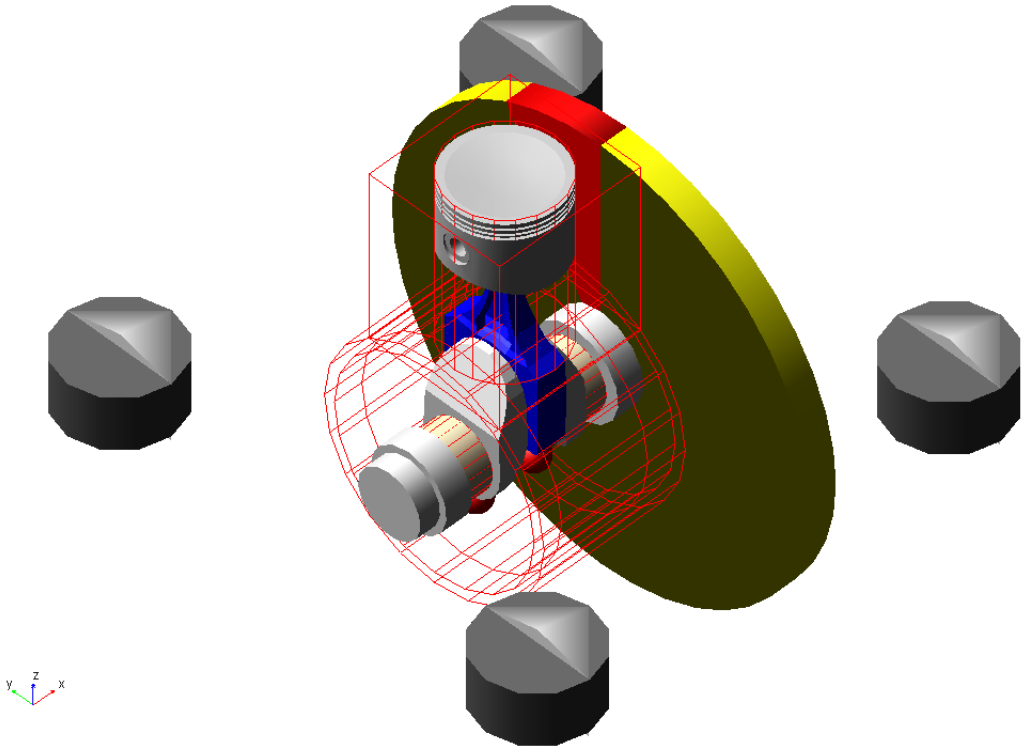

Figure 4.1: Virtual Engine Inline-1 Model

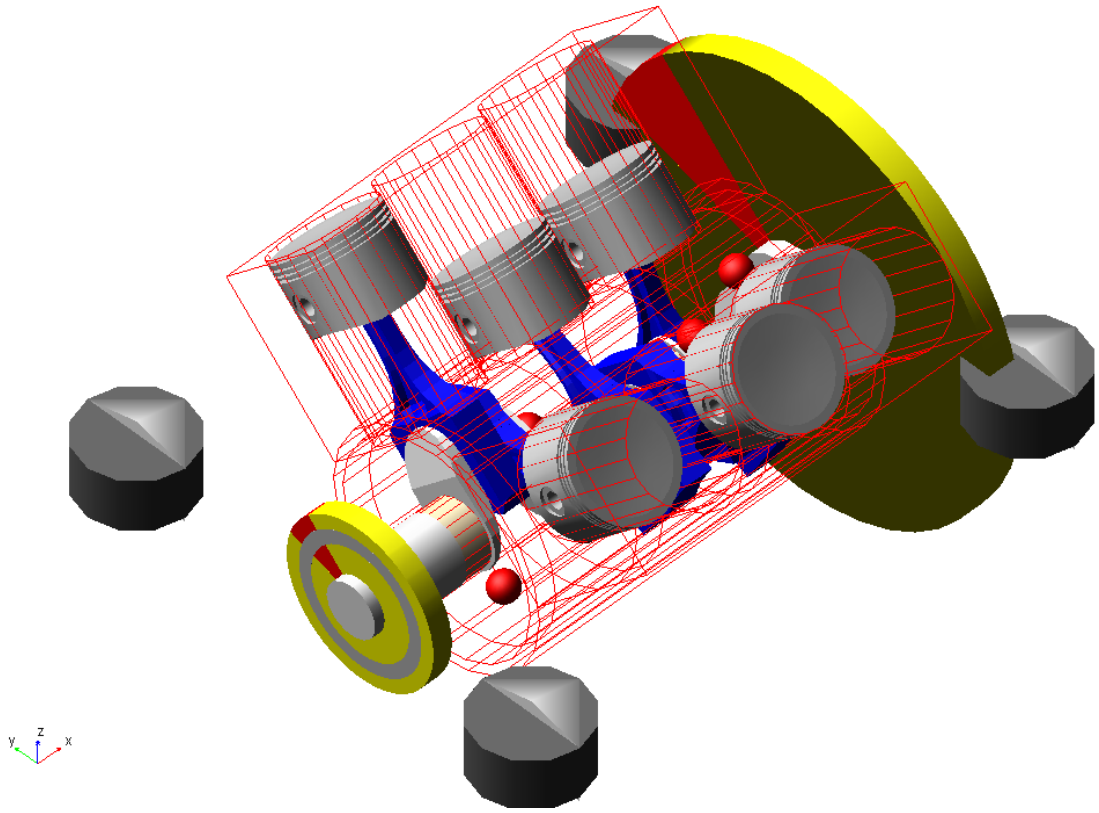

Figure 4.2: Virtual Engine Vee-6 Model

4.1 Inline-1 Engine

The Virtual Engine inline-1 model was acquired by using the FEV Virtual Engine template mdids://aengine_shared/templates.tbl/_cranktrain_i1.tpl. That template already existed in the database and was only modified to be able to apply the connecting rod MN file mdids://aengine_shared/flex_bodys.tbl/fev_flex_con_rod.mnf. The piston data file was changed to mdids://private/pistons.tbl/fev_0002.pst while the piston pin was attached to the piston instead of the connecting rod. The engine data which were modified with their new values can be found in Table 4.1; also, the balancing shafts were deactivated.

TABLE 4.1

FEV VIRTUAL ENGINE MODEL DATA

FEV Virtual Engine Data			
Stroke (in)	**Bore Diameter (in)**	**Axial Cylinder Distance (in)**	**Effective Connecting Rod Length (in)**
3.11	3.03	3.425	4.72
Piston Pin Outside Diameter (in)	**Piston Pin Length (in)**	**Piston Boss Spacing (in)**	**Piston Height (in)**
0.787	2.83	1.30	2.165
Bearing Position (in)	**Thrust Main Bearing #**	**Crank-Connecting Rod Ratio**	**Connecting Rod-Stroke Ratio**
1.71	2	0.33	1.52
Crank Pin (in)		**Crank Main Pin (in)**	
diameter	**length**	**diameter**	**length**
1.73	0.866	1.89	0.83
Compression Height (in)		**Total Displacement (L):**	
1.18		0.368	

The used connecting rod interface node identification numbers were number 6 for the crank pin marker and number 1 for the piston pin marker; those were required to correctly attach the MN file to the connecting rod. Constraint bearings were used for the crank pin bearings and the piston bearings, not hydrodynamic flex bearings. The test rig was adjusted so that there was only one connector with a stiffness of 1.3E+006 and a damping of 54.6. The gas force was changed to the Otto cycle gas force file mdids://aengine_shared/gas_force.tbl/fev_otto_001.gaf; the gas force plot for an actual run can be seen in Figure 4.3. A sampling of positions for the inline-1 engine can be seen in Figure 4.4.

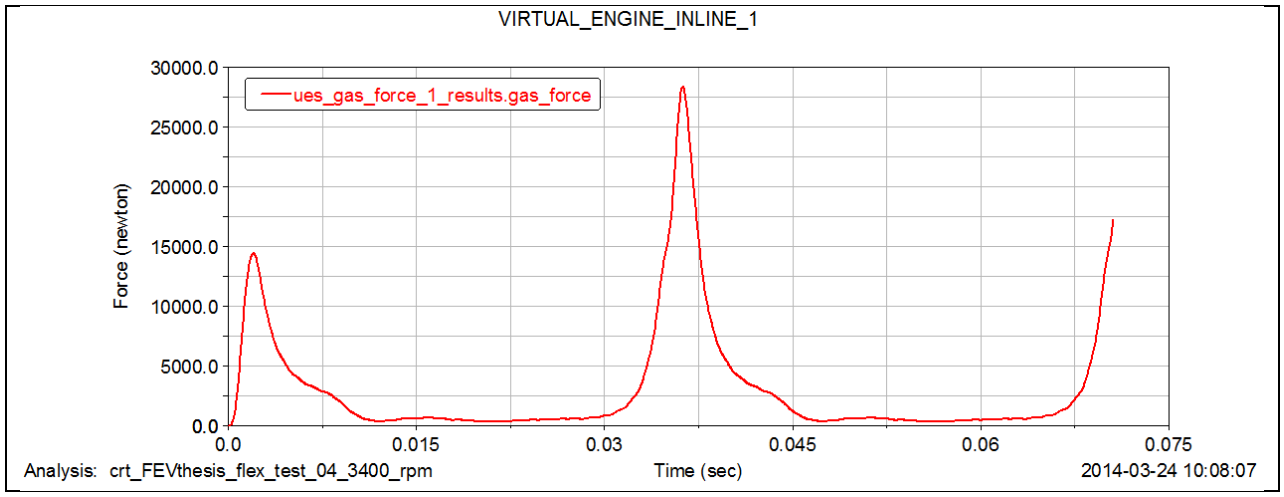

Figure 4.3: Virtual Engine Inline-1 Gas Force

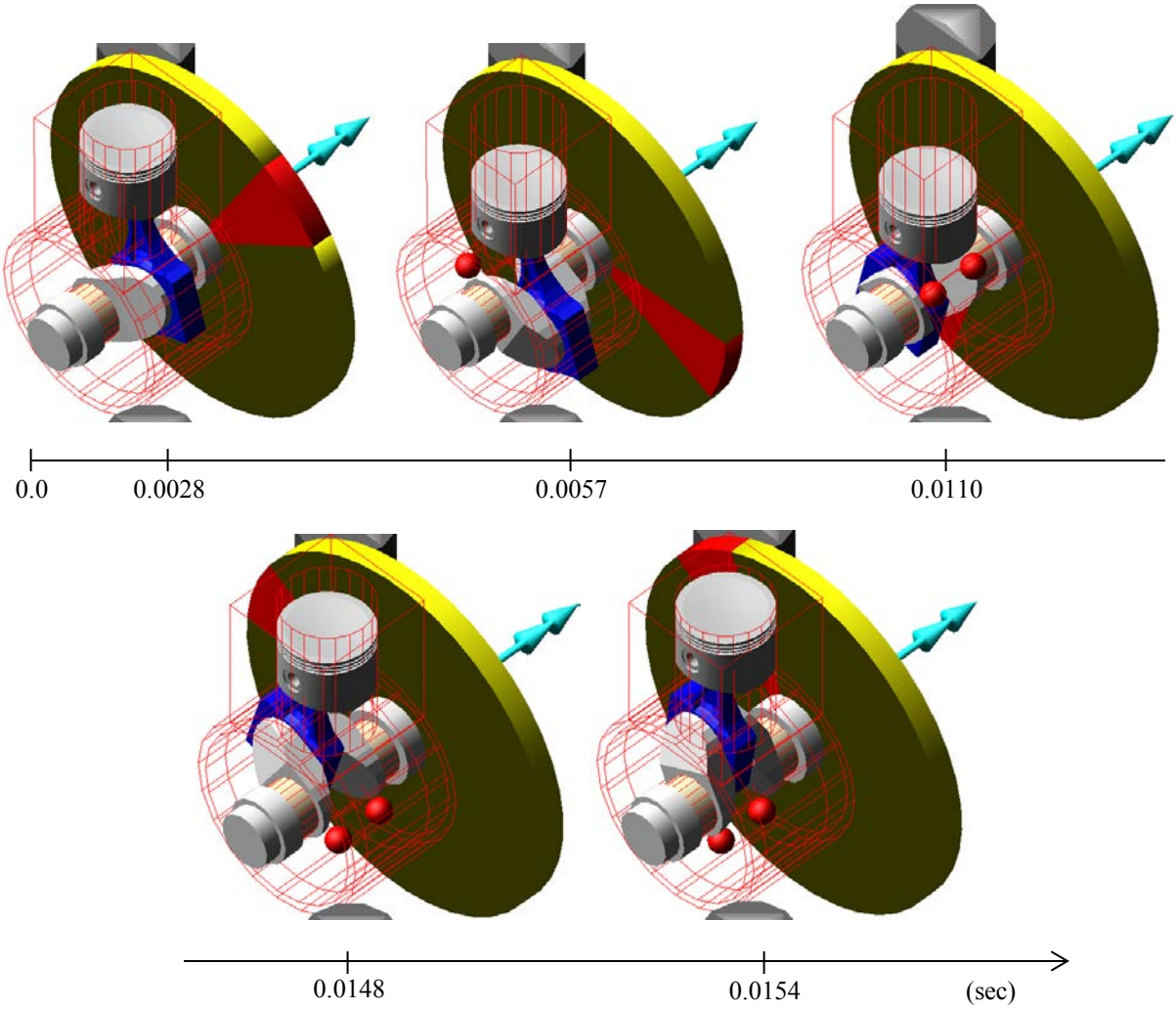

Figure 4.4: Virtual Engine Inline-1 Positions

4.2 Vee-6 Engine

The vee-6 model was created from the FEV Virtual Engine database template mdids://aengine_shared/templates.tbl/_cranktrain_v6.tpl. The modifications to the Virtual Engine vee-6 data were the same as those for the inline-1 data; the total displacement and the extra data required by a vee engine (Table 4.2) were the only differences. The gas forces for the vee-6 model, as they appeared during an actual run, can be seen in Figure 4.5. A sample of positions for the vee-6 engine can be seen in Figure 4.6.

TABLE 4.2

FEV VIRTUAL ENGINE VEE-6 DATA

Virtual Engine Vee-6 Data			
Number of Banks	**Number of Cylinders**	**Bank Angle (deg)**	**Bank Offset (in)**
2	6	45	0.866
Firing Order	**Cylinder Order**		**Total Displacement (L)**
	Bank 1 (left side)	**Bank 2 (right side)**	
1-4-2-5-3-6	1, 2, 3	4, 5, 6	2.207

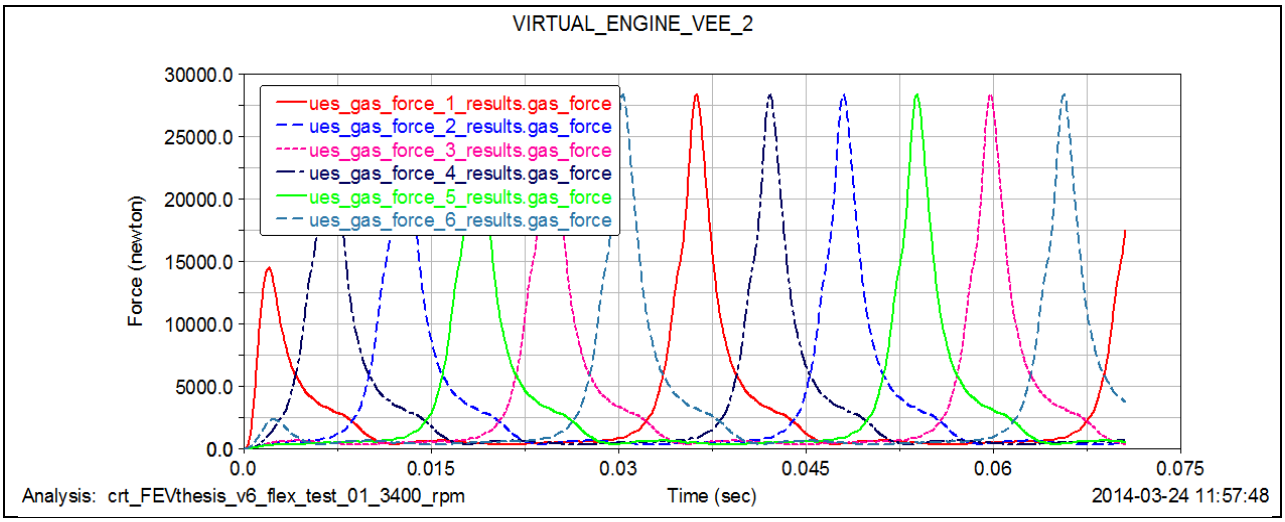

Figure 4.5: Virtual Engine Vee-6 Gas Forces

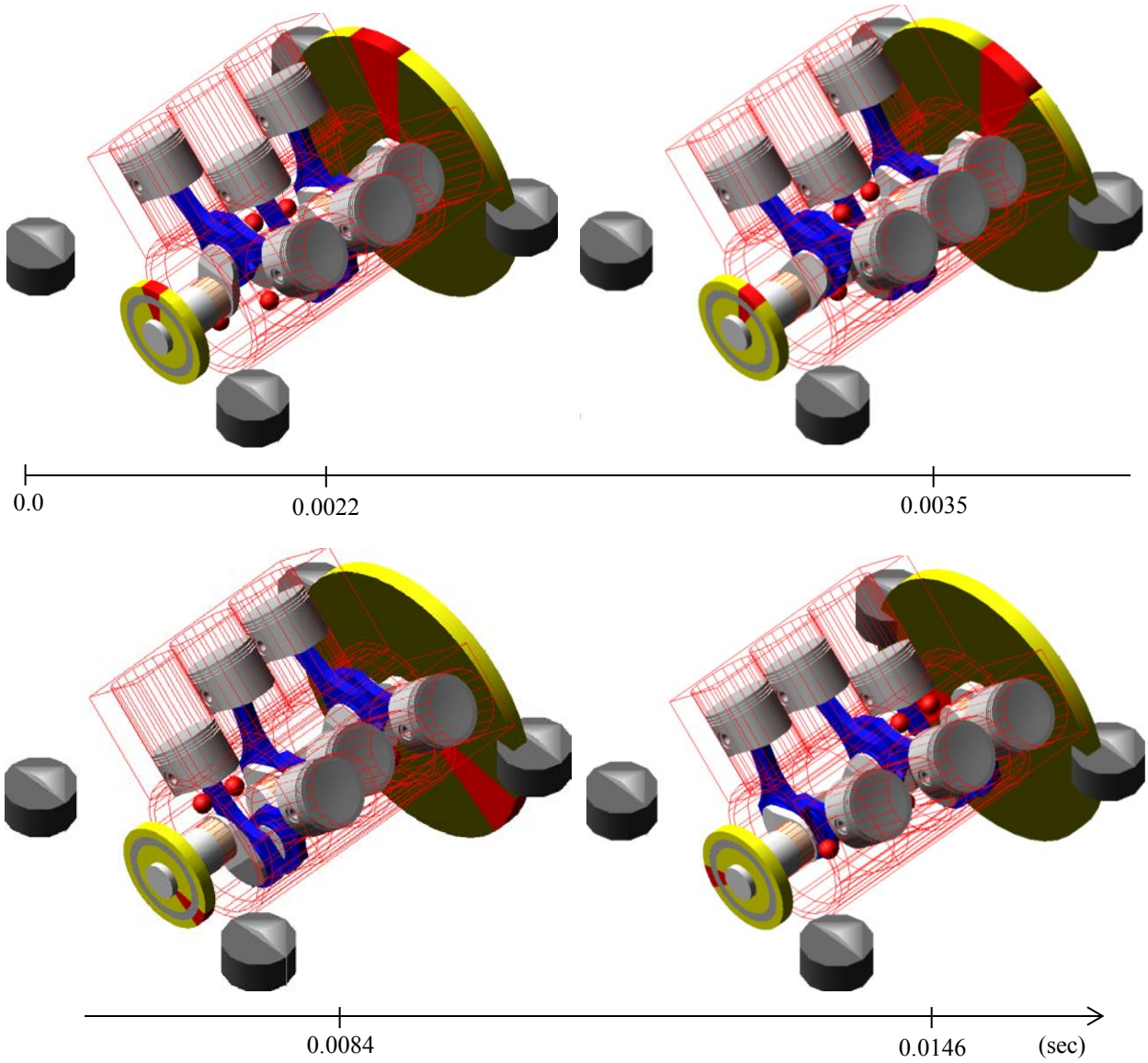

Figure 4.6: Virtual Engine Vee-6 Positions

CHAPTER 5

RESULTS AND DISCUSSION

Both Adams/View and Virtual Engine automatically disabled the rigid body modes for dynamic analysis so that singularities would not arise in the analysis [19]. From the Adams/View and Virtual Engine models, the piston positions, velocities, and accelerations along the cylinder axis were graphically collected. From the piston pin joints in the Adams/View models and the piston pin bearings in the Virtual Engine models, the forces in the y- and z-directions, the force magnitudes, and the angular velocities about the x-axis were collected. These forces and angular velocities were also collected for the crank pin joints in the Adams/View models and the crank pin bearings in the Virtual Engine models with the addition of one graph, that of the forces in the x-direction.

Due to the variance in marker orientation between the Adams/View results and the Virtual Engine results, a global orientation was assigned to the graph titles found in Appendices D through O so as to not confuse the reader. The y-axis was vertical and pointed up, the z-axis was horizontal and pointed left, while the x-axis was horizontal and came out of the page towards the reader. This orientation system was also true for the local coordinates with respect to the cylinder orientation, for all cases; what this means is that the graphs with same title could be compared to each other.

5.1 MSC Adams/View Results

The connecting rod natural frequencies with their respective mode numbers were collected from the Adams/View MN files for both the cast iron and the aluminum connecting rods (Table 5.1). (The MN files' natural frequencies for the cast iron models were the same, this

was also true for the aluminum connecting rod MN files; what this means was that the MN file natural frequency data only had to be collected once from each MN file type.)

TABLE 5.1

ADAMS/VIEW MN FILE NATURAL FREQUENCIES

	Adams/View MN Files			
	Mode #	**Frequency (Hz)**	**Mode #**	**Frequency (Hz)**
Cast Iron	1	-0.001148	6	0.0008836
	2	-0.000749	7	2497.13
	3	-0.000545	8	4500.31
	4	-0.000270	9	5343.91
	5	0.0006883	10	6320.94
Aluminum	1	-0.001258	6	0.0019009
	2	-0.001083	7	2510.15
	3	-0.000676	8	4464.16
	4	-0.000335	9	5310.46
	5	0.0011542	10	6350.51

The front views of the cast iron and aluminum flex connecting rods with their rigid body mode shapes and corresponding mode numbers can be seen in Figures 5.1 and 5.2, respectively. Appendices B and C show both the side and front profiles for the mode shapes for the same models. As stated earlier, since the rigid body mode shapes were the same between the inline-1 models and the vee-2 models within their respective material types, only one set of results for each material type was required.

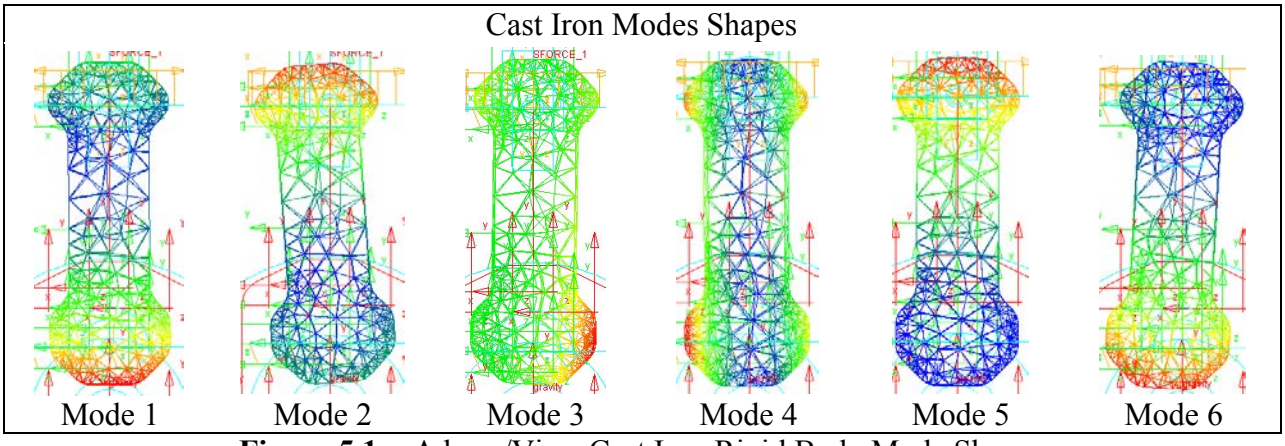

Figure 5.1: Adams/View Cast Iron Rigid Body Mode Shapes

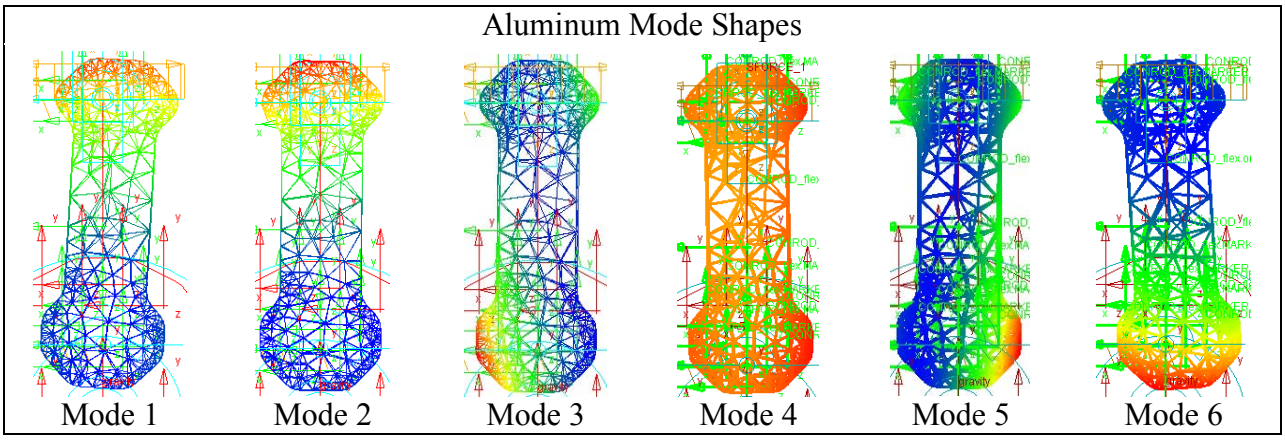

Figure 5.2: Adams/View Aluminum Rigid Body Mode Shapes

When determining the systems' natural frequencies for static analysis using normal mode vibrational analysis, Adams/View had two different options: without damping effects and with damping effects. The 'un-damped' results were of unknown stability since their real eigenvalues were all equal to zero. (The term 'un-damped natural frequency is only correct when the system experiences proportional damping or is a single degree of freedom system [20].) The damped results were all stable since their real eigenvalues were all negative [20]. The data which was collected directly from the systems with the flexible connecting rods were their natural frequencies (Tables 5.2 and 5.3).

TABLE 5.2

ADAMS/VIEW INLINE-1 LINEAR NATURAL FREQUENCIES

	'Un-damped'		**Damped**		
	Mode #	**Frequency (Hz)**	**Mode #**	**Frequency (Hz)**	**Real Eigenvalues**
Cast Iron	1	737.004	1	741.04	-34.26
	2	3776.24	2	4904.86	-3433.43
	3	3959.79	3	3968.53	-1830.43
	4	4831.4	4	3948.61	-1212.15
	5	5718.48	5	15491.02	-15017.9
Aluminum	1	2590.63	1	15013.0	-14900.6
	2	3835.48	2	2596.56	-498.78
	3	4270.39	3	4437.82	-3586.04
	4	5680.79	4	3982.34	-1838.71
	5	8682.14	5	10661.7	-9879.69

TABLE 5.3

ADAMS/VIEW VEE-2 LINEAR NATURAL FREQUENCIES

	'Un-damped'		Damped		
	Mode #	**Frequency (Hz)**	**Mode #**	**Frequency (Hz)**	**Real Eigenvalues**
Cast Iron	1	652.97	1	655.50	-25.61
	2	2931.2	2	3076.39	-1836.2
	3	3894.89	3	5054.82	-3592.02
	4	3975.42	4	4074.42	-1973.29
	5	4158.13	5	4210.49	-2189.72
Aluminum	1	2623.55	1	2631.25	-514.34
	2	3235.24	2	4586.19	-3713.43
	3	3389.74	3	17979.7	-17765.0
	4	3909.64	4	4579.87	-3610.75
	5	4403.16	5	3527.02	-2097.34

5.2 FEV Virtual Engine Results

The connecting rod natural frequencies for the Virtual Engine models were also the same, among each other, since they all referenced the same MN file; these frequencies can be found in Table 5.4. The results were extracted from the connecting rod MN file by using MSC Adams/ Flex Student Version 2013. They could be compared to the Adams/View connecting rod natural frequencies found in Table 5.1.

TABLE 5.4

VIRTUAL ENGINE MN FILE NATURAL FREQUENCIES

Virtual Engine MN File			
Mode #	**Frequency (Hz)**	**Mode #**	**Frequency (Hz)**
1	-0.052213	6	0.0401374
2	-0.014609	7	1161.01
3	0.0013412	8	1777.98
4	0.0024632	9	2008.12
5	0.0067525	10	4649.66

A trial using different test rig stiffness and damping values than mentioned earlier was performed. The values for stiffness and damping were estimated from the model data for an

engine idle speed of 600 rpm, a damping loss factor of 0.05, and a safety margin of 20 percent; these settings resulted in a stiffness of 874.5 and a damping of 3.479. The results for this test rig were very different from any generated by the other Virtual Engine test rig as well as those generated by the Adams/View models. The results did not show any patterns so were not used in this report. For future research, the test rig effects would be good to investigate further.

5.3 Discussion

The peak pressures for the Virtual Engine models at 3400 rpm were 6 Newtons per millimeter square which was equivalent to 870 psi versus the Adams/View pressures of 600 psi. The Virtual Engine gas force peaked around 28,000 Newtons which was about 6,300 lb_{force}; Adams/View gas force was about 7,500 lb_{force}. The difference in gas force peaks was due the difference in piston areas between the models of the two programs; all of the engine models were run with roughly the same parameters thereby allowing comparison between like models.

The first six modes in Tables 5.1 and 5.4 were the connecting rod rigid body modes, and the remainder of the modes in those tables was their flex frequencies. The data in those two tables were compared to what was found in Chegini et al. [13] and Quinghui et al. [14]; but due to differences in modeling, boundary conditions, and finite element programs used, only some frequencies were similar. The Adams/View and Virtual Engine results were all similar enough that they could be compared. The rigid body frequencies were very low; therefore, they could be safely passed through without causing resonance. The flex frequencies were high enough that, under normal operating conditions, no connecting rod would ever reach those frequencies.

From the natural frequencies in Tables 5.2 and 5.3 compared to those in Tables 5.1 and 5.4, it could be seen that the systems' initial frequencies were lower than the connecting rods' first flex frequencies; therefore, the systems would reach resonance before the connecting rods.

In Tables 5.2 and 5.3, it could also be seen that the systems with cast iron connecting rods had lower initial frequencies than those same systems with aluminum connecting rods; this was due to the softer aluminum connecting rods absorbing the vibrational energy better than the stiffer cast iron connecting rods.

From Figures 5.3-5.5, the midpoint deformation of the inline-1 flexible connecting rods for the two programs can be seen. The midpoint deformation for the cast iron and aluminum rods are seen to be about the same, around 9.0E-005 inches, excluding the initial deformation found in the cast iron model. For the Virtual Engine model, there was no deformation. The midpoint deformations for all models were essentially zero; therefore, they could be disregarded.

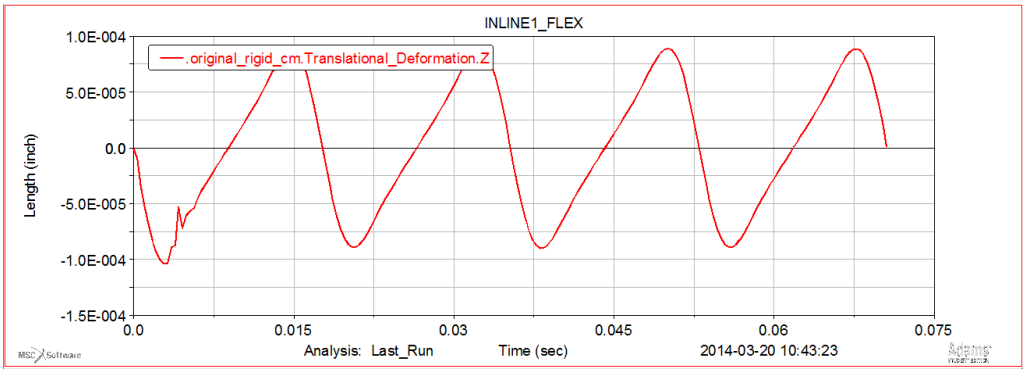

Figure 5.3: Adams/View Cast Iron Inline-1 Connecting Rod Center of Mass Z Deformation

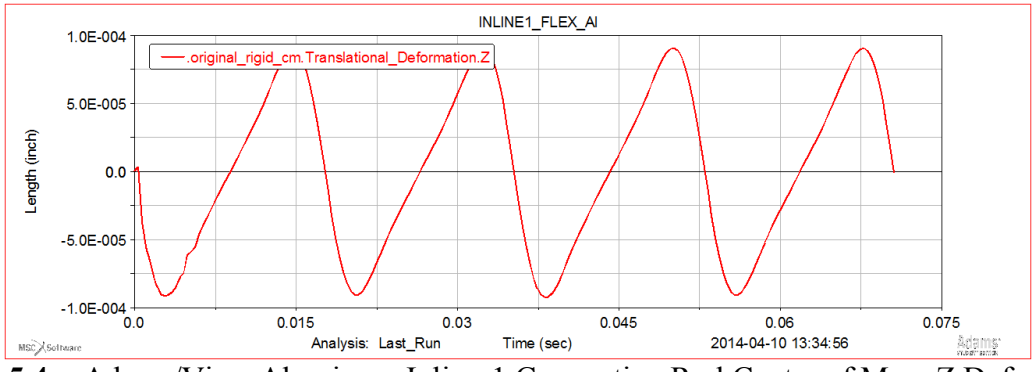

Figure 5.4: Adams/View Aluminum Inline-1 Connecting Rod Center of Mass Z Deformation

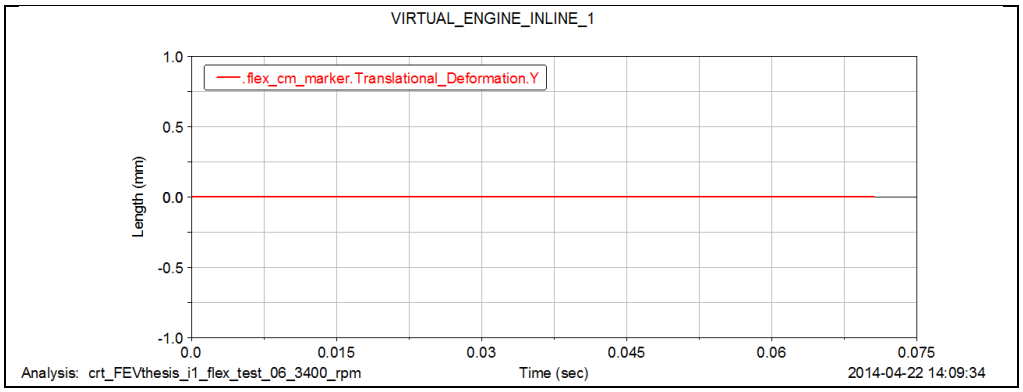

Figure 5.5: Virtual Engine Inline-1 Connecting Rod Center of Mass Z Deformation

The Adams/View piston displacements, velocities, and accelerations were compared to analytical and actual engine data [15, 16, 17, 18]; to verify that the results seemed reasonable, they were also compared to Virtual Engine. Due to the differences in connecting rod-stroke ratios and rpms, the velocities and accelerations were different; but the results appeared to be within appropriate range. Some comparisons of the Adams/View piston accelerations can be seen in Figures 5.6-5.13; the data from one model was plotted in the same graph as the data for a different model to see how they compared to each other.

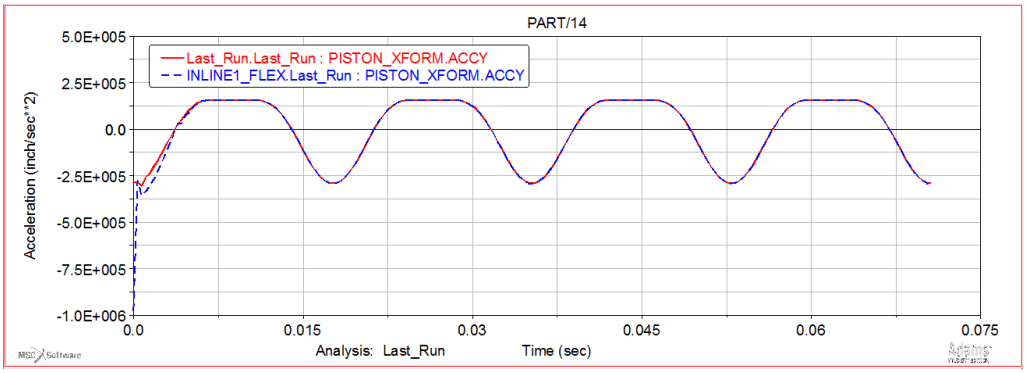

Figure 5.6: Cast Iron Rigid (red) and Flex (blue) Inline-1 Piston Accelerations

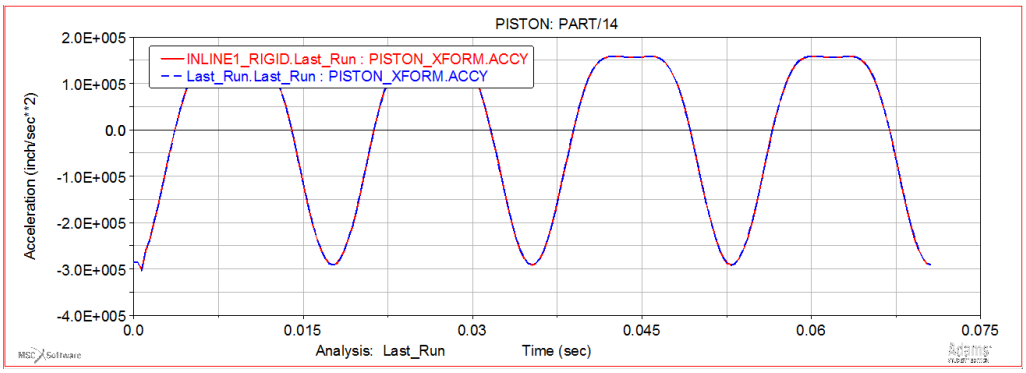

Figure 5.7: Cast Iron (red) and Aluminum (blue) Rigid Inline-1 Piston Accelerations

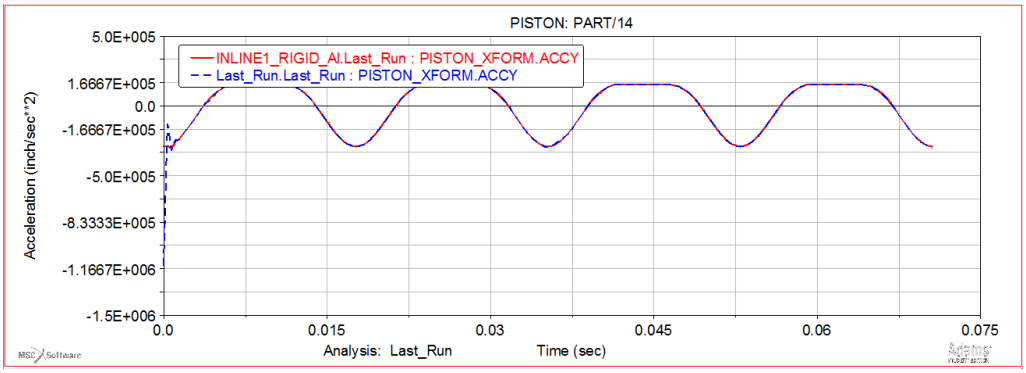

Figure 5.8: Aluminum Rigid (red) and Flex (blue) Inline-1 Piston Accelerations

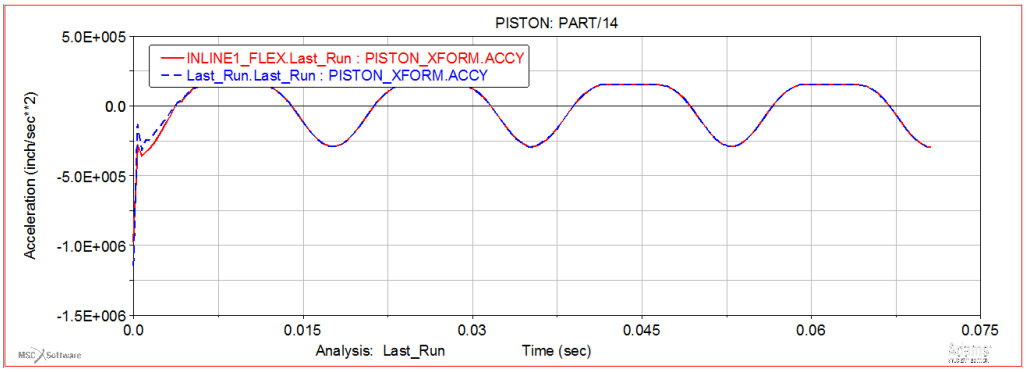

Figure 5.9: Cast Iron (red) and Aluminum (blue) Flex Inline-1 Piston Accelerations

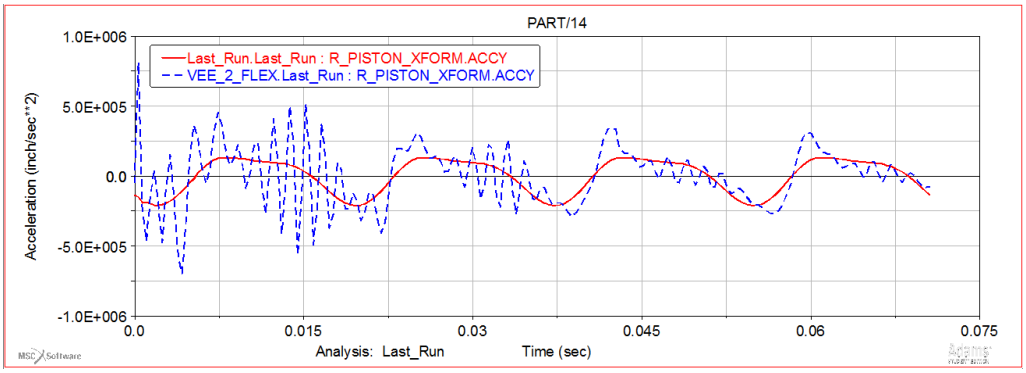

Figure 5.10: Cast Iron Rigid (red) and Flex (blue) Vee-2 Right Piston Accelerations

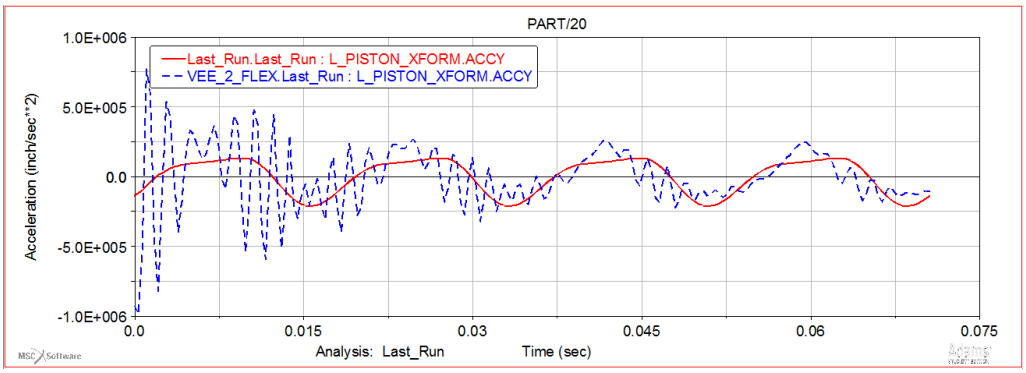

Figure 5.11: Cast Iron Rigid (red) and Flex (blue) Vee-2 Left Piston Accelerations

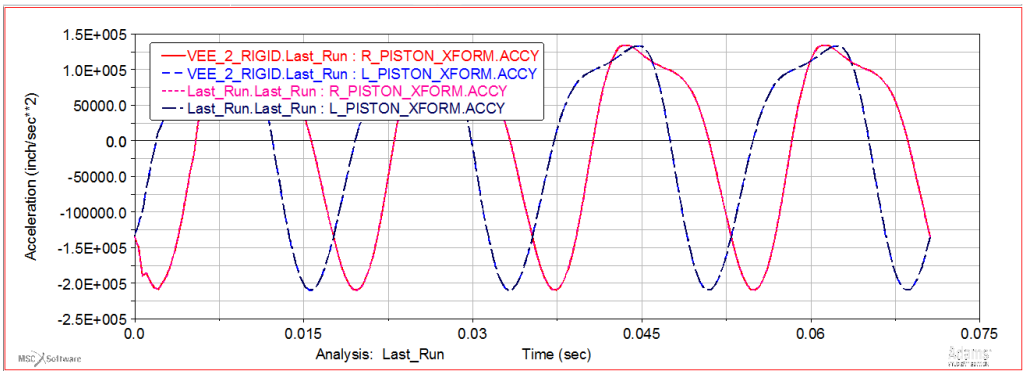

Figure 5.12: Cast Iron and Aluminum Rigid Vee-2 Piston Accelerations

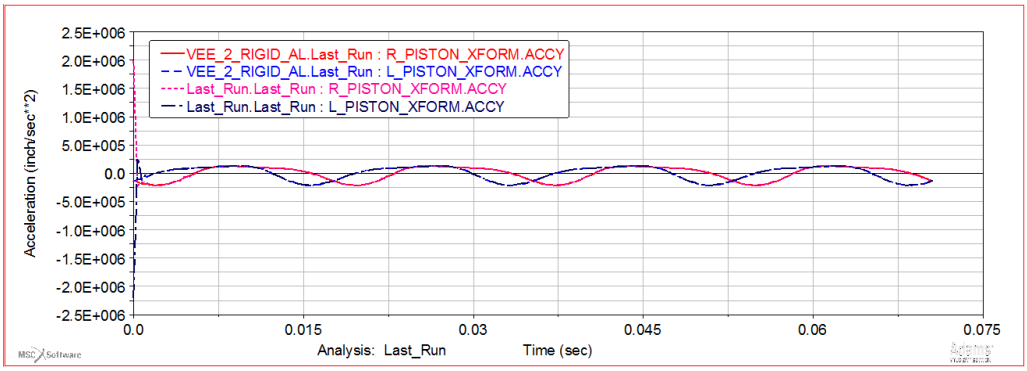

Figure 5.13: Aluminum Rigid and Flex Vee-2 Piston Accelerations

Due to the perfect matching of the Adams/View piston acceleration data among the respective engine types, one does not see any anomalies except for the initial spikes and the cast iron flex vee-2 model's oscillations. The initial spikes in the acceleration plots were caused by the systems starting up. The cast iron flex vee-2 initial spike was half of the respective aluminum spike, but the oscillations were three times greater than the rigid results for the first 360 degrees. Even though the cast iron flex vee-2 results initially had major oscillations, the

oscillations started to damp out and the results began to join up with the cast iron vee-2 rigid results (Figures 5.10 and 5.11); this was evidence that the system's natural frequencies were stable thereby backing up the data found in Table 5.3. Since the aluminum flex vee-2 model results did not have the oscillations that the cast iron flex model had, it was further evidence that aluminum connecting rods absorb system vibrational energy much better than stiffer cast iron connecting rods; Figures 5.3 and 5.4 also back this up.

The Virtual Engine piston accelerations for the flexible models can be seen in Figures 5.14 and 5.15. The rigid and flex results for the Virtual Engine models were the same between the respective engine types except for the startup spike found in the inline-1 flex model. The rigid piston accelerations can be found in Appendices L and N.

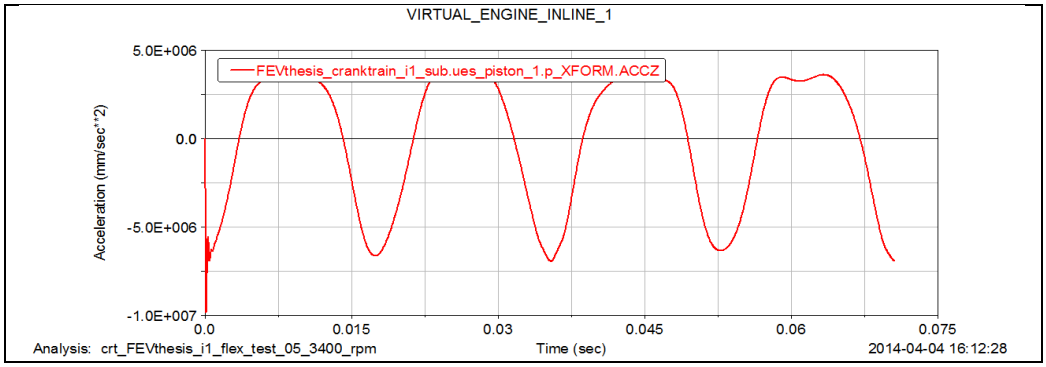

Figure 5.14: Virtual Engine Flex Inline-1 Piston Acceleration

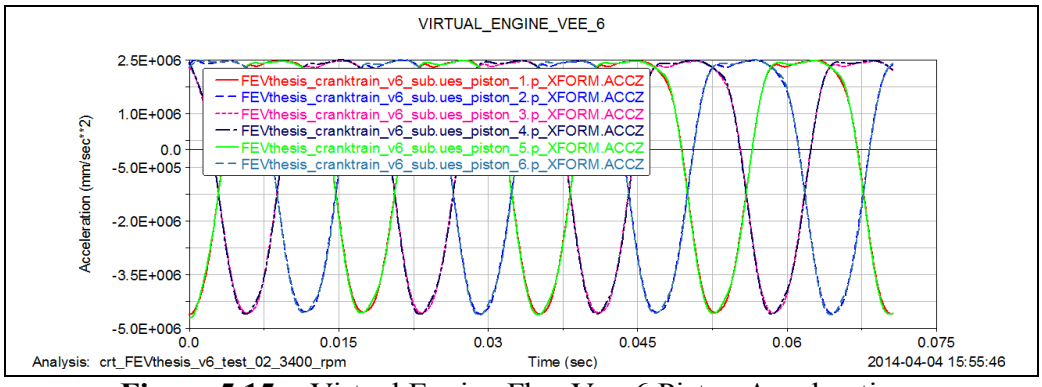

Figure 5.15: Virtual Engine Flex Vee-6 Piston Accelerations

The piston pin joint forces for all of the Adams/View models and the Virtual Engine models had similar values once the Newtons were converted to pounds-force; this was also true

for the crank pin joint forces. An example is the piston pin joint y forces which for the Adams/ View inline-1 models (Figure 5.16) were approximately -1000 to 6500 lb_{force} and for the Virtual Engine models (Figure 5.17) were approximately -562 to 5845 lb_{force}. The Adams/View vee-2 models (Figure 5.18) were approximately -1000 to 5000 lb_{force}, while those of the Virtual Engine vee-6 models (Figure 5.19) were the same as the inline-1 models. Though Figures 5.16 through 5.19 are only a sample of the piston pin joint y data, what was stated holds true for the rest of the piston pin joint y data found in the Appendices.

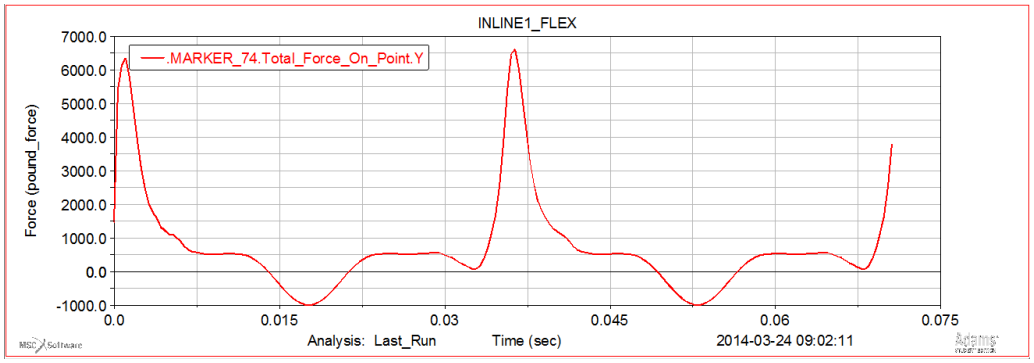

Figure 5.16: Adams/View Cast Iron Flex Inline-1 Piston Pin Joint Y Force

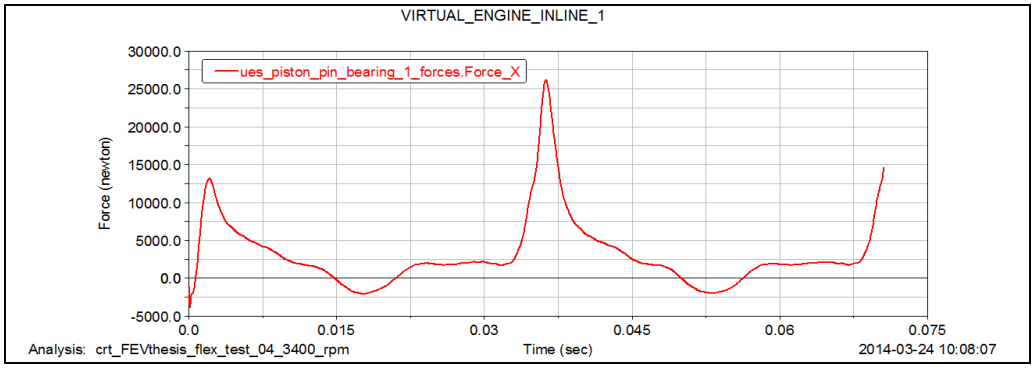

Figure 5.17: Virtual Engine Flex Inline-1 Piston Pin Joint Y Force

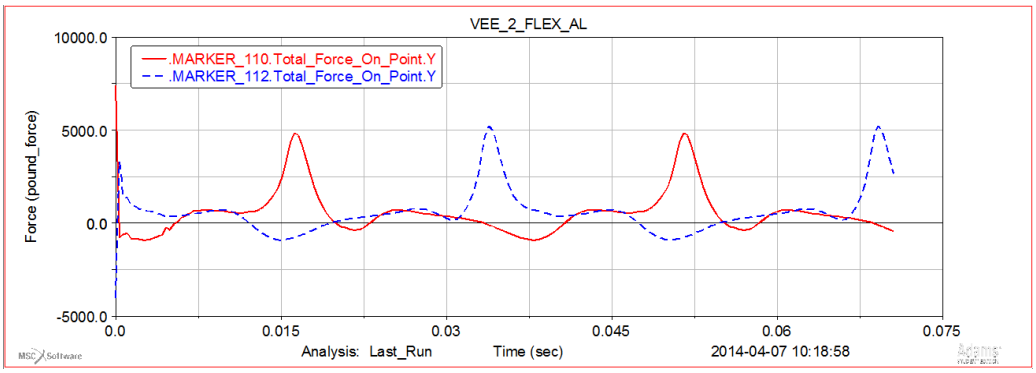

Figure 5.18: Adams/View Aluminum Flex Vee-2 Piston Pin Joint Y Forces

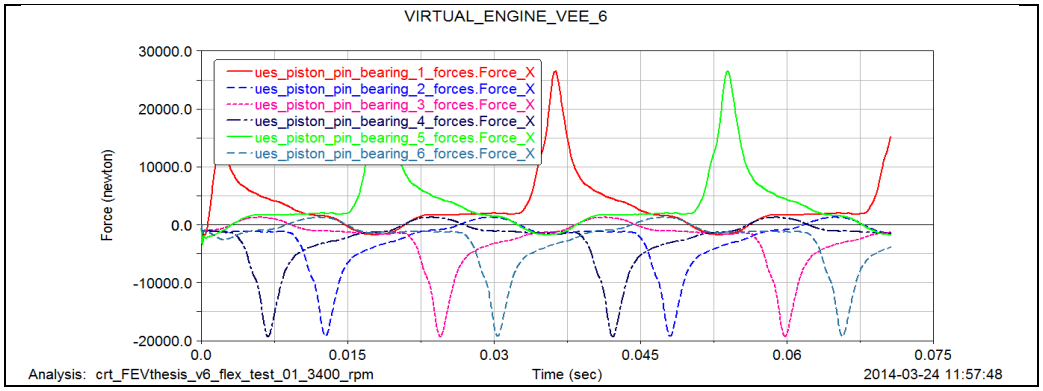

Figure 5.19: Virtual Engine Flex Vee-6 Piston Pin Joint Y Forces

The piston pin joint velocities for all of the models were close, approximately -6,000 to 6,000 rpm for the Adams/View models and approximately -7,000 to 7,000 rpm for the Virtual Engine models. This was also true for the crank pin joint angular velocities with the Adams/View models approximately 14,700 to 26,300 rpm and the Virtual Engine models approximately 14,000 to 27,500 rpm. For virtually all of the models except the cast iron flex vee-2 results, the initial startup disturbances were settled by the first 360 degrees.

The Adams/View and Virtual Engine force and angular velocity graph results found in the Appendices are almost identical in shape. All of the inline models cross-check quite well among each other; this was also true for the vee models. It was proof that simplified engine models could be used for basic analysis rather than having to create complex models.

CHAPTER 6

CONCLUSIONS AND RECOMMENDATIONS

6.1 Conclusions

The purpose of this research was to determine what effects the vibrations of connecting rods had on the overall performance of Otto cycle engines. Dynamic and vibrational analysis was conducted using the programs MSC Adams/View and FEV Virtual Engine. The Adams/ View models were composed of simplified cranktrains and forces, while those of Virtual Engine were modeled after actual dimensions and workings. Inline and vee engine configurations were modeled; the results from the two programs were then compared. The data was also checked against static analysis from literature sources as well as having the general piston performance cross-checked against actual engine data.

The Adams/View rigid body frequencies were similar to those of a real connecting rod design used in the Virtual Engine models. All of the system frequencies were of a high enough frequency and had stable eigenvalues so as not to cause destructive resonance; the connecting rod rigid body modes were of very low frequencies resulting in safe passage during startup and shutdown. Since all of the models were run at steady-state, any interference at the very beginning of all graphs could be ignored due to the spikes having been caused by the models being suddenly started at a high rpm rather than gradually building up to it as real engines do.

Even though the units were different between Adams/View and Virtual Engine, when converted, the results were the same or similar. When looking at the results, one has to remember that those from Adams/View were of idyllic form (i.e. they had no friction, etc.) while those of Virtual Engine were of realistic form (i.e. they were similar to what would be found in a real engine).

From the results, it was determined that the vibrations of connecting rods do not greatly affect the overall performance of an Otto cycle engine unless a connecting rod was damaged or had a casting defect thereby reducing its natural frequencies. Also, it was determined that a simplified connecting rod and engine model were capable of producing accurate enough results for general, overall engine analysis. Though the aluminum connecting rod energy absorption was good for preventing system vibrations, it would have to be compared to the drawback of losing structural strength before one could make a decision as to modifying the connecting rod material for real engines. There are many other factors in connecting rod design which would have to be considered as well.

6.2 Recommendations

For future research using Adams/View, one could apply different forces which are found in actual engines, vary the mesh, and adjust the rpm. Stroke length and connecting rod dimensions would also be good items to adjust. For the Virtual Engine models, it was suggested that one try hydrodynamic bearings with a new connecting rod MN file. Different test rig configurations, test results, and connecting rod models could also be studied. A flexible crankshaft, different engine types, and different number of cylinders could be studied further. One could also look at how engine operating temperatures would affect the vibrational results.

REFERENCES

REFERENCES

[1] Metso. "Vibration Analysis," *Scribd*, May 2011. http://www.scribd.com/doc/203678040/Vibration-Analysis (accessed June 6, 2013).

[2] Genta, G. Dynamics of Rotating Systems, New York: Springer, 2005.

[3] Nissan Automotive. "VQ35HR-VQ25HR Engine Technology Overview," *Nissan Global.* n.d. http://www.nissan-global.com/EN/DOCUMENT/PDF/TECHNOLOGY/technology_overview/VQ_E_070802_X-1a-02.pdf (accessed September 13, 2013).

[4] Lichty, L. C. Internal Combustion Engines, 6th ed., New York: McGraw-Hill Book Company, Inc., 1951.

[5] Palm III, W. J. System Dynamics, 2nd ed., New York: McGraw-Hill, 2010.

[6] Mourelatos, Z. P. "A crankshaft system model for structural dynamic analysis of internal combustion engines," *Computers & Structures*, June 2001. http://data.obitet.net/makale/makale/internalcombustionengines/006.pdf (accessed April 8, 2014).

[7] Furuhama, S., and M. Takiguchi. "Measurement of Piston Frictional Force in Actual operating Diesel Engine," *SAE Technical Paper 790855*, February 1979. http://papers.sae.org/790855/ (accessed April 8, 2014).

[8] Yang, J., L. Pu, Z. Wang, Y. Zhou, and X. Yan. "Fault Detection in a Diesel Engine by Analysing the Instantaneous Angular Speed," *Mechanical Systems and Signal Processing*: 549-564, May 2001. http://www.sciencedirect.com/science/article/pii/S088832700091344X (accessed May 8, 2014).

[9] Kaminski, T., M. Wendeker, K. Urbanowicz, and G. Litak. "Combustion Process in a Spark Ignition Engine: Dynamics and Noise level Estimation," *Chaos: An Interdisciplinary journal of Nonlinear Science*: 461-466, 2004. http://scitation.aip.org/content/aip/journal/chaos/14/2/10.1063/1.1739011 (accessed Apri1 8, 2014).

[10] de Jalon, J. G., J. Cuadrado, A. Avello, and J. M. Jimenez. "Kinematic and Dynamic Simulation of Rigid and Flexible Systems with Fully Cartesian Coordinates," *Computer-Aided Analysis of Rigid and Flexible Mechanical Systems*: 258-323, 1993.

REFERENCES (continued)

[11] Garnier, T., C. Grente, and D. Bonneau. "Three-Dimensional EHD Behavior of the Engine Block/Crankshaft Assybly for a Four Cylinder inline Automotive Engine," *Journal of Tribology*: 721-730, October 1999. http://tribology.asmedigitalcollection.asme.org/article.aspx?articleid=1465969 (accessed April 8, 2014).

[12] Tevatia, A., S. B. Lal, and S. K. Srivastava. "Finite Element Fatigue Analysis of Connecting Rods of Different Cross-Sections," *International Journal of Mechanics & Solids*: 45-53, 2011. http://eds.b.ebscohost.com/eds/detail?vid=2&sid=c17cef74-2a1c-4561-911d-34813fb3d54c%40sessionmgr198&hid=115&bdata=JnNpdGU9ZWRzLWxpdmU%3d#db=a9h&AN=74649724 (accessed April 8, 2014).

[13] Chegini, H., A. Najjariyan, M. Ramjbarkohan, M. Abad, M. Mohammadi, S. Farakhzad, and H. Agangari. "Modal Analysis of Connecting Rod of Nissan Z24 Engine by Finite Element Method," *Journal of Science and today's world*: 54-58, November 2012. http://www.academia.edu/2308141/Modal_Analysis_of_Connecting_Rod_of_Nissan_Z24_Engine_by_Finite_Element_Method (accessed May 21, 2013).

[14] Qinghui, Z., Wang Yunying, and Ji Wei. "The Finite Element Anlysis of Connecting Rod of Diesel Engine," *Measuring Technology and Mechatronics Automation*: 870-873, March 2010. http://ieeexplore.ieee.org/stamp/stamp.jsp?tp=&arnumber=5459521 (accessed August 27, 2013).

[15] Norton, R. L. Design of Machinery: An Introduction to the Sysnthesis and Analysis of Mechanisms and Machines, 5th ed, New York: McGraw-Hill, 2012.

[16] Kane, J. *Comparing NASCAR Cup engines to Formula One engines, by EPI Inc*, November 2011. http://www.epi-eng.com/piston engine technology/comparison of cup to f1.htm (accessed May 21, 2013).

[17] FTL Racing. *index.* n.d. http://www.ftlracing.com/rsratio.htm (accessed May 21, 2013).

[18] EPI, Inc. *Piston Motion: The Obvious and not-so-Obvious, by EPI, Inc*, September 2012. http://www.epi-eng.com/piston_engine_technology/piston_motion_basics.htm (accessed May 21, 2013).

[19] MSC Software. "Flex_2013," *MSC SimCompanion-2-Adams/Flex help-Adams 2013.* September 2013. http://simcompanion.mscsoftware.com/infocenter/index?page=content&id=DOC10403&cat=1VMO50&actp=LIST (accessed March 14, 2014).

REFERENCES (continued)

[20] MSC Software. "adams_vibration_mdr3_help," *MSC SimCompanion-2-Using Adams/Vibration.* October 2009. http://simcompanion.mscsoftware.com/infocenter/index?page=content&id=DOC9311&cat=11P7155&actp=LIST (accessed June 20, 2013).

BIBLIOGRAPHY

BIBLIOGRAPHY

Bernard, S. J., E. O. Waters, and C. W. Phelps. Principles of Machine Design, New York: The Ronald Press Company, 1955.

Black, P. H., and O. E. Adams, Jr. Machine Design, 3rd ed., New York: McGraw-Hill Book Company, 1968.

Budynas, R. G., and J. K. Nisbett. Shigley's Mechanical Engineering Design, 9th ed., New York: McGraw-Hill, 2008.

da Silva, M. R. M. C. Intermediate Dynamics: Complemented with Simulations and Animations, New York: McGraw-Hill, 2004.

Friswell, M. I., J. E. T. Penny, S. D. Garvey, and A. W. Less. Dynamics of Rotating Machines, New York: Cambridge University Press, 2010.

Logan, D. L. A First Course in the Finite Element Method, 5th ed., Stamford: Cengage Learning, 2012.

Meirovitch, L. Fundamentals of Vibrations, New York: McGraw-Hill, 2001.

Pye, D. R. The Internal Combustion Engine, Volume 1, 2nd ed., London: Oxford University Press, 1937.

Stone, R. Introduction to Internal Combustion Engines, 2nd ed., Warrendal: Society of Automotive Engineers, Inc., 1993.

Taylor, C. F., and E. S. Taylor. The Internal Combustion Engine, 1st ed., Scranton: International Textbook Company, 1938.

Thomson, W. T., and M. D. Dahleh. Theory of Vibration with applications, 5th ed., Upper Saddle River: Prentice Hall, 1998.

APPENDICES

APPENDIX A

NORMALIZED PRESSURE DATA FOR 720 CRANK ANGLE DEGREES

Column									
1	**2**	**3**	**4**	**5**	**6**	**7**	**8**	**9**	**10**
0.638	0.782	0.259	0.099	0.012	0	0	0	0	0
0.667	0.761	0.252	0.098	0.01	0	0	0	0	0
0.696	0.741	0.245	0.095	0.008	0	0	0	0	0
0.726	0.721	0.238	0.091	0.007	0	0	0	0	0
0.756	0.701	0.231	0.09	0.007	0	0	0	0	0
0.784	0.682	0.223	0.087	0.006	0	0	0	0	0
0.812	0.663	0.218	0.086	0.005	0	0	0	0	0
0.837	0.642	0.211	0.082	0.005	0	0	0	0	0
0.863	0.623	0.206	0.079	0.006	0	0	0	0	0
0.887	0.603	0.2	0.076	0.006	0	0	0	0	0
0.909	0.584	0.194	0.073	0.005	0	0	0	0	0
0.929	0.566	0.188	0.069	0.004	0	0	0	0	0
0.946	0.547	0.181	0.066	0.003	0	0	0	0	0
0.962	0.529	0.177	0.064	0.004	0	0	0	0	0
0.974	0.512	0.172	0.062	0.004	0	0	0	0	0
0.984	0.494	0.166	0.059	0.003	0	0	0	0	0
0.992	0.478	0.163	0.057	0.003	0	0	0	0	0
0.997	0.462	0.158	0.054	0.003	0	0	0	0	0
0.999	0.446	0.153	0.05	0.003	0	0	0	0	0
1	0.432	0.148	0.047	0.002	0	0	0	0	0
1	0.417	0.143	0.045	0.001	0	0	0	0	0
0.997	0.404	0.139	0.041	0	0	0	0	0	0
0.99	0.391	0.135	0.037	0	0	0	0	0	0
0.982	0.378	0.131	0.034	0	0	0	0	0	0
0.972	0.366	0.129	0.032	0	0	0	0	0	0
0.96	0.355	0.126	0.028	0	0	0	0	0	0
0.947	0.342	0.123	0.026	0	0	0	0	0	0
0.932	0.33	0.119	0.023	0	0	0	0	0	0
0.917	0.32	0.115	0.021	0	0	0	0	0	0
0.9	0.31	0.112	0.019	0	0	0	0	0	0
0.88	0.3	0.11	0.018	0	0	0	0	0	0
0.861	0.292	0.107	0.016	0	0	0	0	0	0
0.843	0.283	0.105	0.015	0	0	0	0	0	0
0.822	0.275	0.103	0.014	0	0	0	0	0	0
0.802	0.267	0.101	0.013	0	0	0	0	0	0

APPENDIX A (continued)

Column									
11	**12**	**13**	**14**	**15**	**16**	**17**	**18**	**19**	**20**
0	0	0	0	0	0	0	0.009	0.03	0.135
0	0	0	0	0	0	0	0.008	0.031	0.141
0	0	0	0	0	0	0	0.009	0.032	0.148
0	0	0	0	0	0	0	0.009	0.033	0.155
0	0	0	0	0	0	0	0.009	0.034	0.164
0	0	0	0	0	0	0.001	0.009	0.036	0.172
0	0	0	0	0	0	0.001	0.01	0.039	0.18
0	0	0	0	0	0	0.002	0.01	0.04	0.188
0	0	0	0	0	0	0.003	0.01	0.041	0.197
0	0	0	0	0	0	0.002	0.011	0.042	0.204
0	0	0	0	0	0	0.002	0.011	0.043	0.213
0	0	0	0	0	0	0.002	0.011	0.045	0.224
0	0	0	0	0	0	0.003	0.012	0.045	0.234
0	0	0	0	0	0	0.002	0.013	0.048	0.245
0	0	0	0	0	0	0.003	0.013	0.049	0.256
0	0	0	0	0	0	0.003	0.013	0.049	0.266
0	0	0	0	0	0	0.005	0.014	0.052	0.275
0	0	0	0	0	0	0.005	0.016	0.054	0.286
0	0	0	0	0	0	0.005	0.015	0.055	0.295
0	0	0	0	0	0	0.006	0.015	0.057	0.304
0	0	0	0	0	0	0.007	0.016	0.059	0.314
0	0	0	0	0	0	0.007	0.015	0.062	0.325
0	0	0	0	0	0	0.007	0.015	0.064	0.337
0	0	0	0	0	0	0.008	0.017	0.068	0.351
0	0	0	0	0	0	0.008	0.018	0.071	0.364
0	0	0	0	0	0	0.009	0.019	0.076	0.379
0	0	0	0	0	0	0.008	0.019	0.08	0.394
0	0	0	0	0	0	0.008	0.02	0.083	0.411
0	0	0	0	0	0	0.008	0.021	0.086	0.429
0	0	0	0	0	0	0.008	0.021	0.091	0.448
0	0	0	0	0	0	0.008	0.022	0.094	0.47
0	0	0	0	0	0	0.008	0.023	0.099	0.49
0	0	0	0	0	0	0.008	0.024	0.104	0.512
0	0	0	0	0	0	0.009	0.024	0.109	0.535
0	0	0	0	0	0	0.009	0.026	0.115	0.56
0	0	0	0	0	0	0.009	0.028	0.121	0.584
0	0	0	0	0	0	0.009	0.028	0.129	0.61

APPENDIX B

MSC ADAMS/VIEW CAST IRON RIGID BODY MODE SHAPE RESULTS

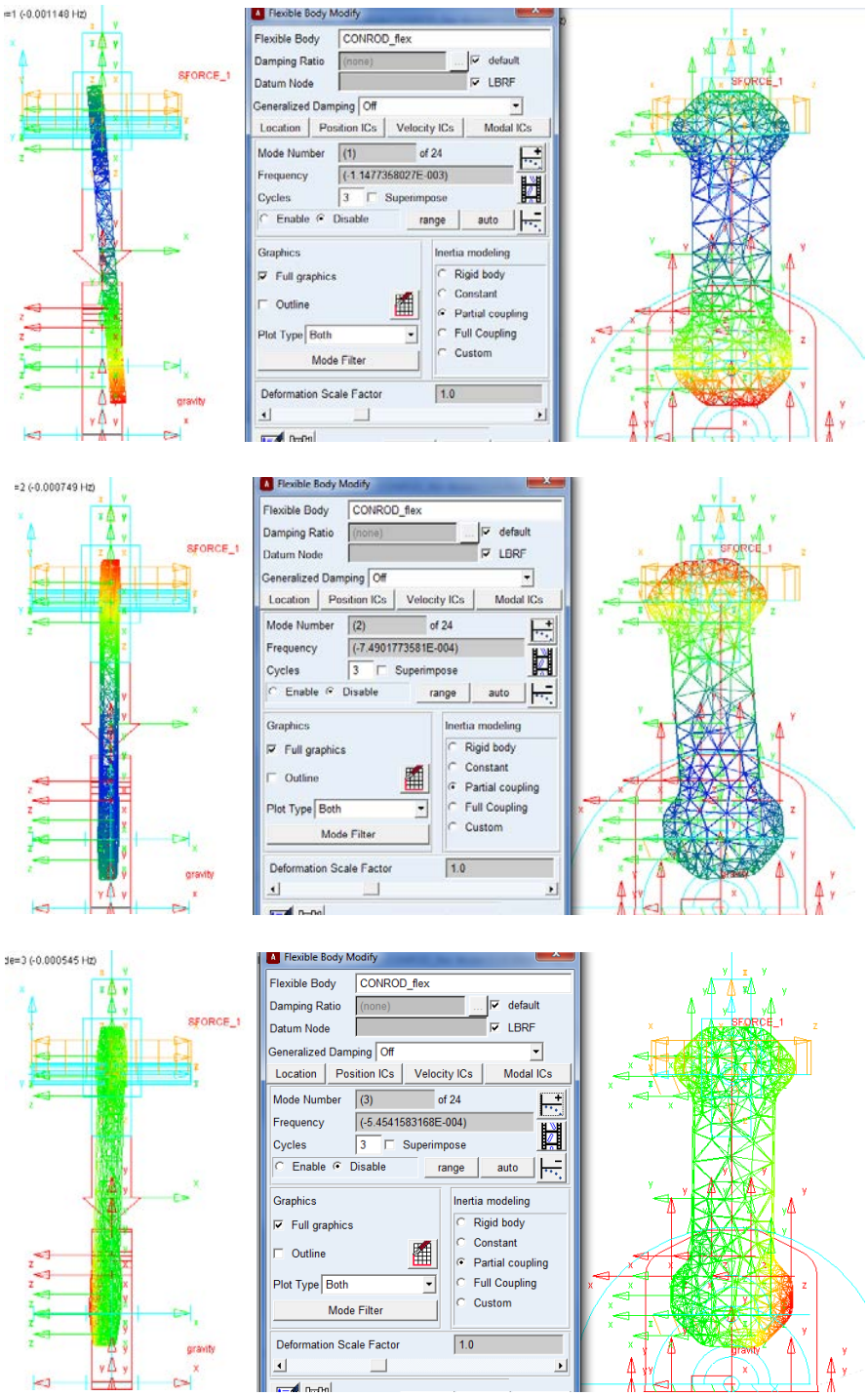

APPENDIX B (continued)

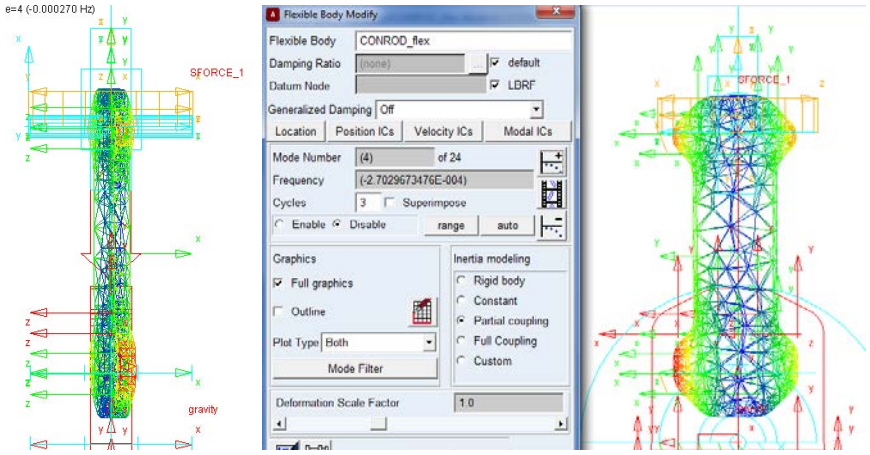

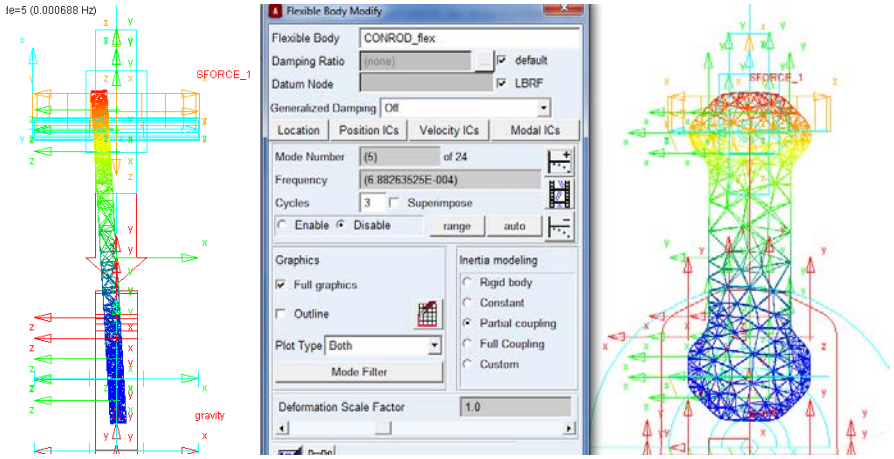

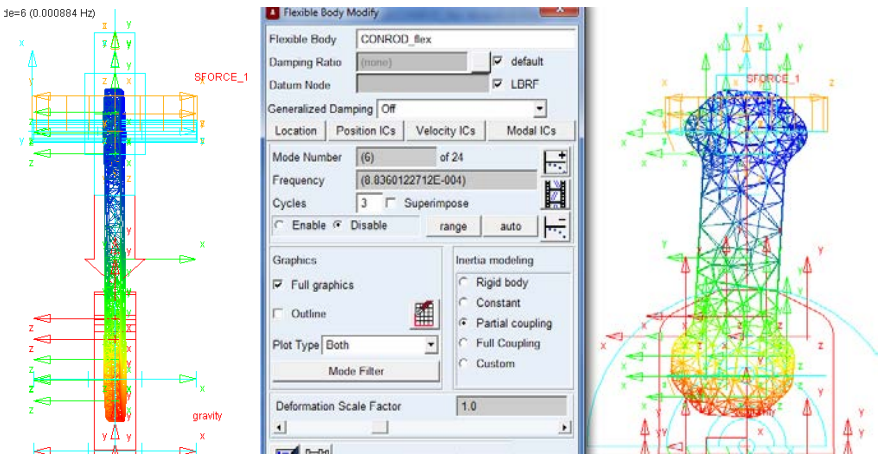

APPENDIX C

MSC ADAMS/VIEW ALUMINUM RIGID BODY MODE SHAPE RESULTS

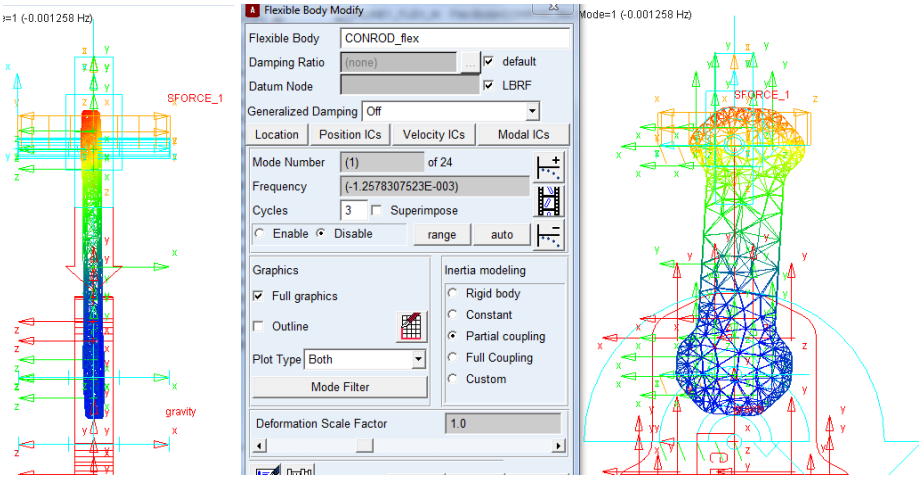

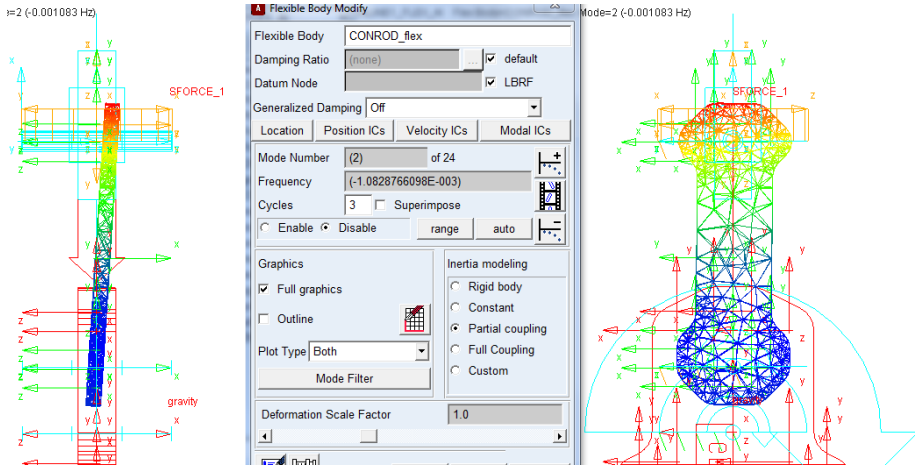

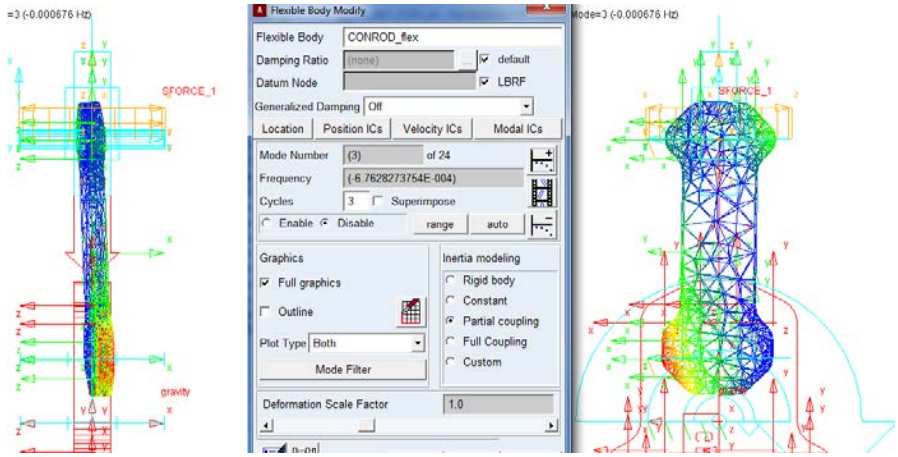

APPENDIX C (continued)

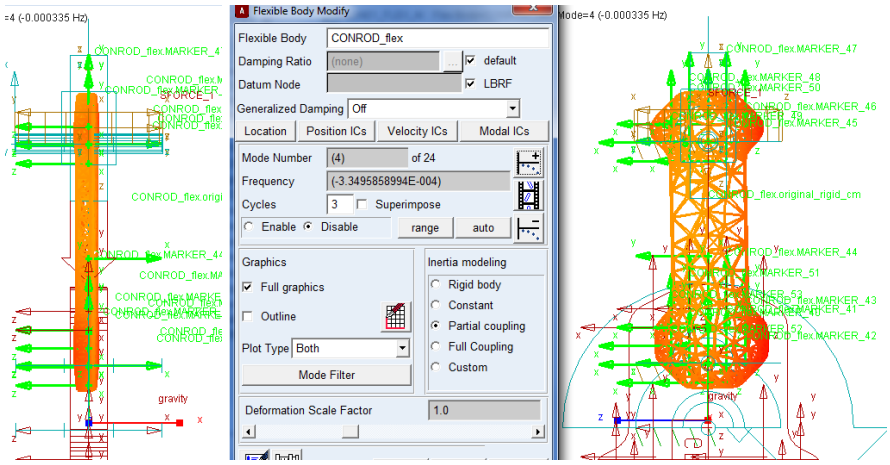

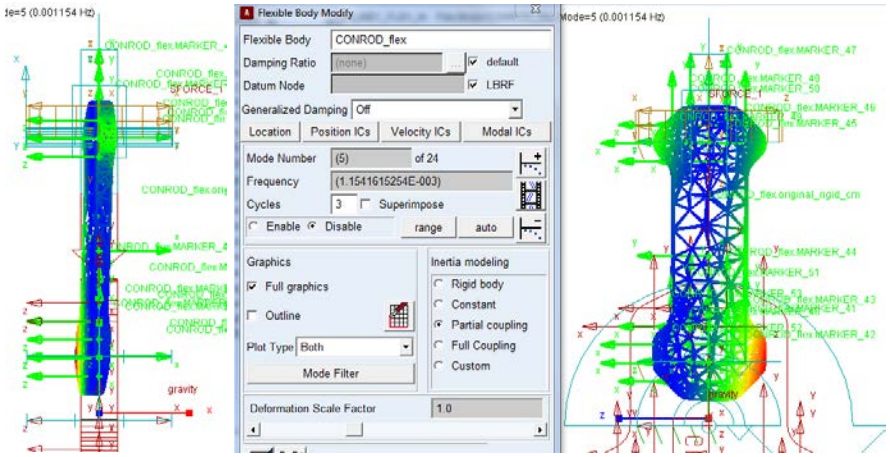

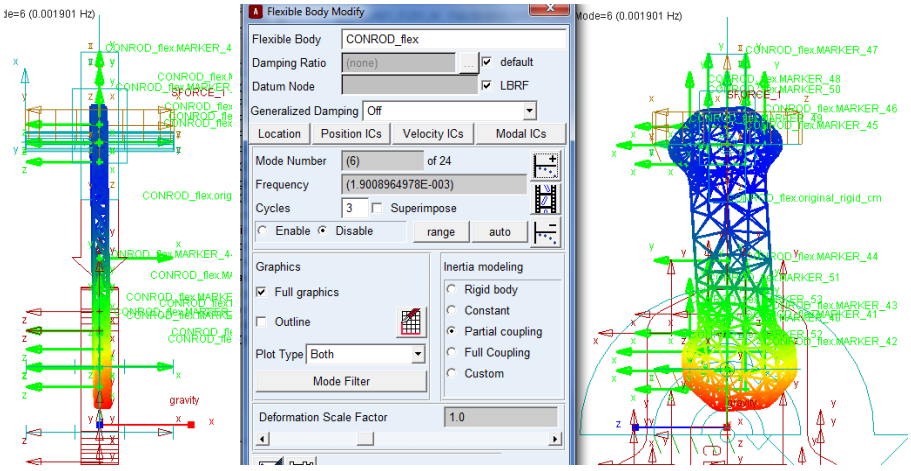

APPENDIX D

MSC ADAMS/VIEW CAST IRON RIGID INLINE-1 RESULTS

Piston Position, Velocity and Acceleration Plots

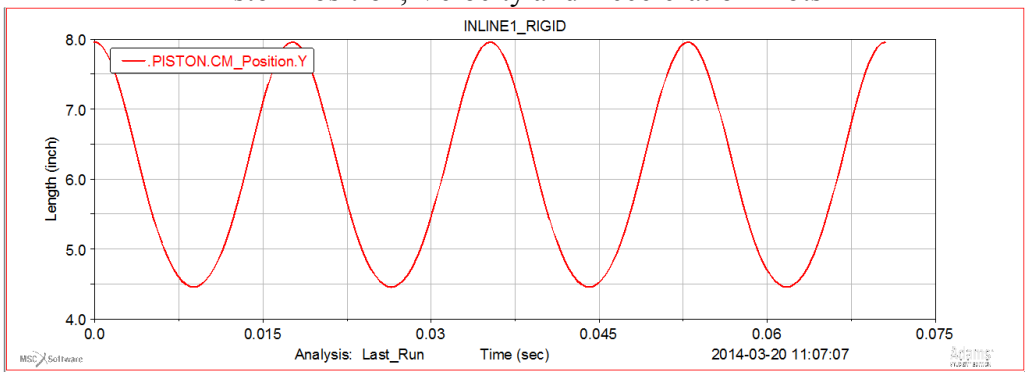

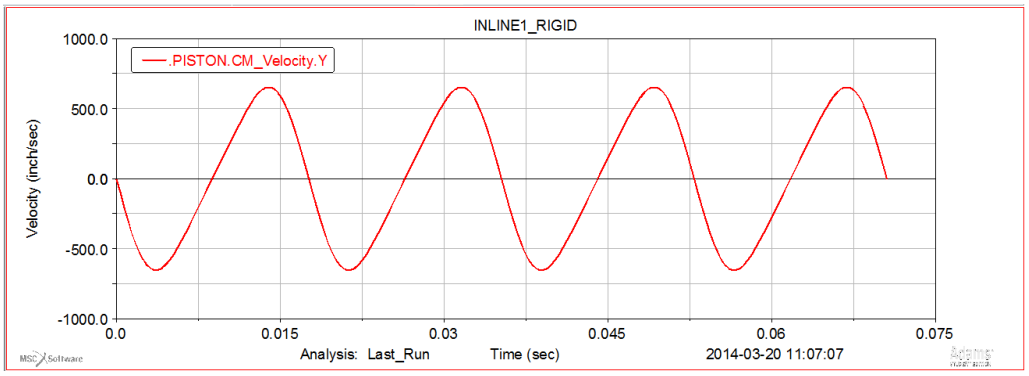

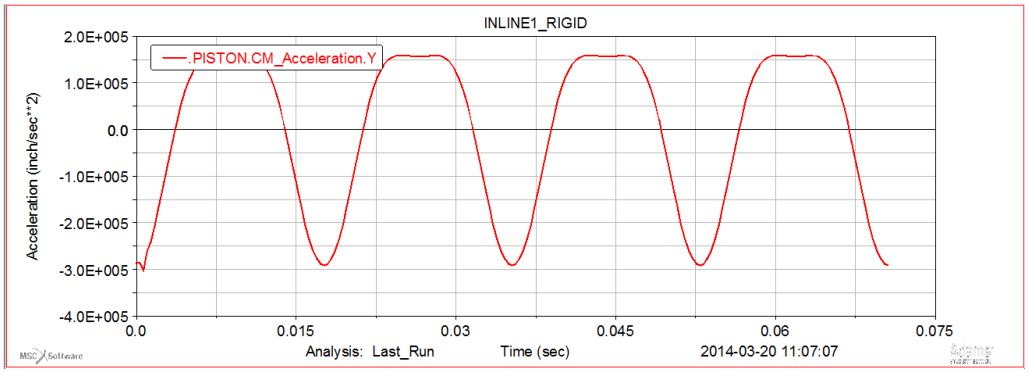

APPENDIX D (continued)

Piston Pin Joint Y Force Plot

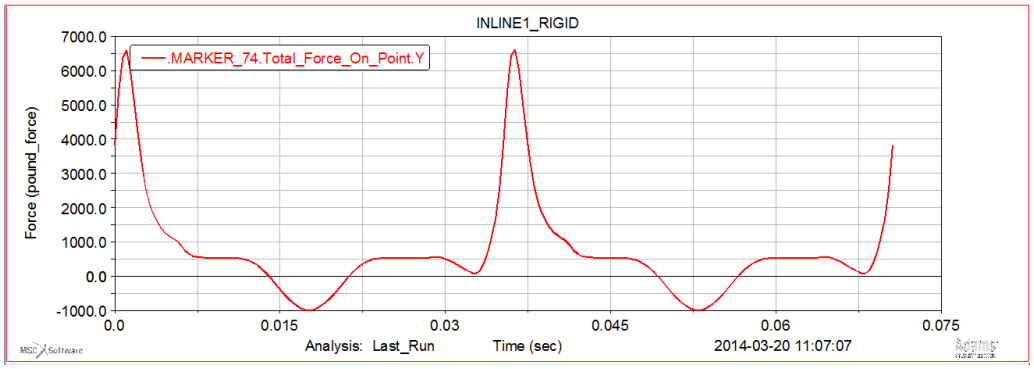

Piston Pin Joint Z Force Plot

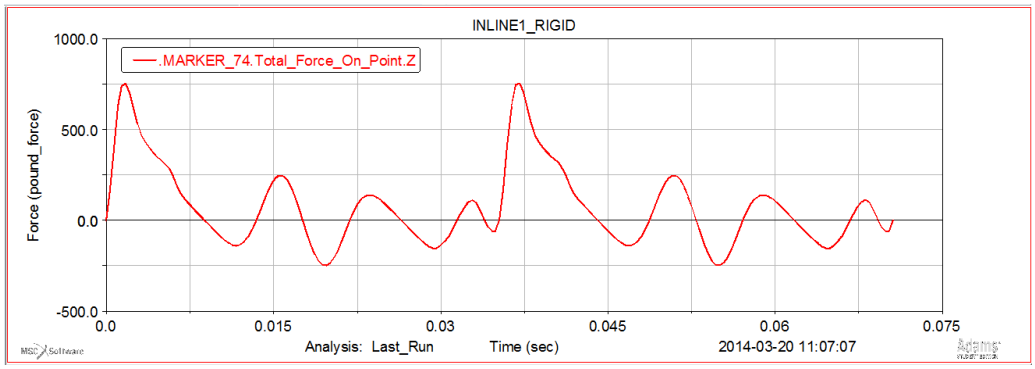

Piston Pin Joint Force Magnitude Plot

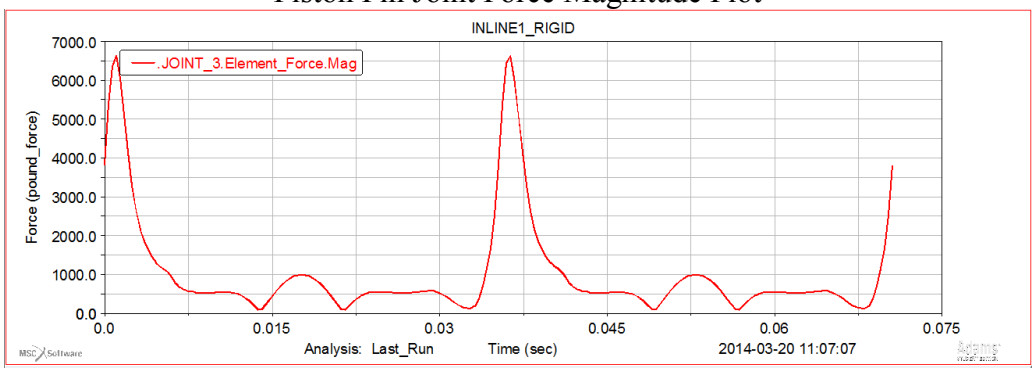

APPENDIX D (continued)

Piston Pin Joint Angular Velocity about X Plot

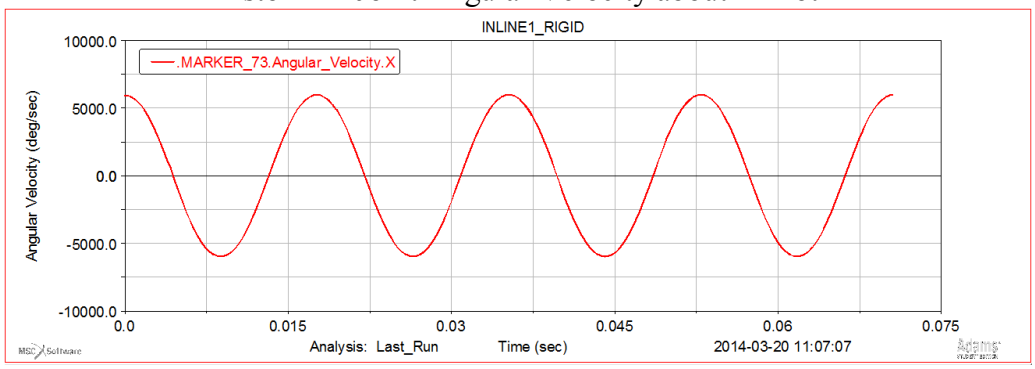

Crank Pin Joint Y Force Plot

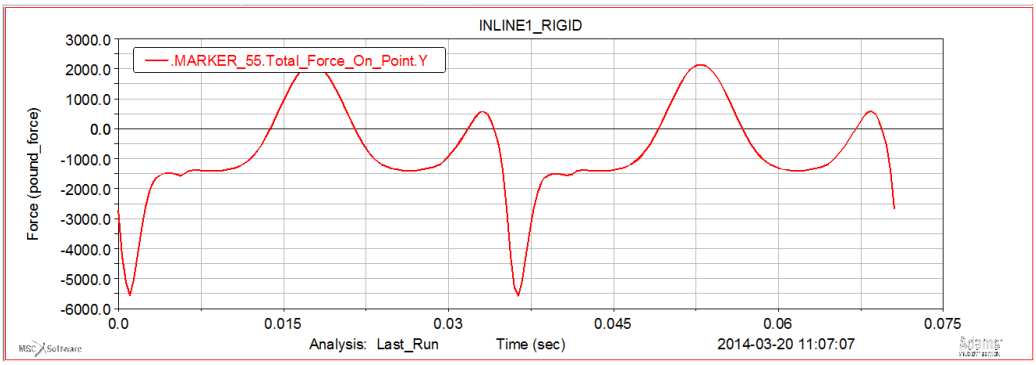

Crank Pin Joint Z Force Plot

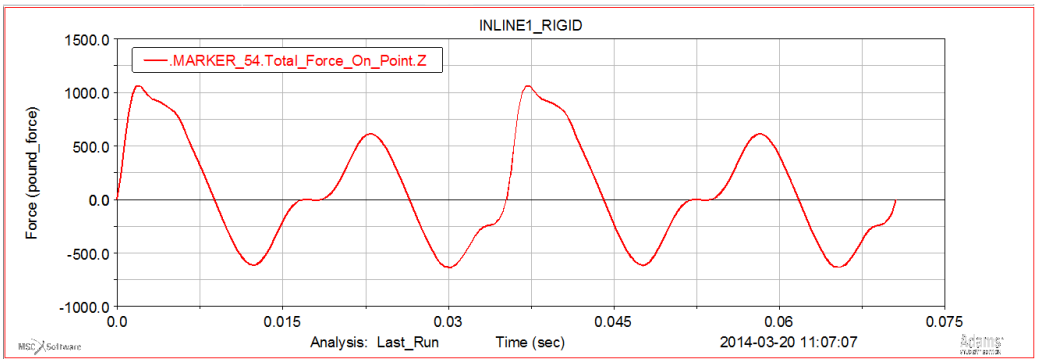

APPENDIX D (continued)

Crank Pin Joint X Force Plot

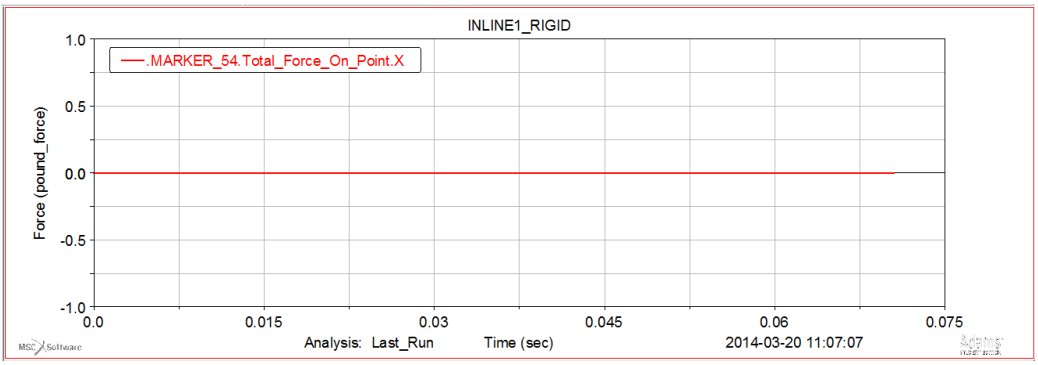

Crank Pin Joint Force Magnitude Plot

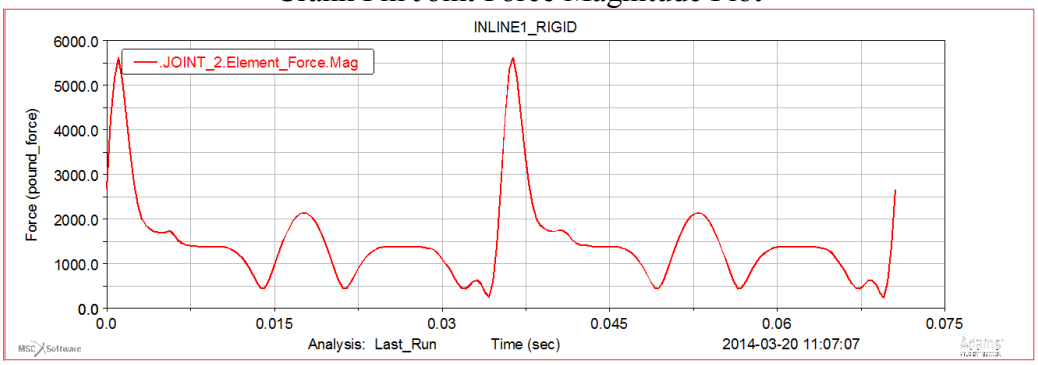

Crank Pin Joint Angular Velocity Magnitude Plot

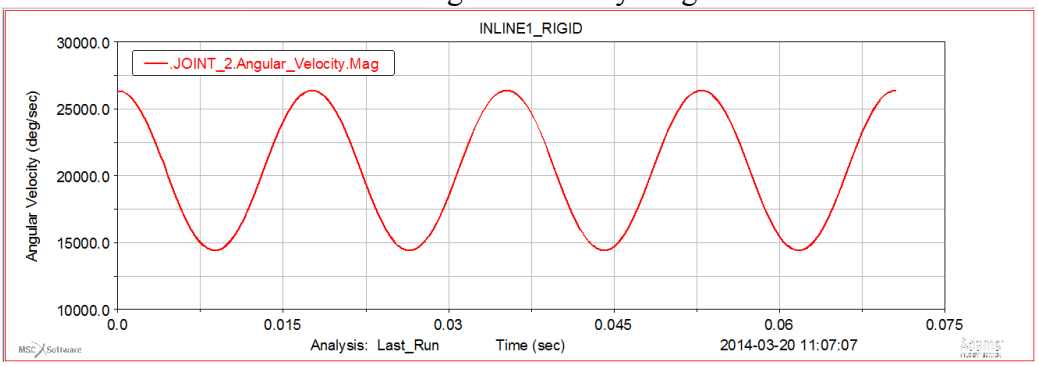

APPENDIX E

MSC ADAMS/VIEW CAST IRON FLEX INLINE-1 RESULTS

Piston Position, Velocity and Acceleration Plots

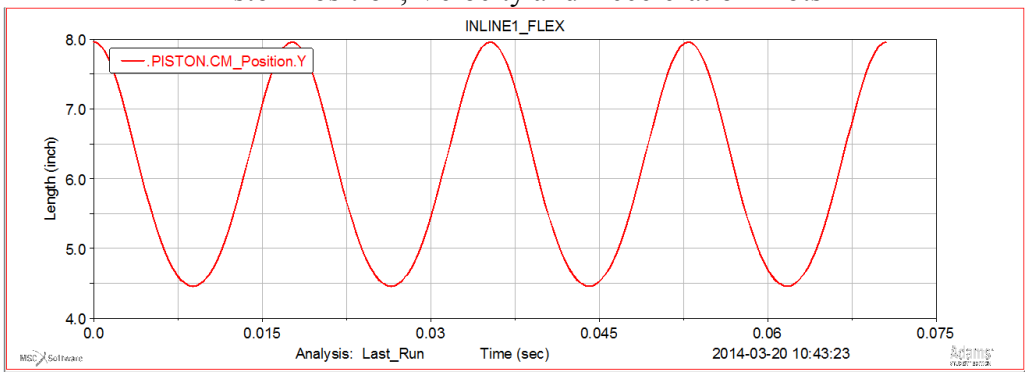

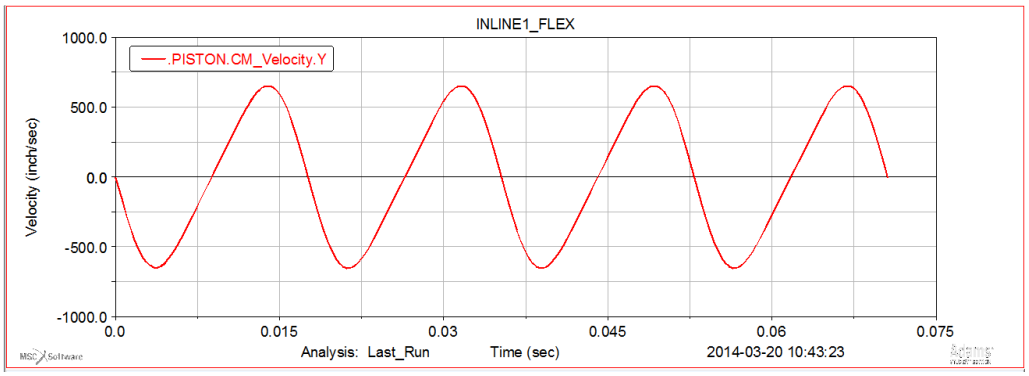

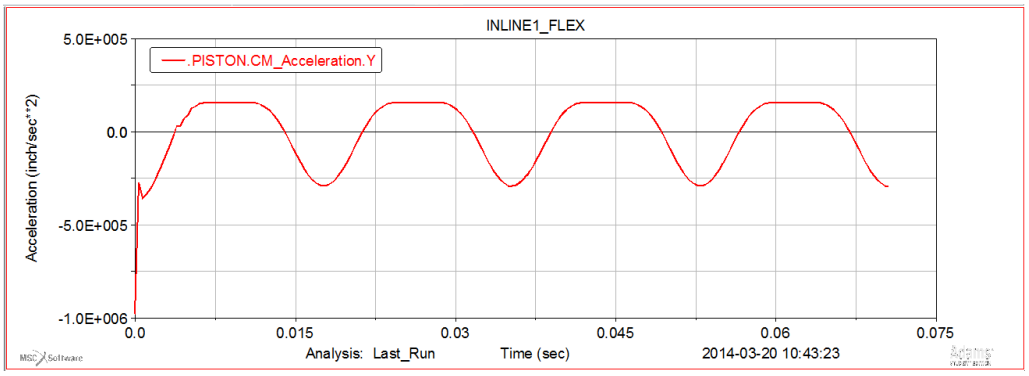

APPENDIX E (continued)

Piston Pin Joint Y Force Plot

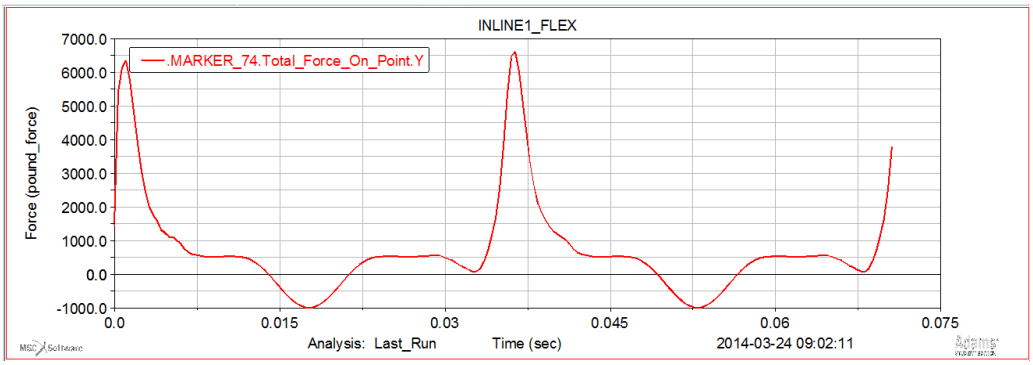

Piston Pin Joint Z Force Plot

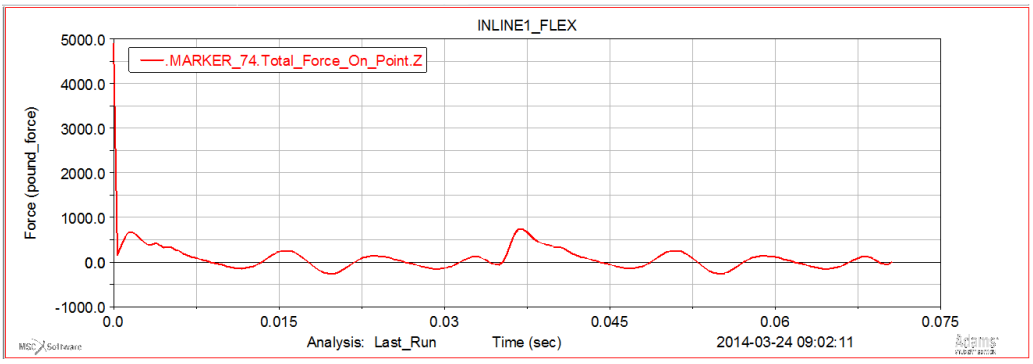

Piston Pin Joint Force Magnitude Plot

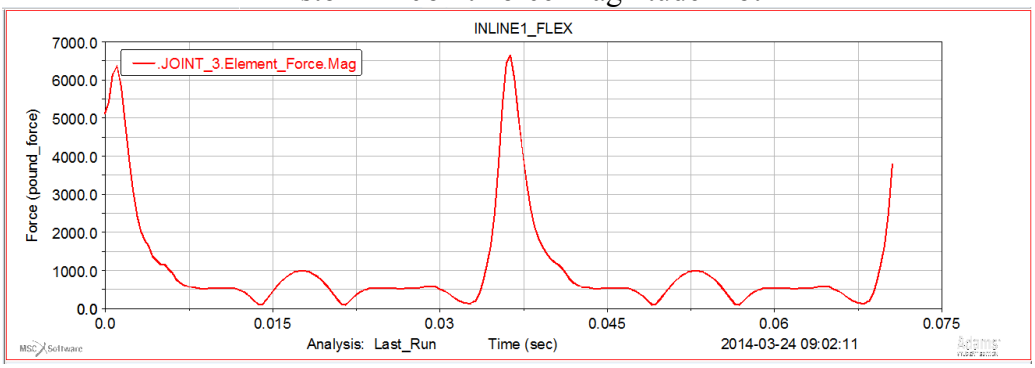

APPENDIX E (continued)

Piston Pin Joint Angular Velocity about X Plot

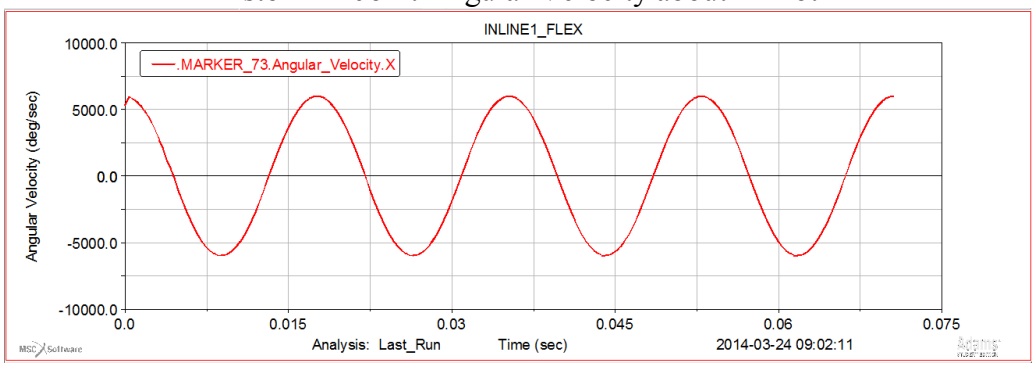

Crank Pin Joint Y Force Plot

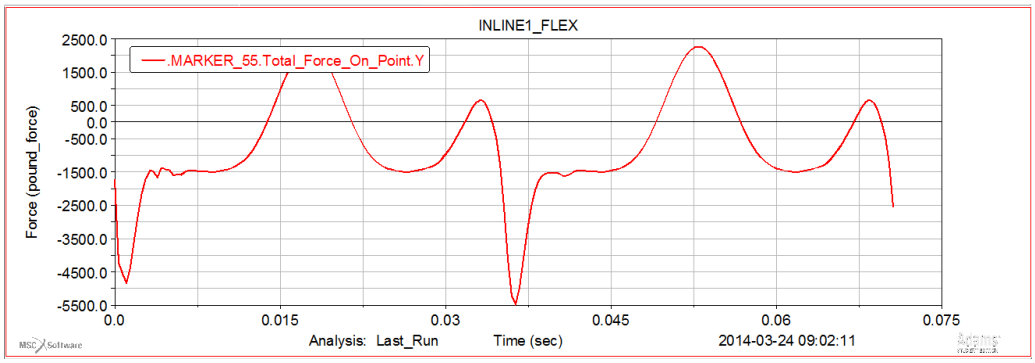

Crank Pin Joint Z Force Plot

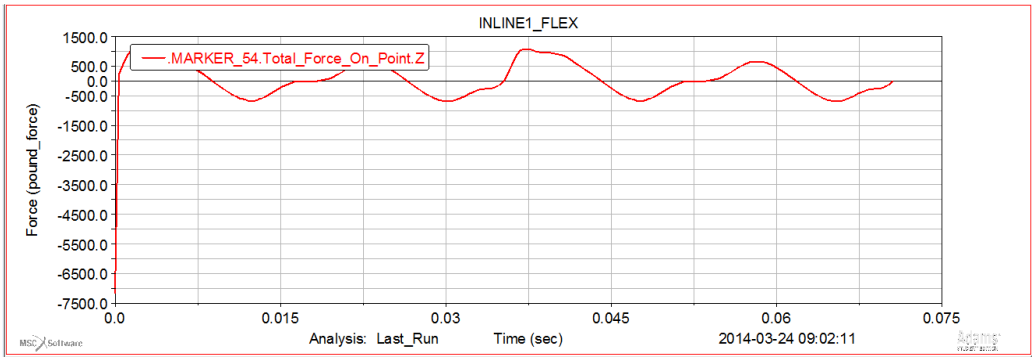

APPENDIX E (continued)

Crank Pin Joint X Force Plot

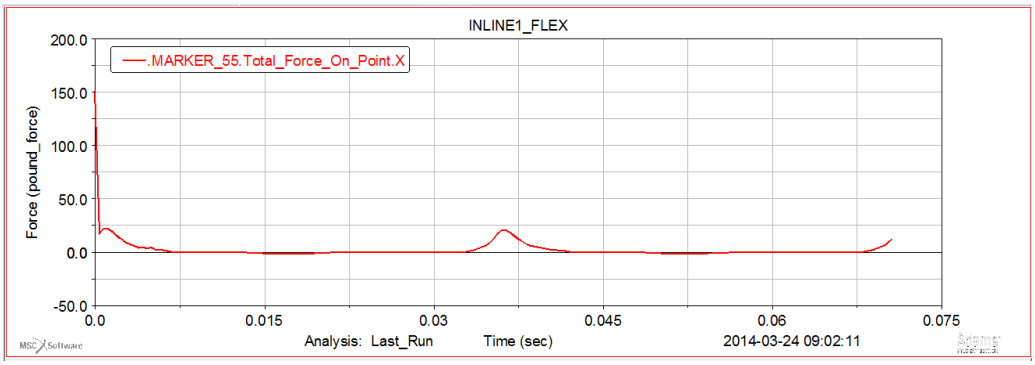

Crank Pin Joint Force Magnitude Plot

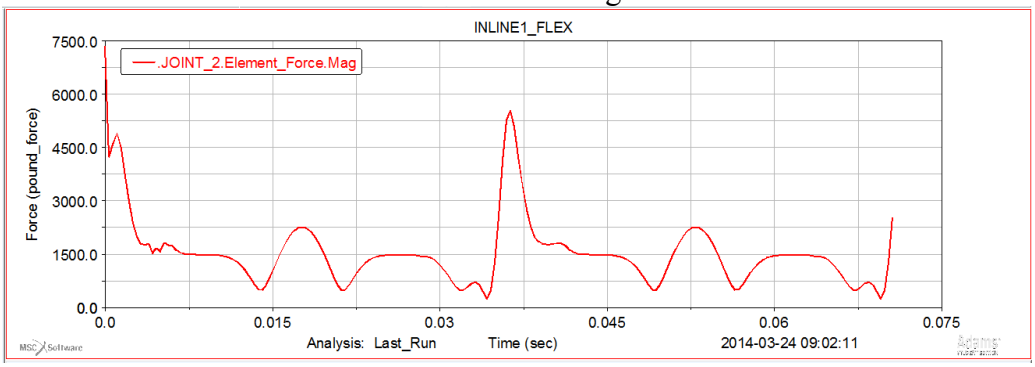

Crank Pin Joint Angular Velocity Magnitude Plot

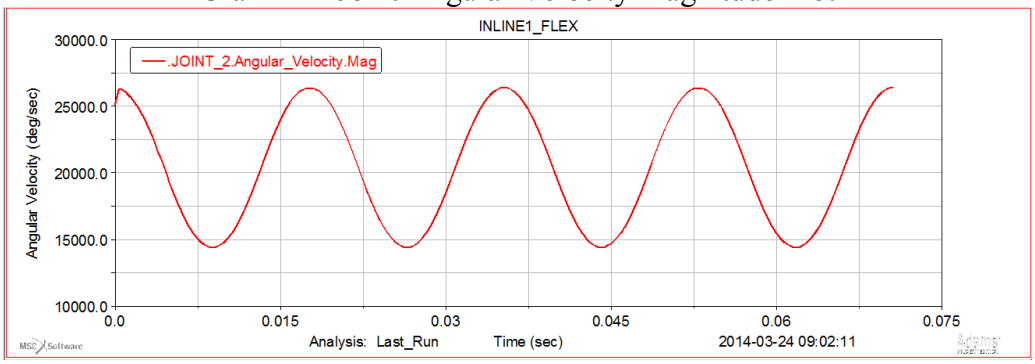

APPENDIX F

MSC ADAMS/VIEW ALUMINUM RIGID INLINE-1 RESULTS

Piston Position, Velocity and Acceleration Plots

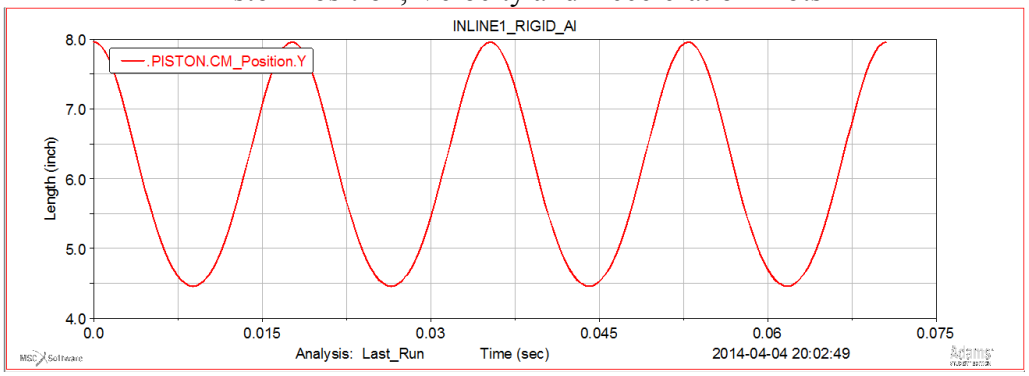

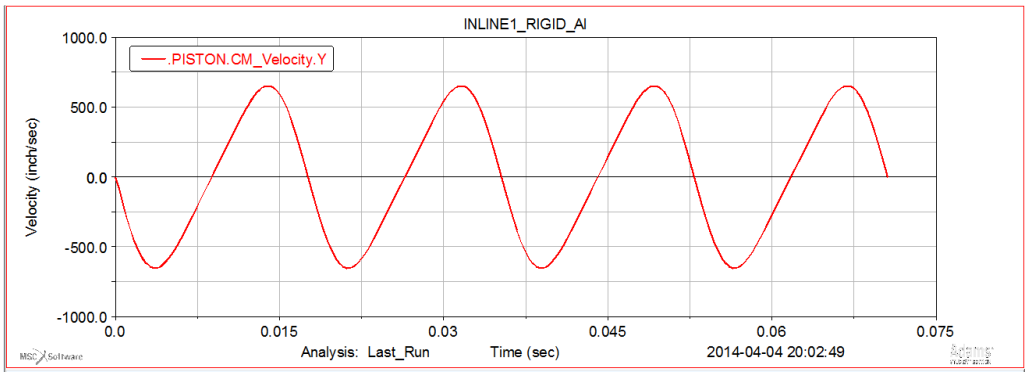

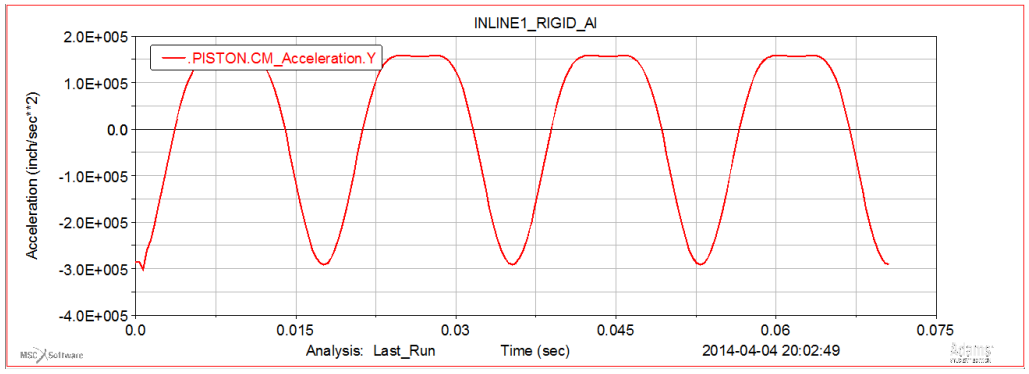

APPENDIX F (continued)

Piston Pin Joint Y Force Plot

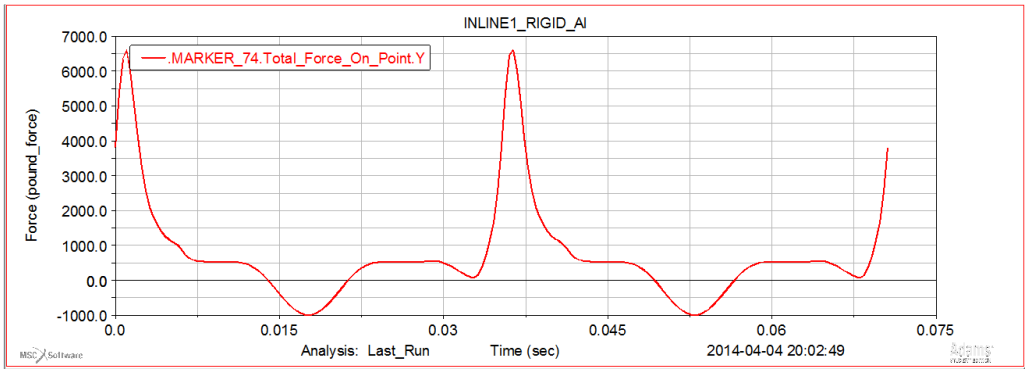

Piston Pin Joint Z Force Plot

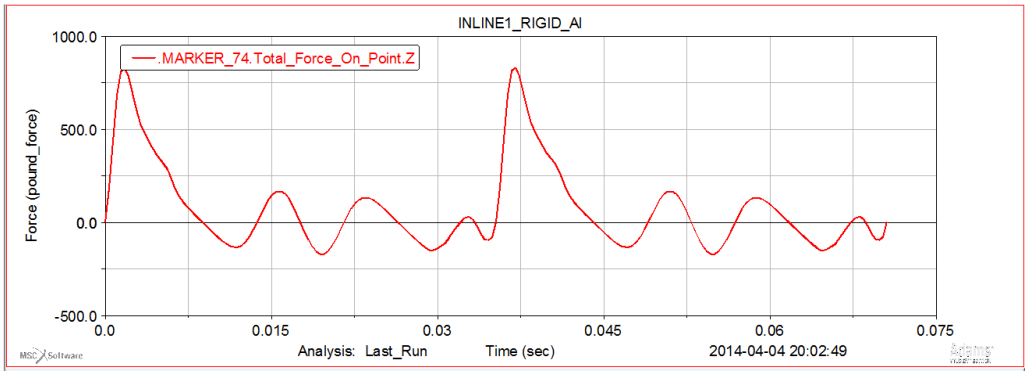

Piston Pin Joint Force Magnitude Plot

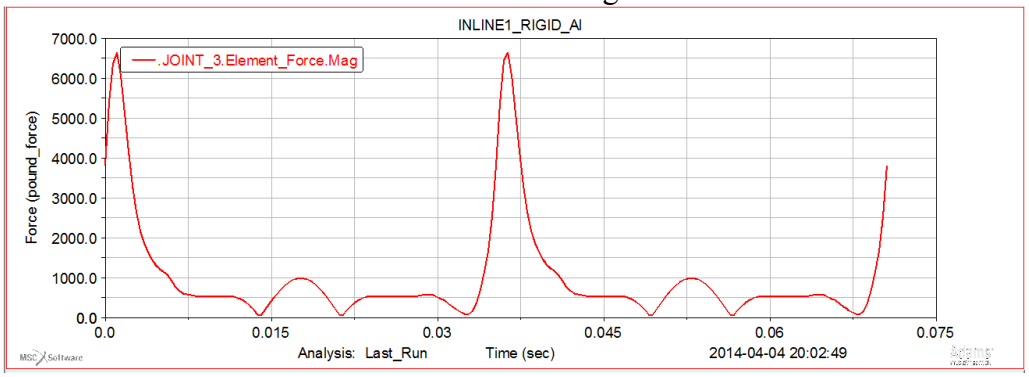

APPENDIX F (continued)

Piston Pin Joint Angular Velocity about X Plot

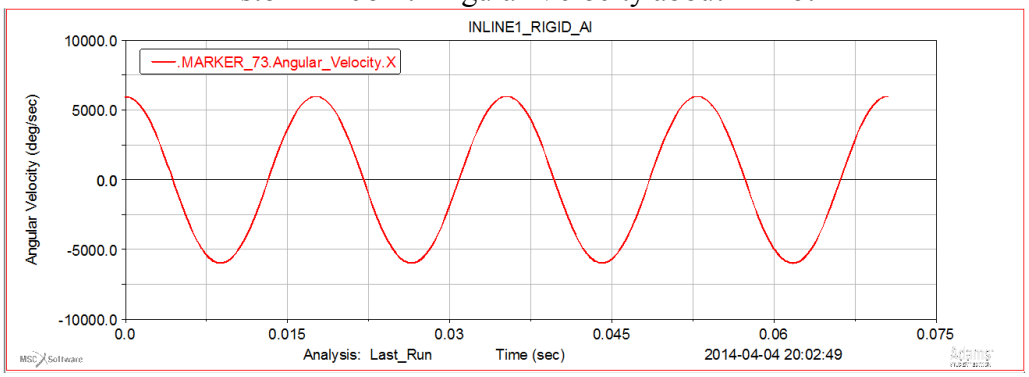

Crank Pin Joint Y Force Plot

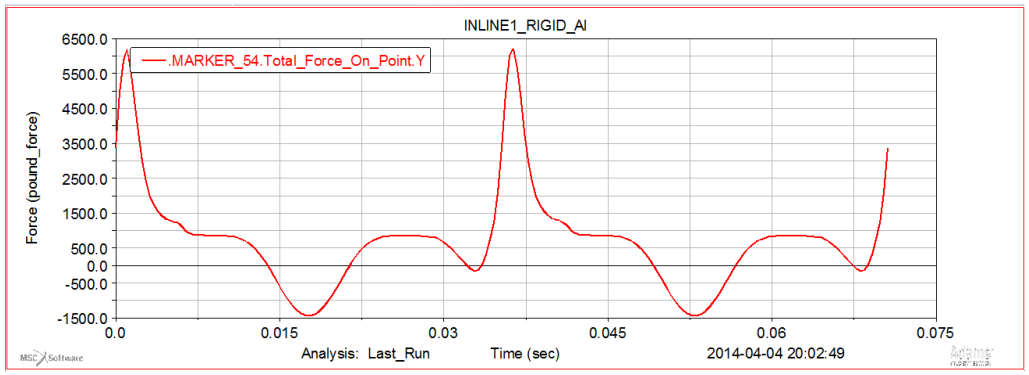

Crank Pin Joint Z Force Plot

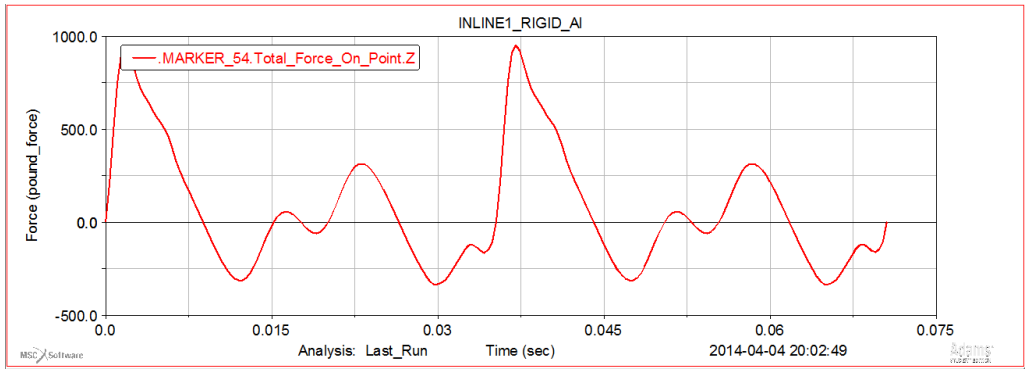

APPENDIX F (continued)

Crank Pin Joint X Force Plot

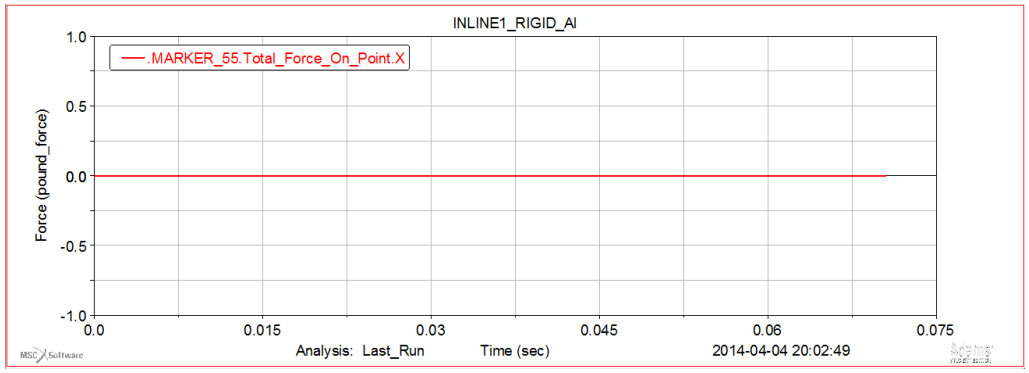

Crank Pin Joint Force Magnitude Plot

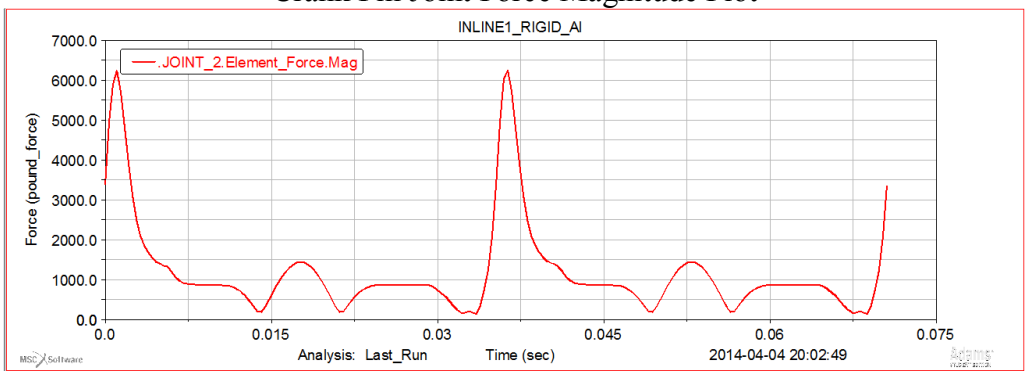

Crank Pin Joint Angular Velocity Magnitude Plot

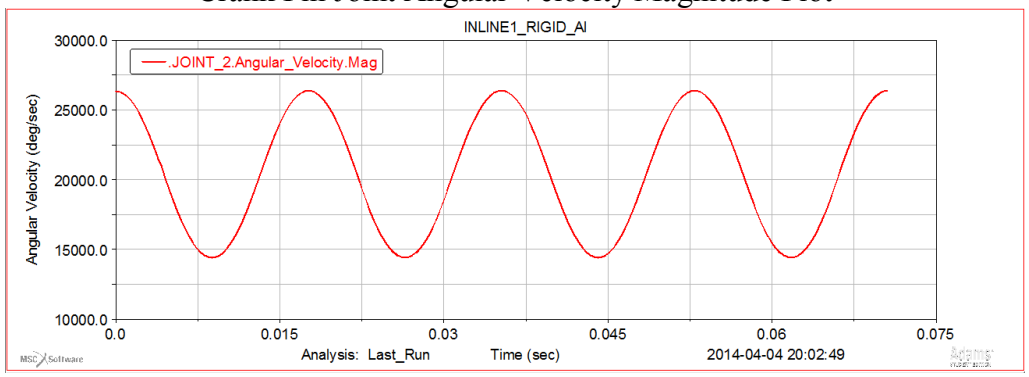

APPENDIX G

MSC ADAMS/VIEW ALUMINUM FLEX INLINE-1 RESULTS

Piston Position, Velocity and Acceleration Plots

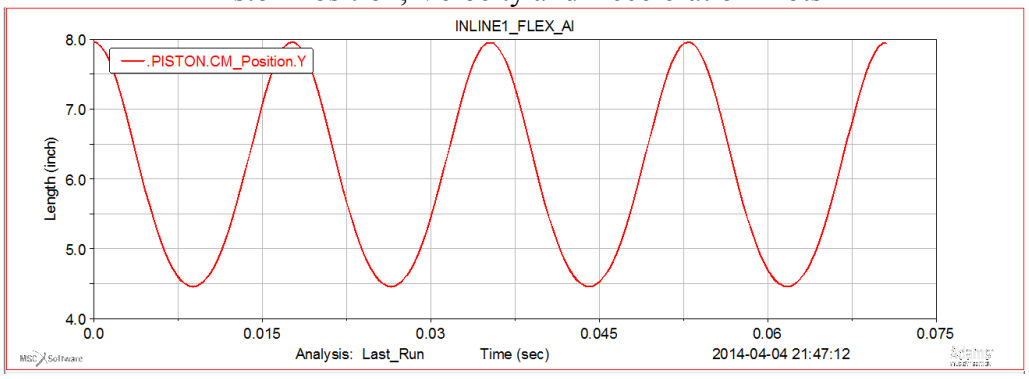

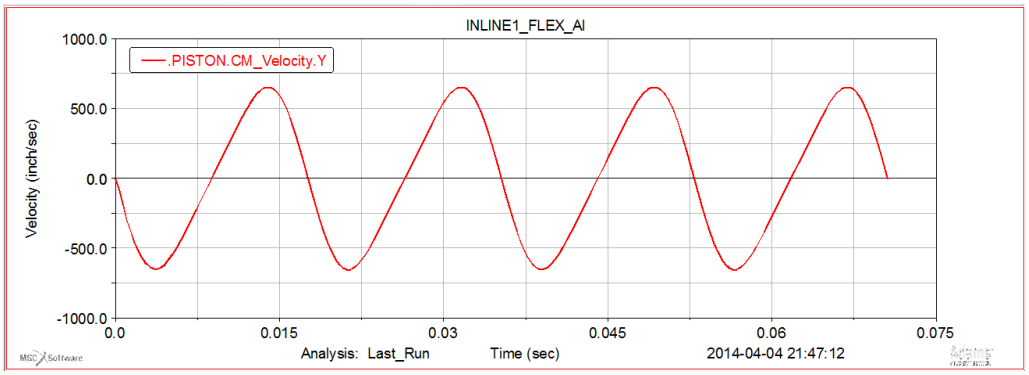

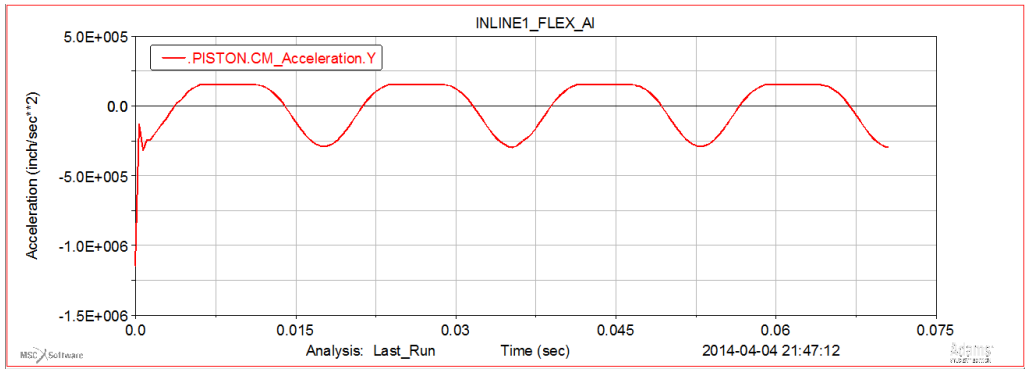

APPENDIX G (continued)

Piston Pin Joint Y Force Plot

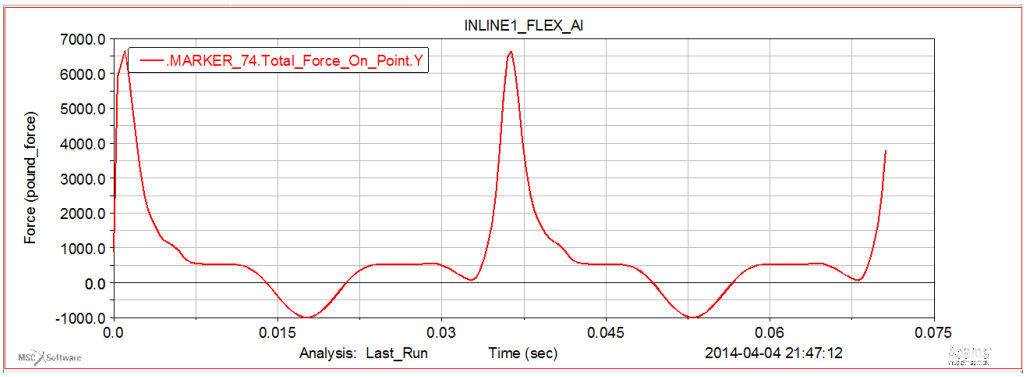

Piston Pin Joint Z Force Plot

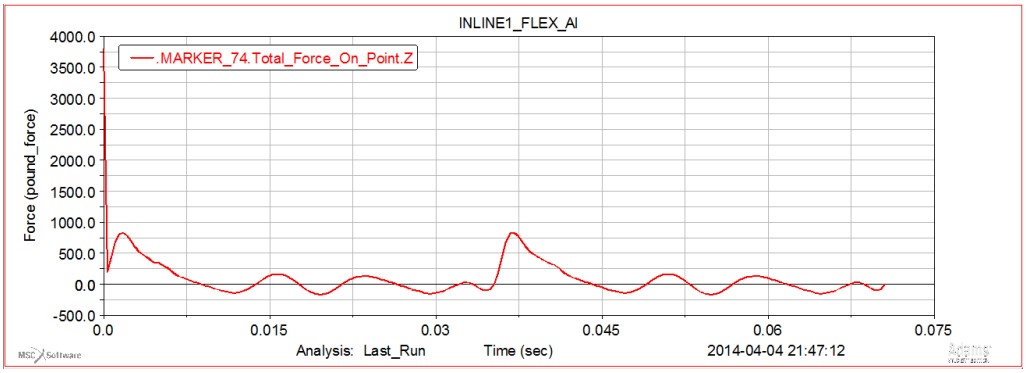

Piston Pin Joint Force Magnitude Plot

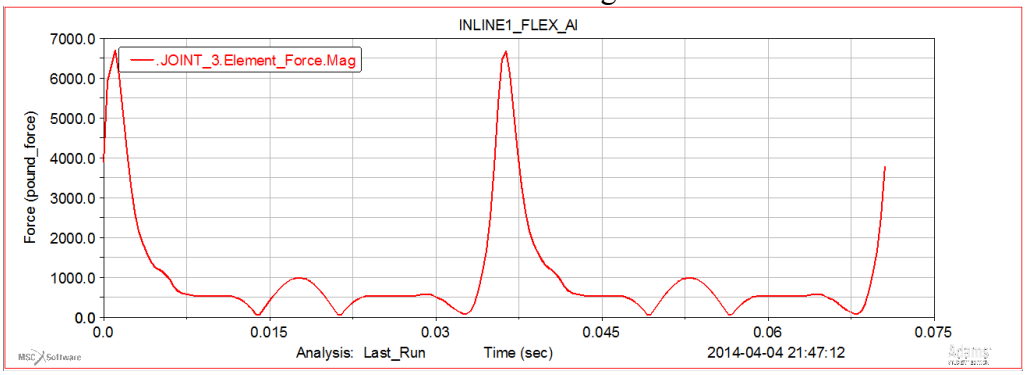

APPENDIX G (continued)

Piston Pin Joint Angular Velocity about X Plot

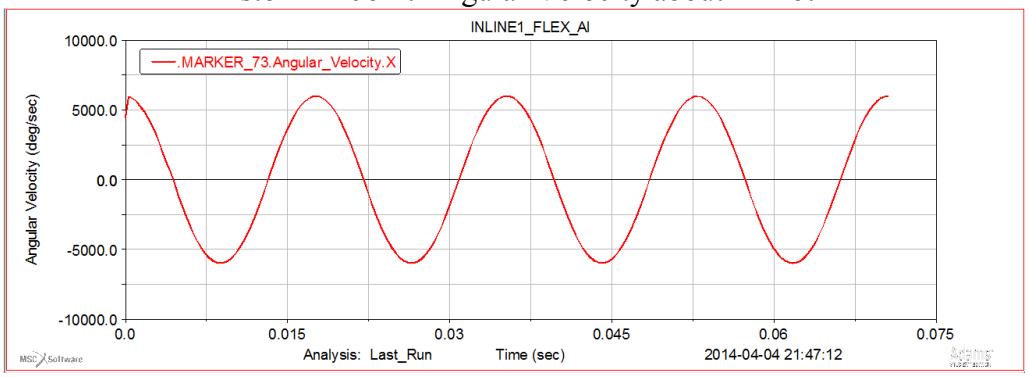

Crank Pin Joint Y Force Plot

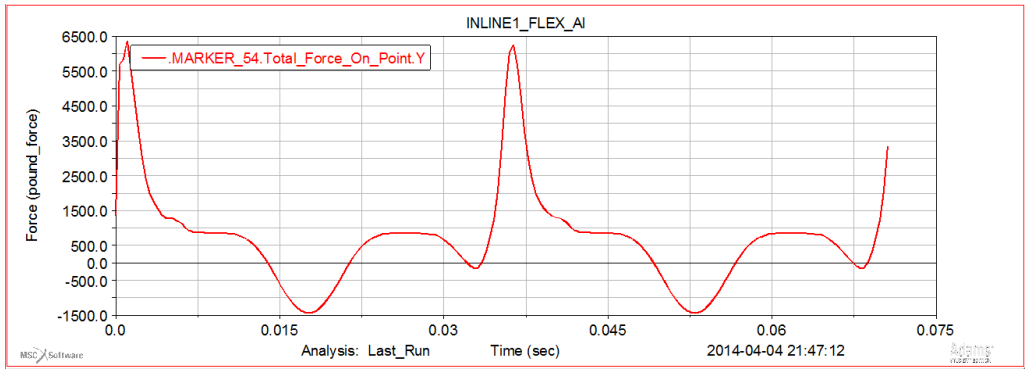

Crank Pin Joint Z Force Plot

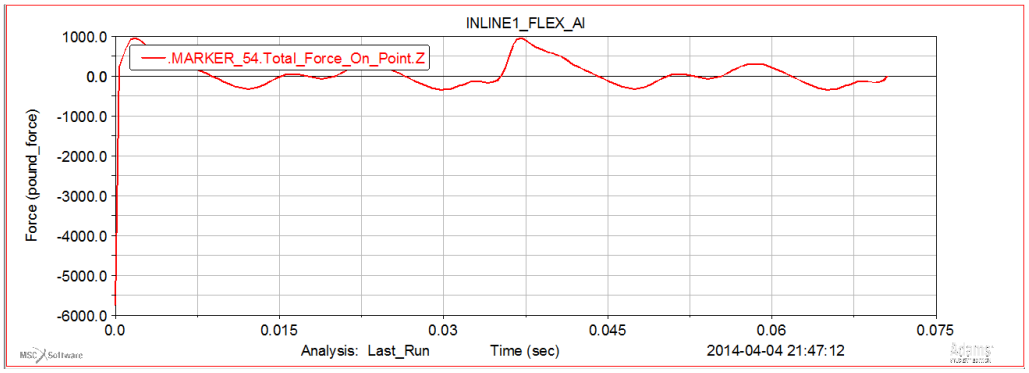

APPENDIX G (continued)

Crank Pin Joint X Force Plot

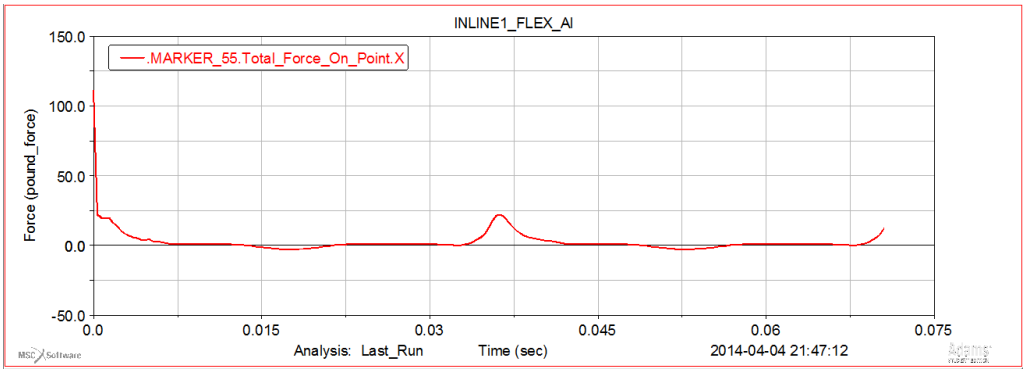

Crank Pin Joint Force Magnitude Plot

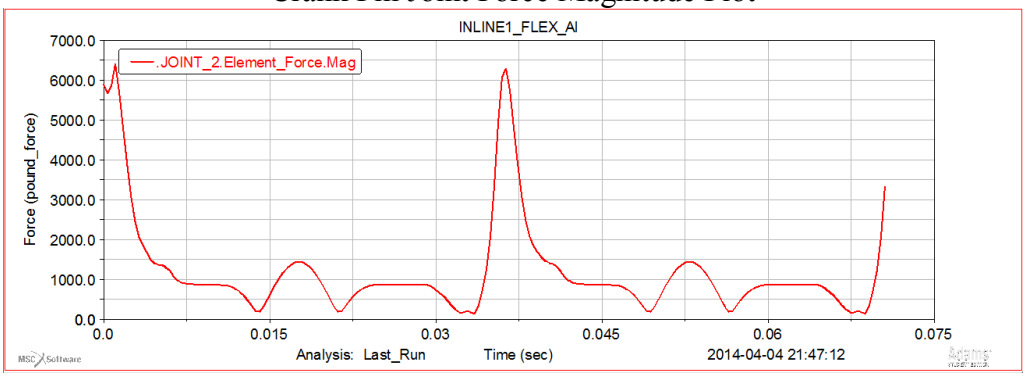

Crank Pin Joint Angular Velocity Magnitude Plot

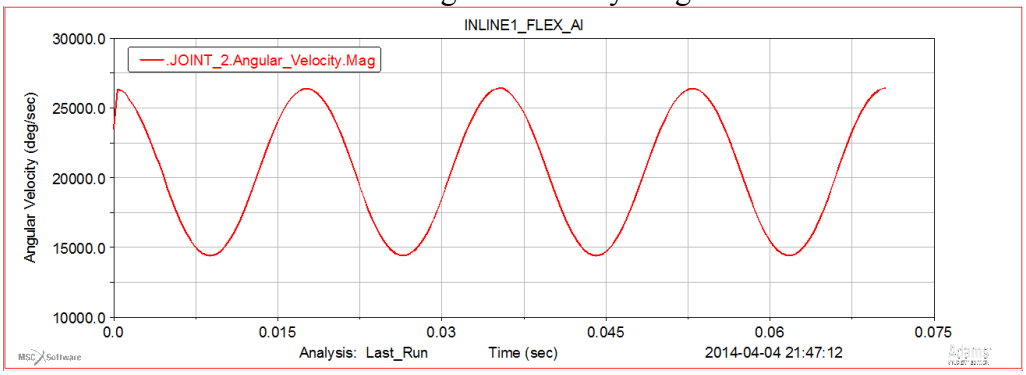

APPENDIX H

MSC ADAMS/VIEW CAST IRON RIGID VEE-2 RESULTS

Piston Position, Velocity and Acceleration Plots

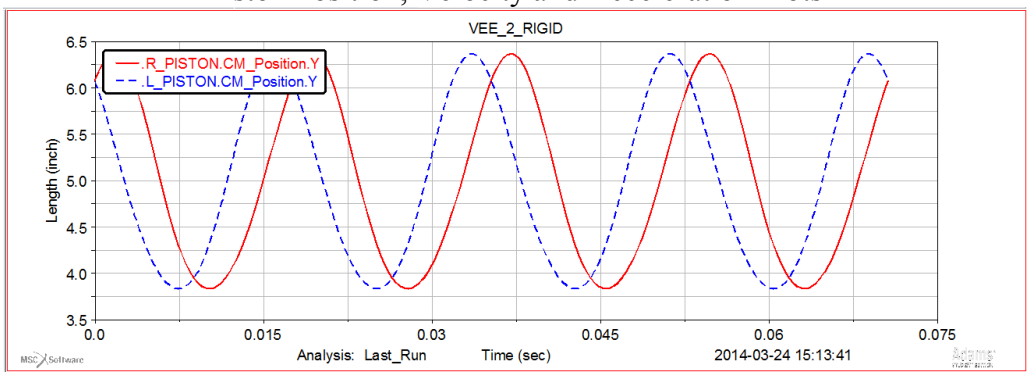

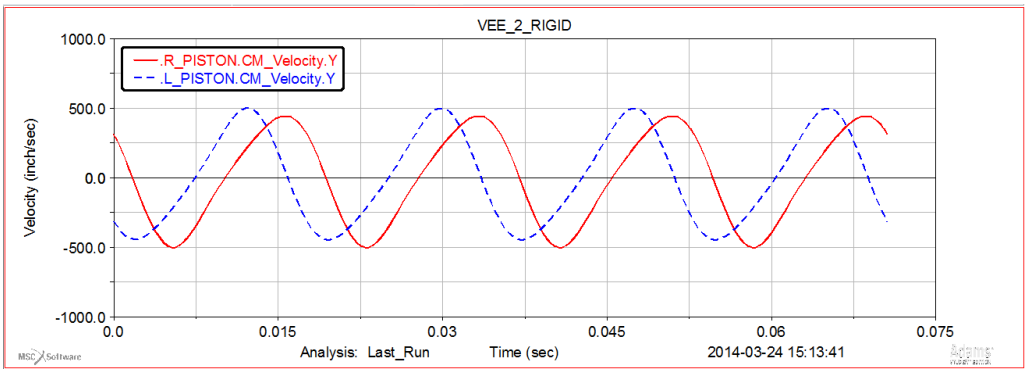

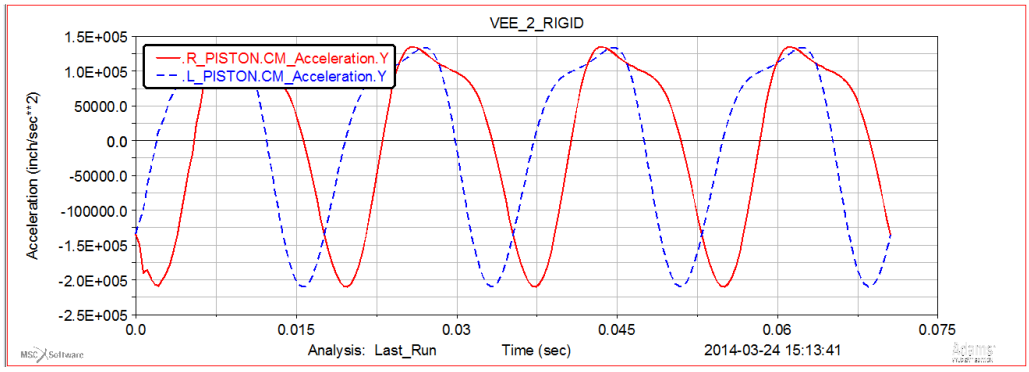

APPENDIX H (continued)

Piston Pin Joint Y Force Plot

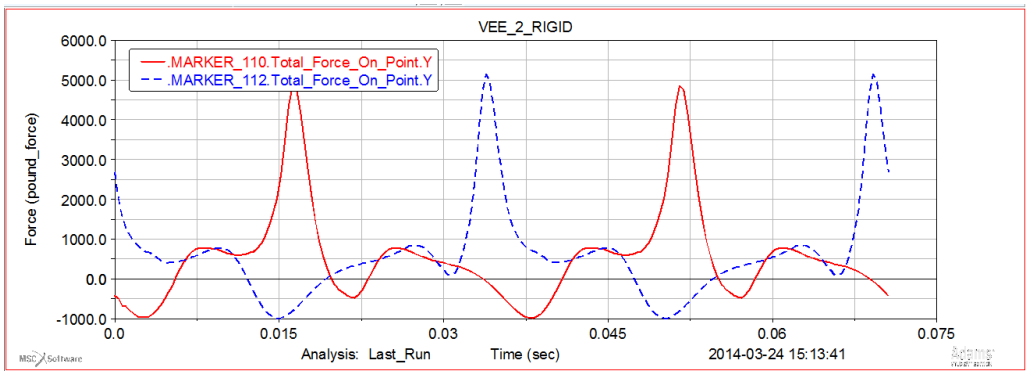

Piston Pin Joint Z Force Plot

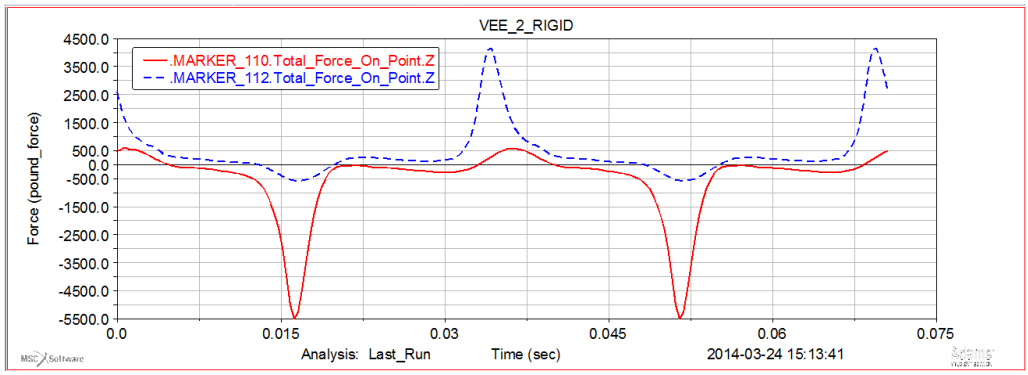

Piston Pin Joint Force Magnitude Plot

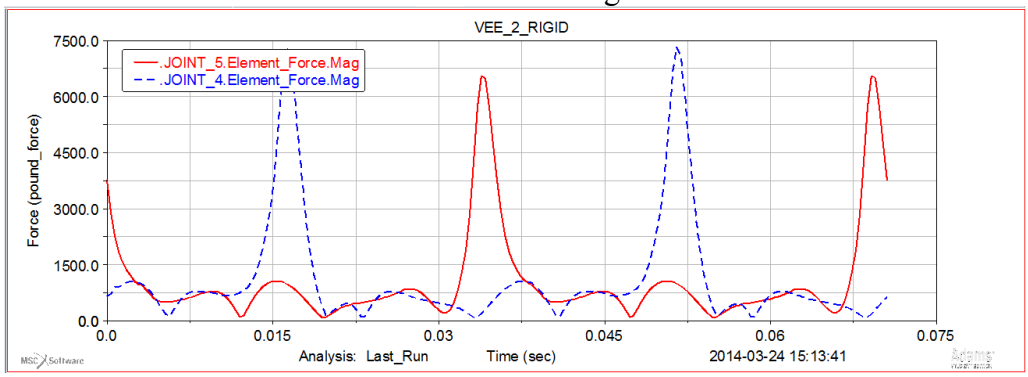

APPENDIX H (continued)

Piston Pin Joint Angular Velocity about X Plot

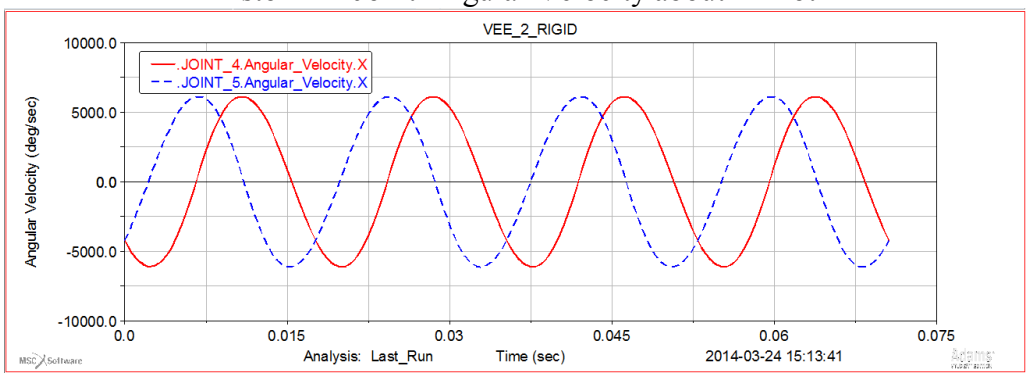

Crank Pin Joint Y Force Plot

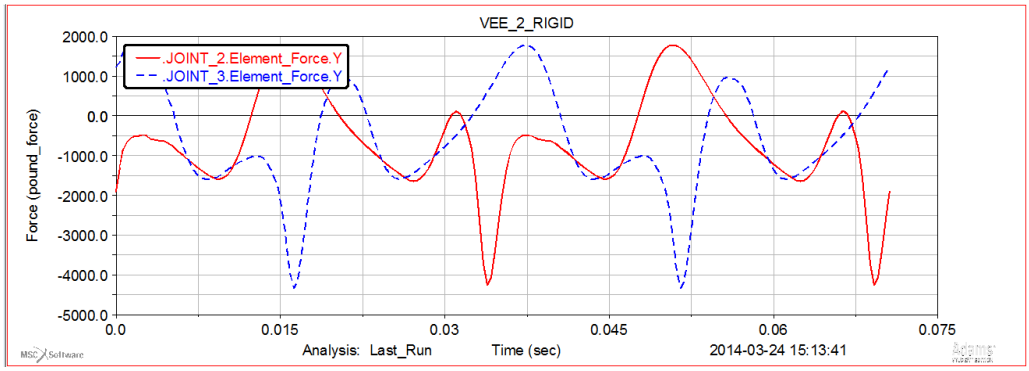

Crank Pin Joint Z Force Plot

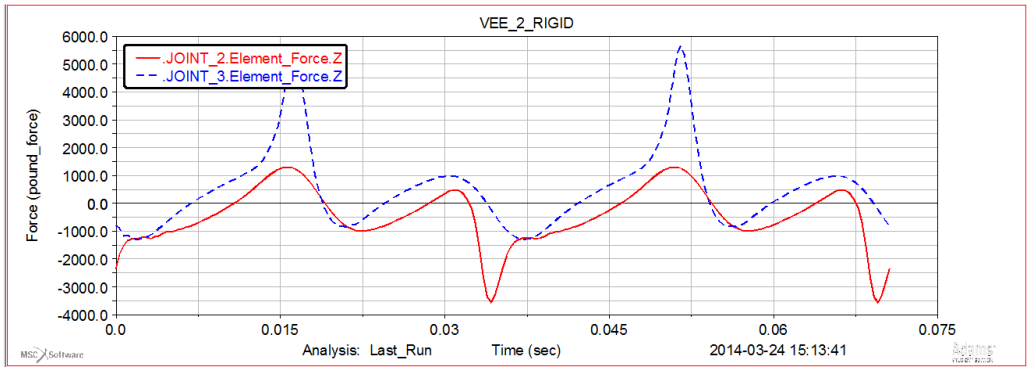

APPENDIX H (continued)

Crank Pin Joint X Force Plot

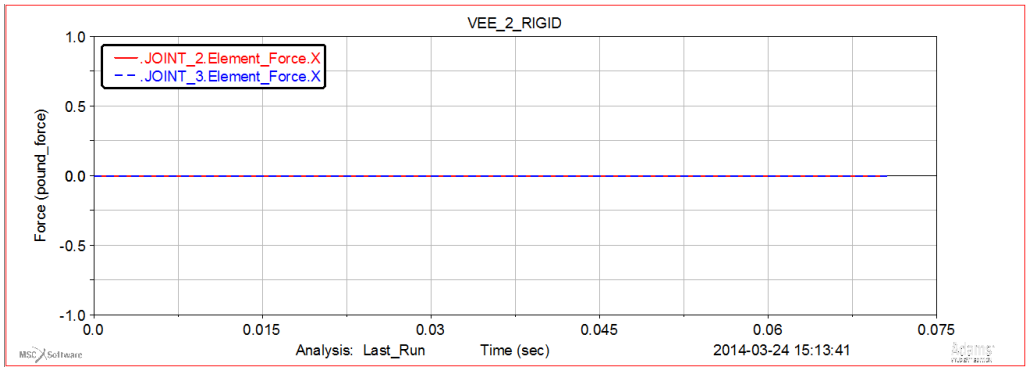

Crank Pin Joint Force Magnitude Plot

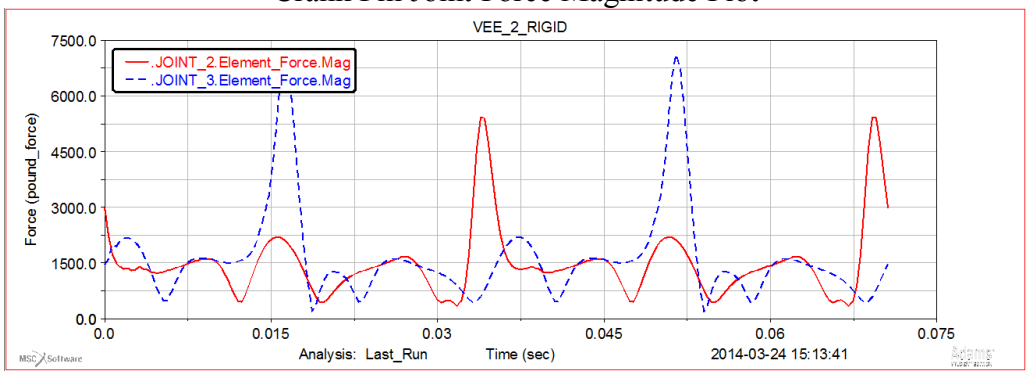

Crank Pin Joint Angular Velocity Magnitude Plot

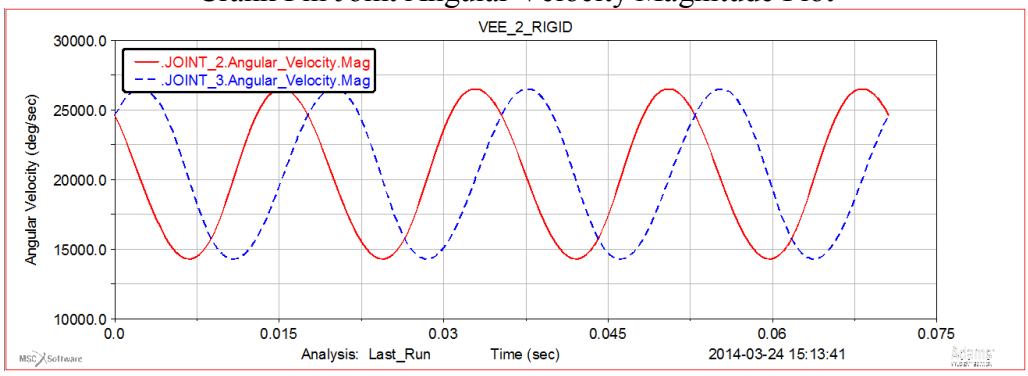

APPENDIX I

MSC ADAMS/VIEW CAST IRON FLEX VEE-2 RESULTS

Piston Position, Velocity and Acceleration Plots

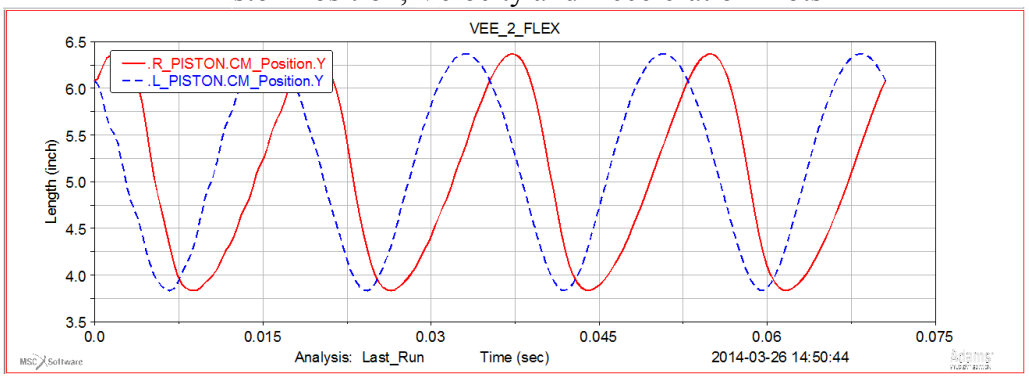

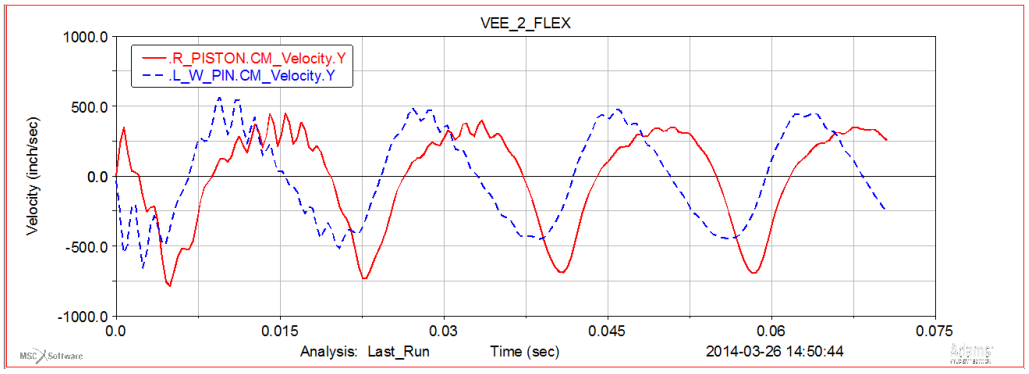

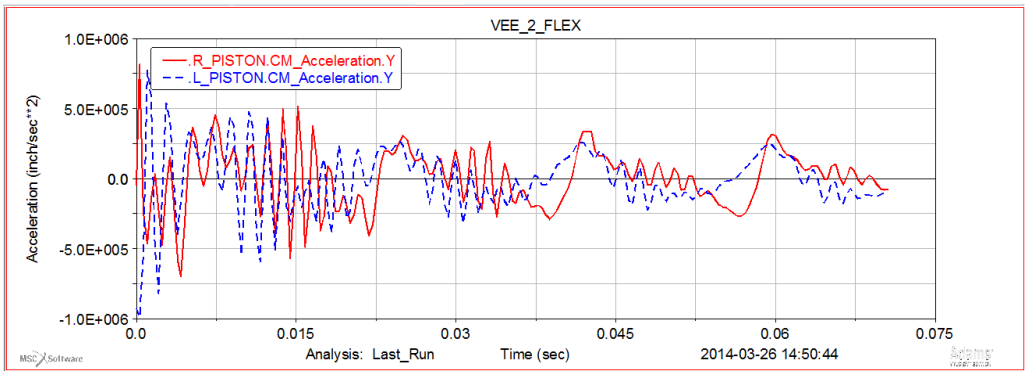

APPENDIX I (continued)

Piston Pin Joint Y Force Plots

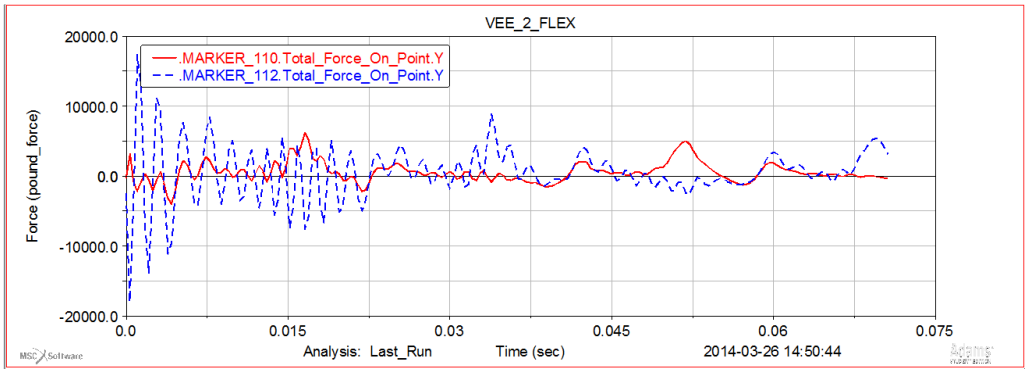

Piston Pin Joint Z Force Plots

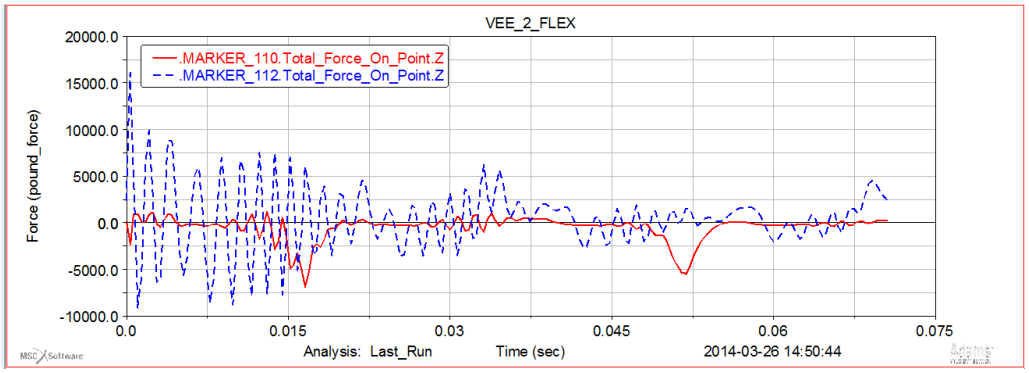

Piston Pin Joint Force Magnitude Plots

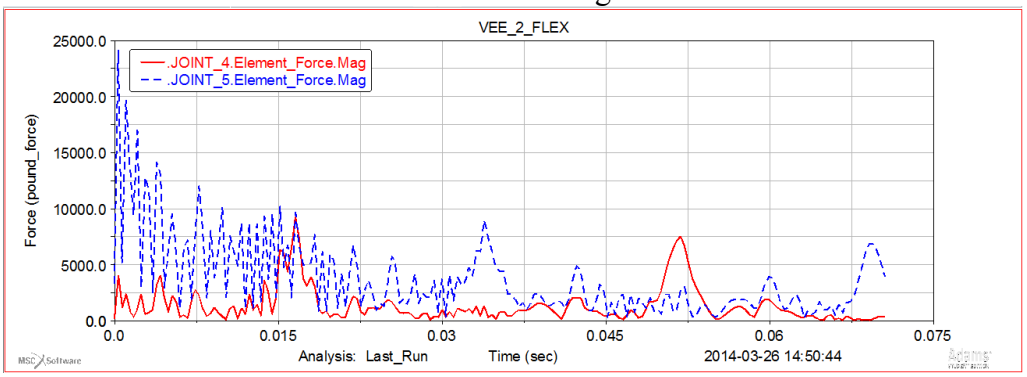

APPENDIX I (continued)

Piston Pin Joint Angular Velocity about X Plots

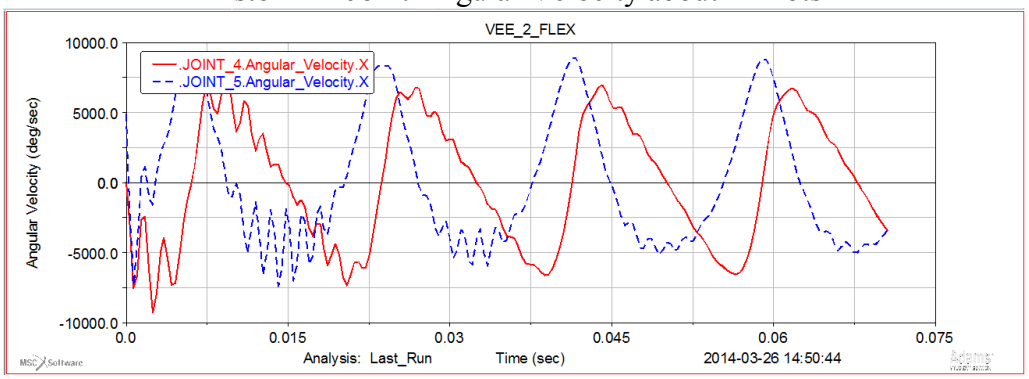

Crank Pin Joint Y Force Plots

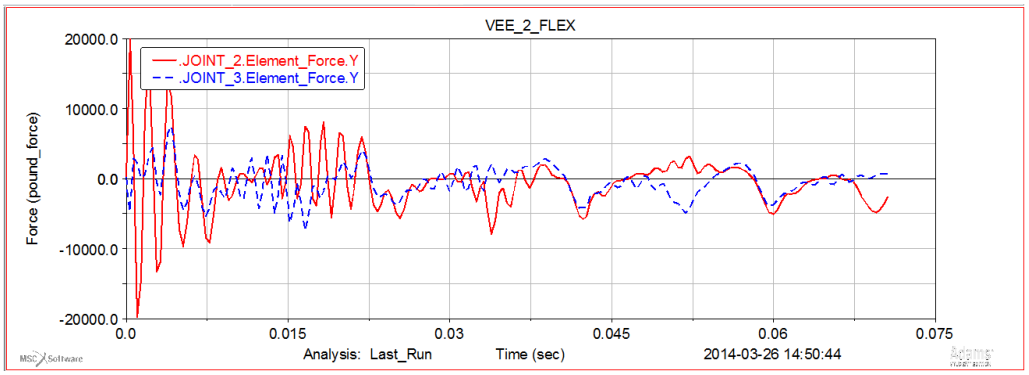

Crank Pin Joint Z Force Plots

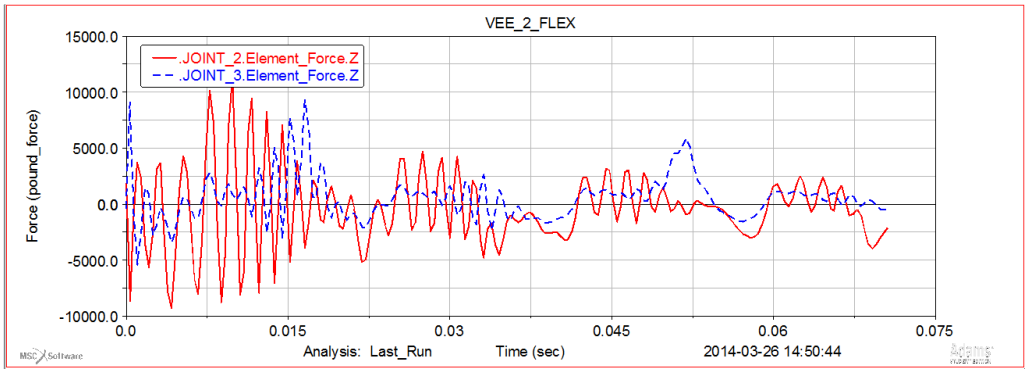

APPENDIX I (continued)

Crank Pin Joint X Force Plots

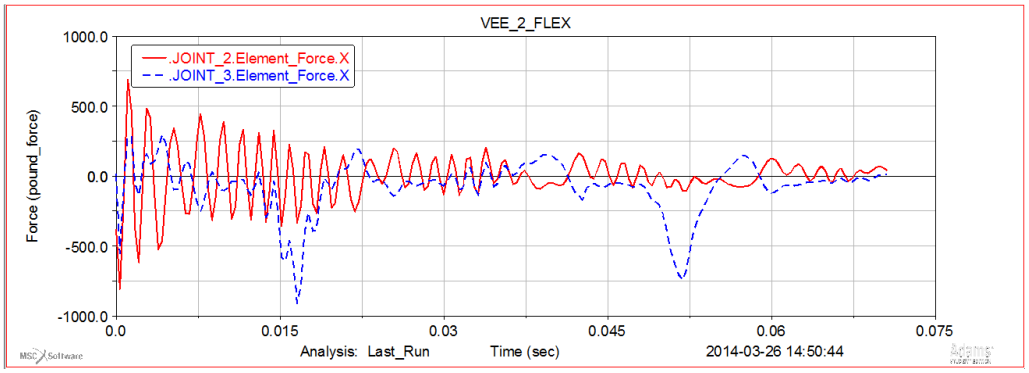

Crank Pin Joint Force Magnitude Plots

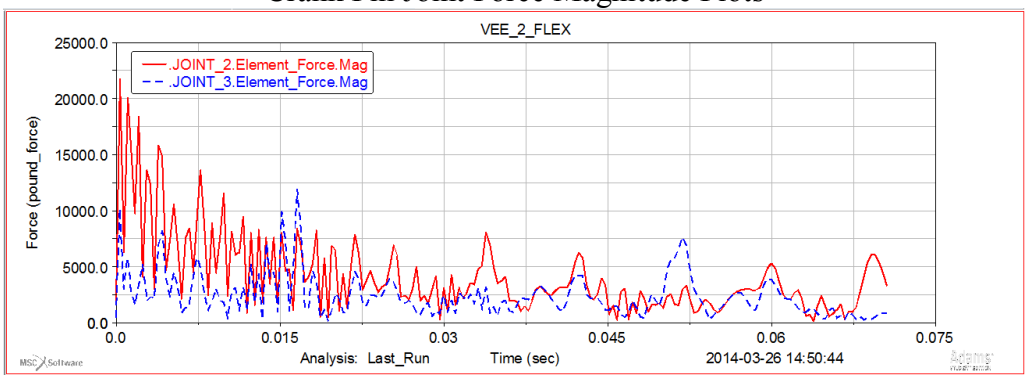

Crank Pin Joint Angular Velocity Magnitude Plots

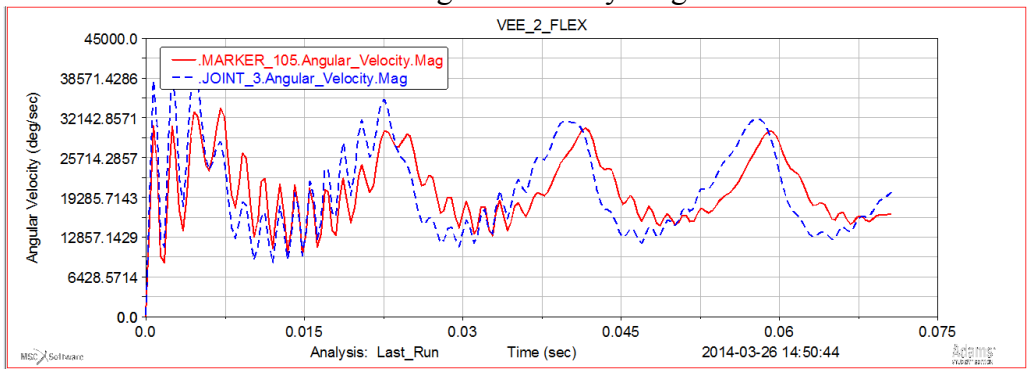

APPENDIX J

MSC ADAMS/VIEW ALUMINUM RIGID VEE-2 RESULTS

Piston Position, Velocity and Acceleration Plots

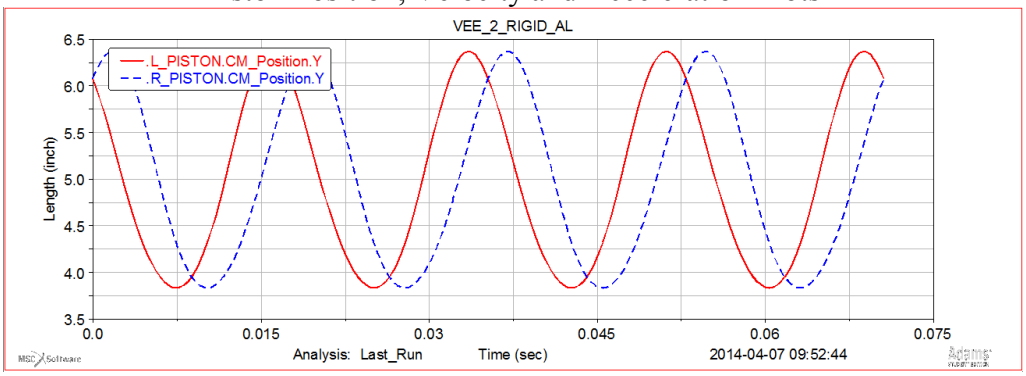

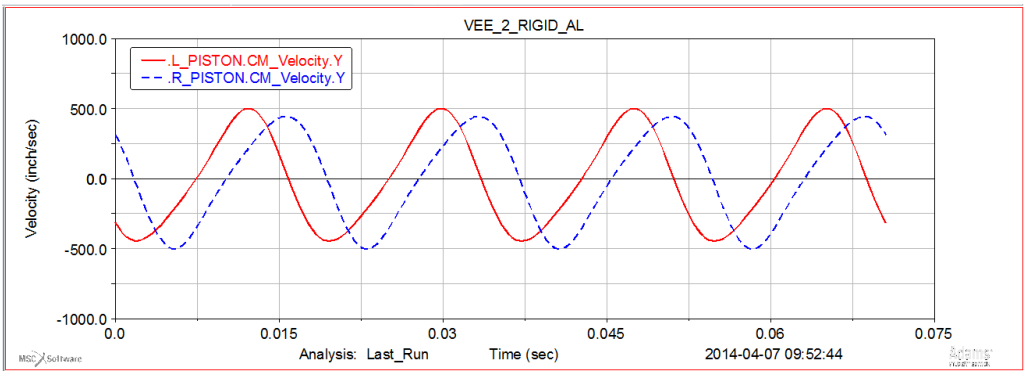

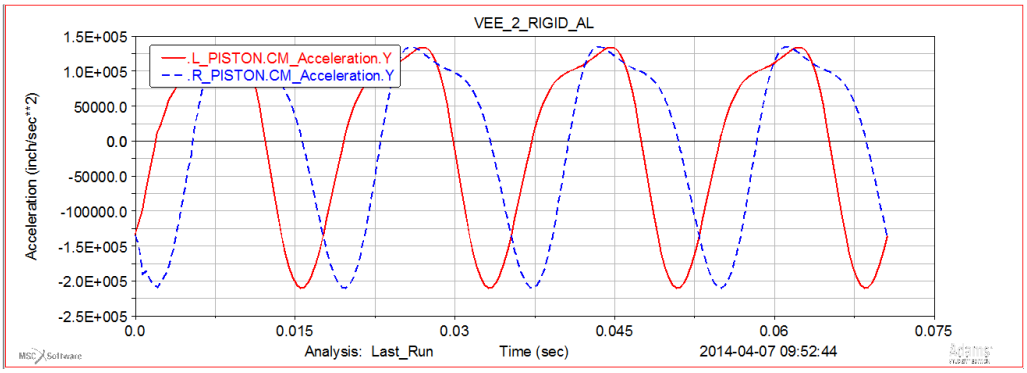

APPENDIX J (continued)

Piston Pin Joint Y Force Plot

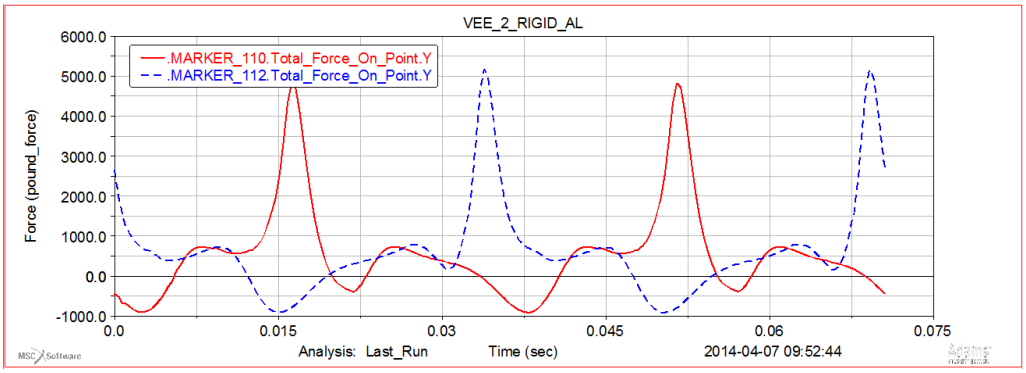

Piston Pin Joint Z Force Plot

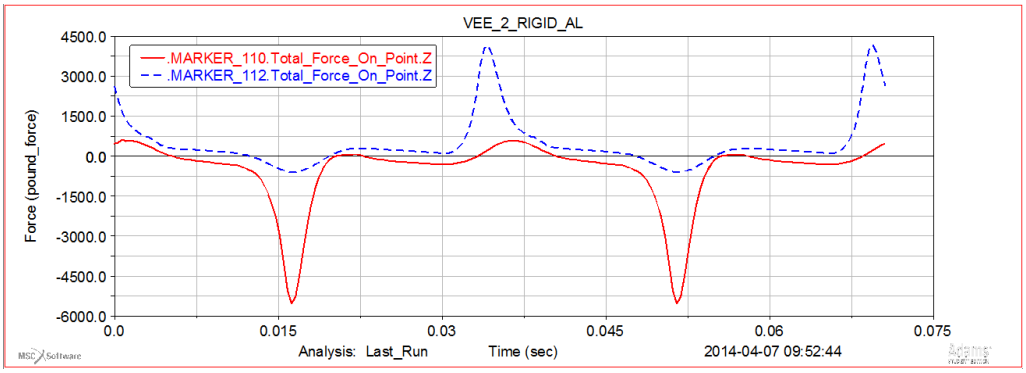

Piston Pin Joint Force Magnitude Plot

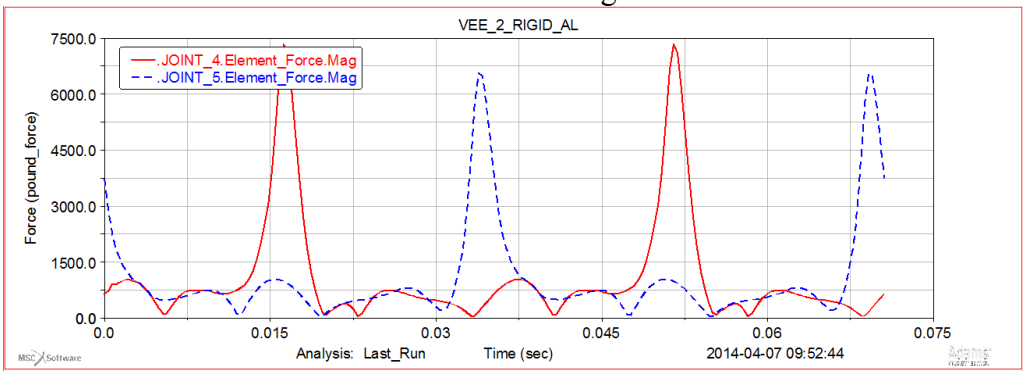

APPENDIX J (continued)

Piston Pin Joint Angular Velocity about X Plot

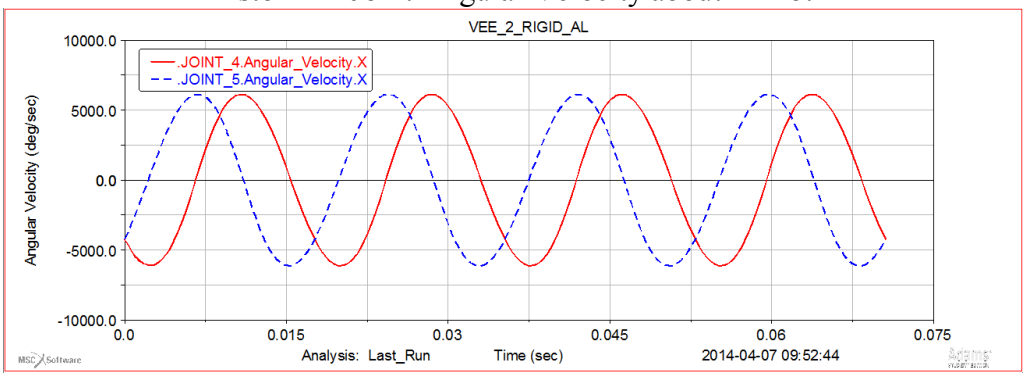

Crank Pin Joint Y Force Plot

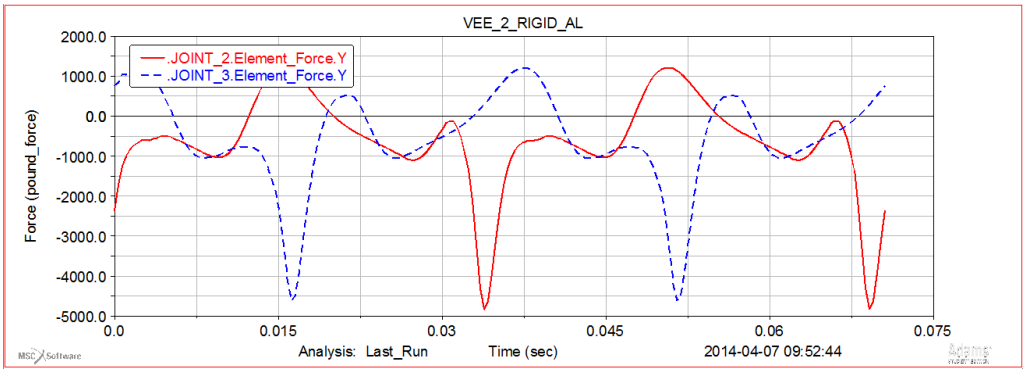

Crank Pin Joint Z Force Plot

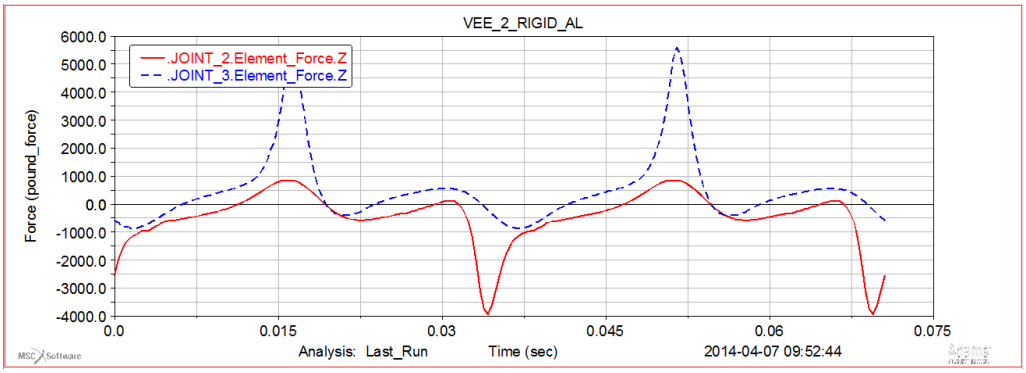

APPENDIX J (continued)

Crank Pin Joint X Force Plot

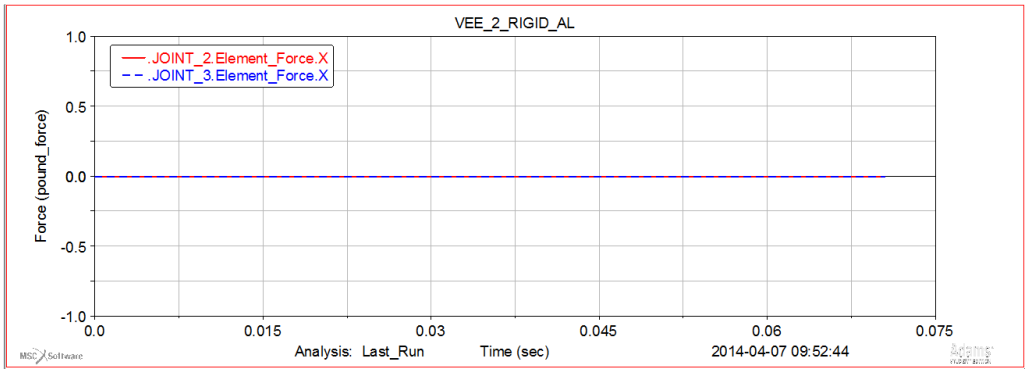

Crank Pin Joint Force Magnitude Plot

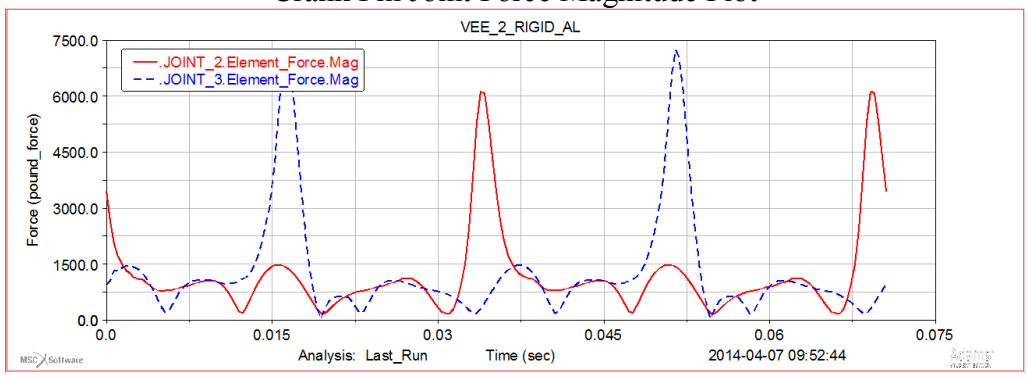

Crank Pin Joint Angular Velocity Magnitude Plot

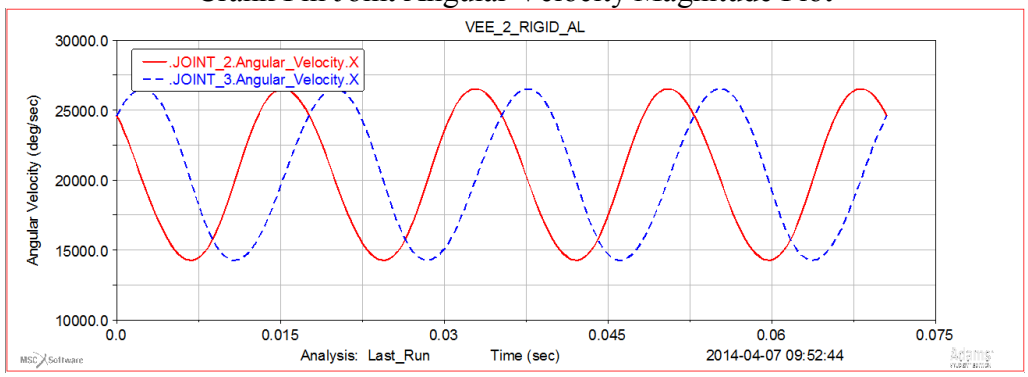

APPENDIX K

MSC ADAMS/VIEW ALUMINUM FLEX VEE-2 RESULTS

Piston Position, Velocity and Acceleration Plots

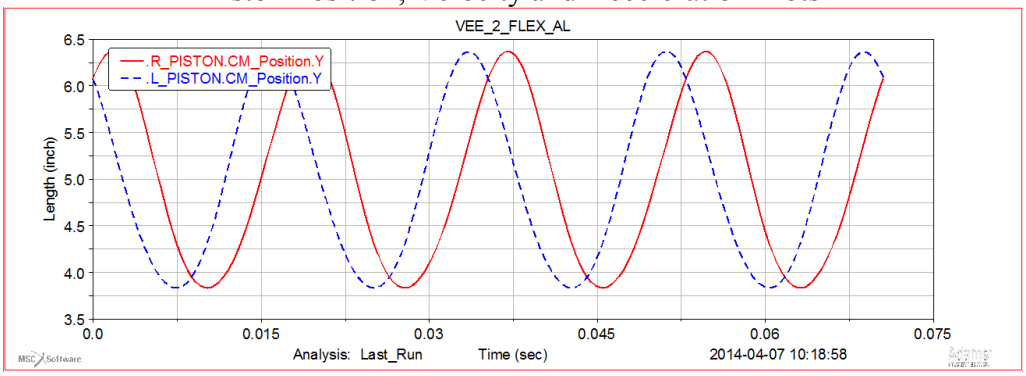

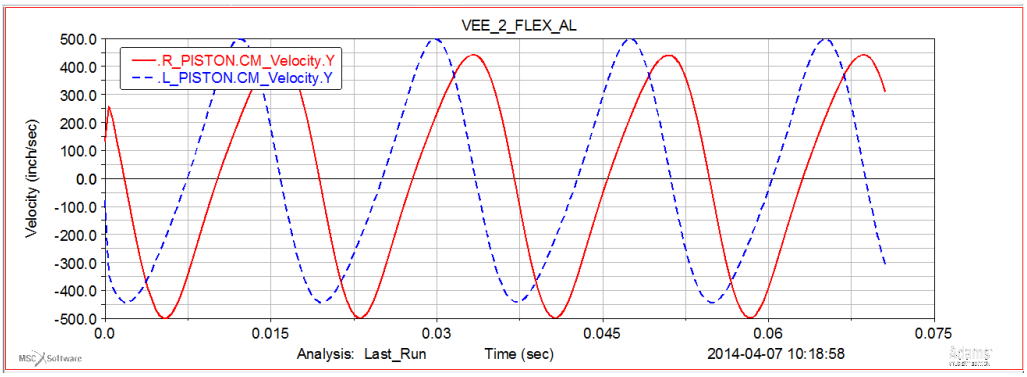

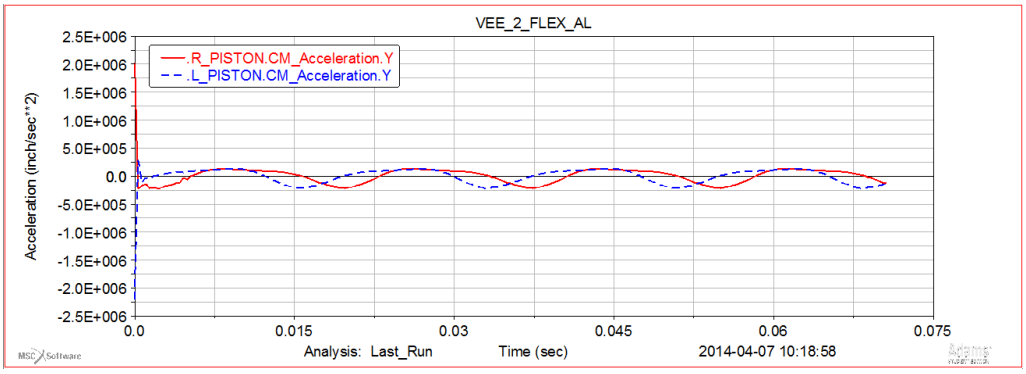

APPENDIX K (continued)

Piston Pin Joint Y Force Plot

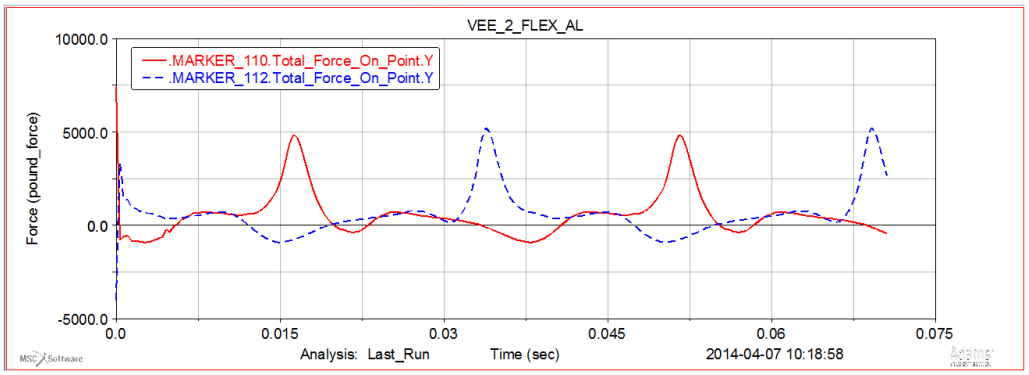

Piston Pin Joint Z Force Plot

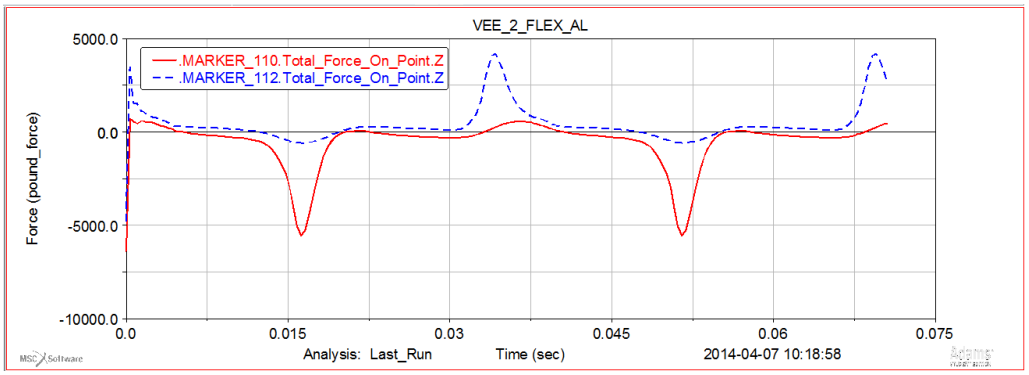

Piston Pin Joint Force Magnitude Plot

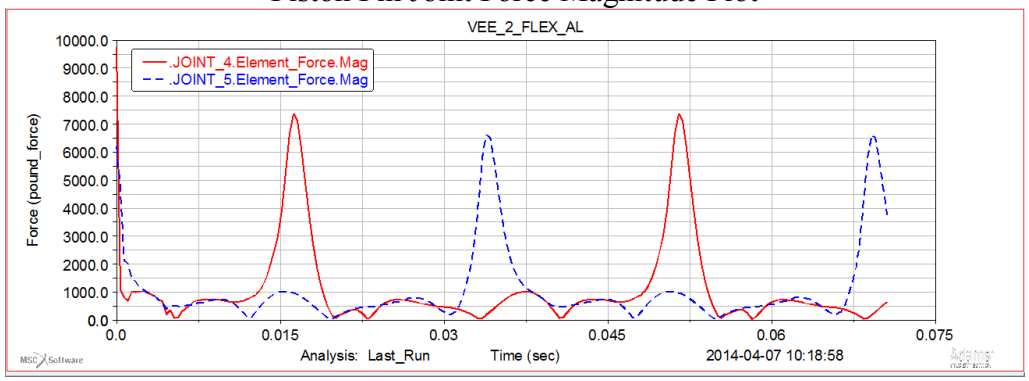

APPENDIX K (continued)

Piston Pin Joint Angular Velocity about X Plot

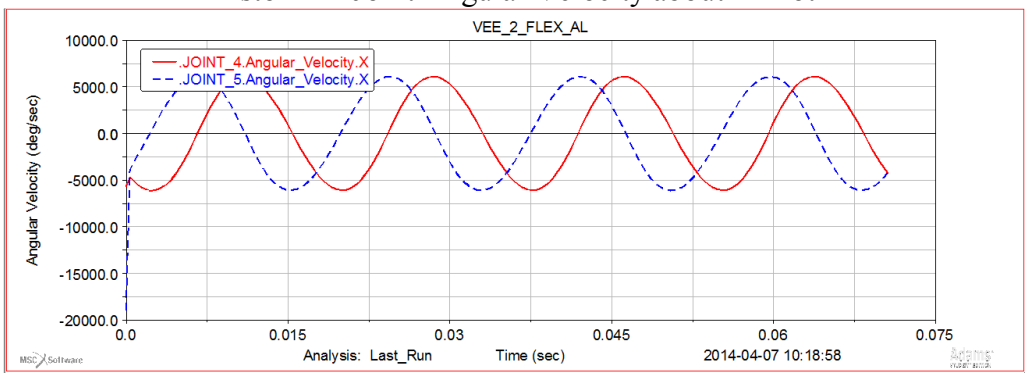

Crank Pin Joint Y Force Plot

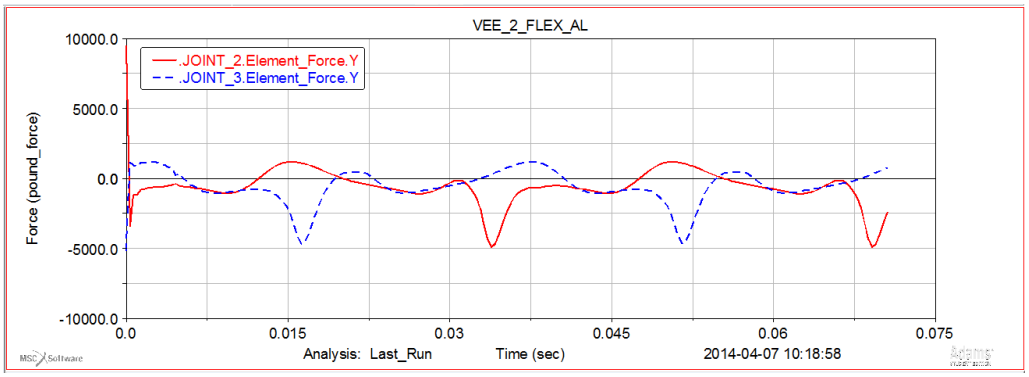

Crank Pin Joint Z Force Plot

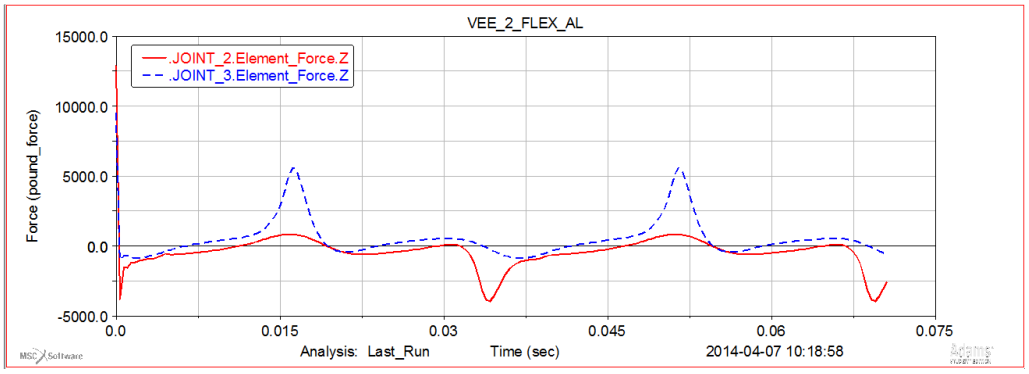

APPENDIX K (continued)

Crank Pin Joint X Force Plot

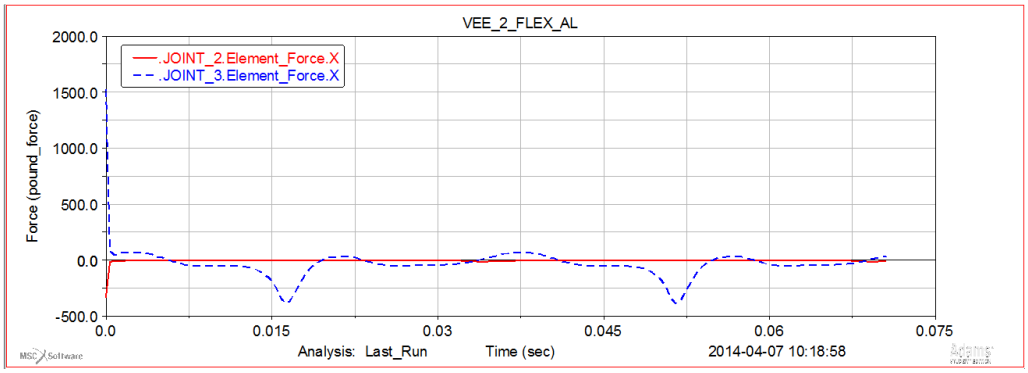

Crank Pin Joint Force Magnitude Plot

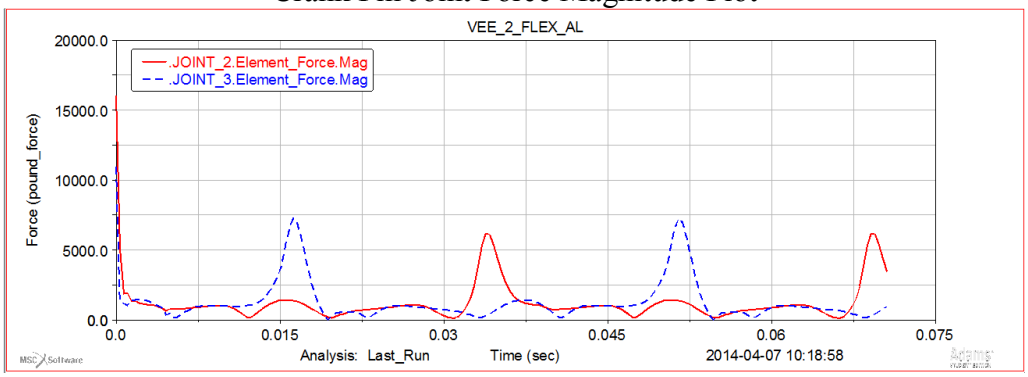

Crank Pin Joint Angular Velocity Magnitude Plot

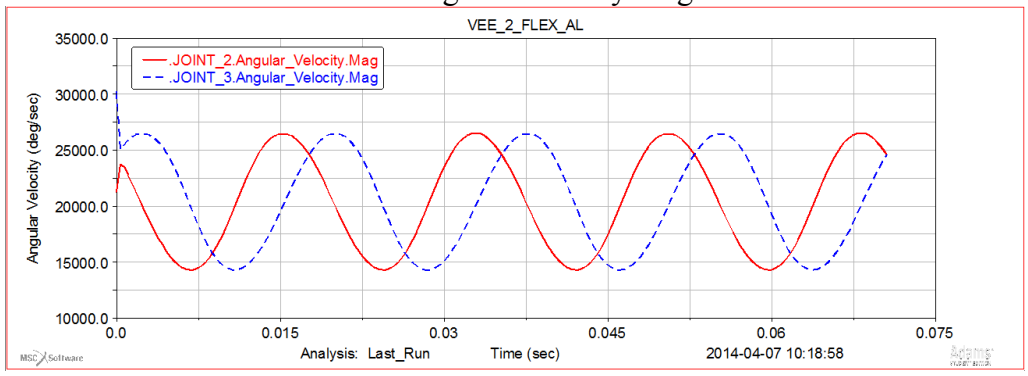

APPENDIX L

FEV VIRTUAL ENGINE RIGID INLINE-1 RESULTS

Piston Position, Velocity and Acceleration Plots

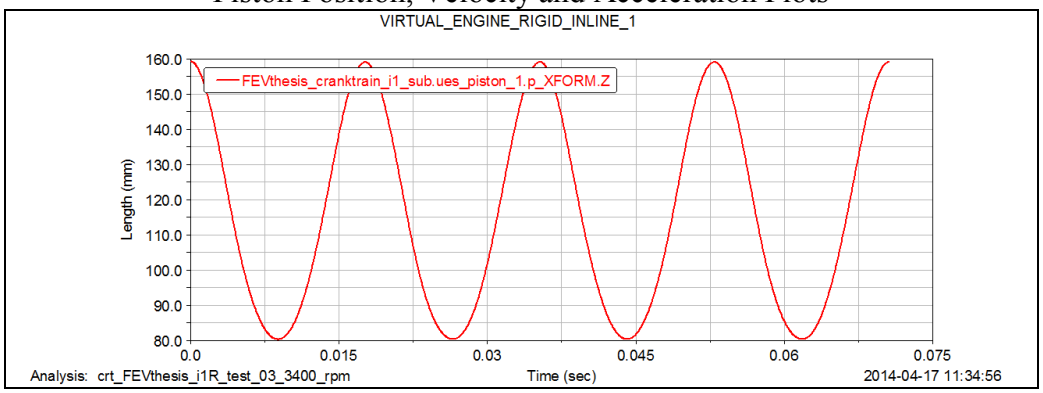

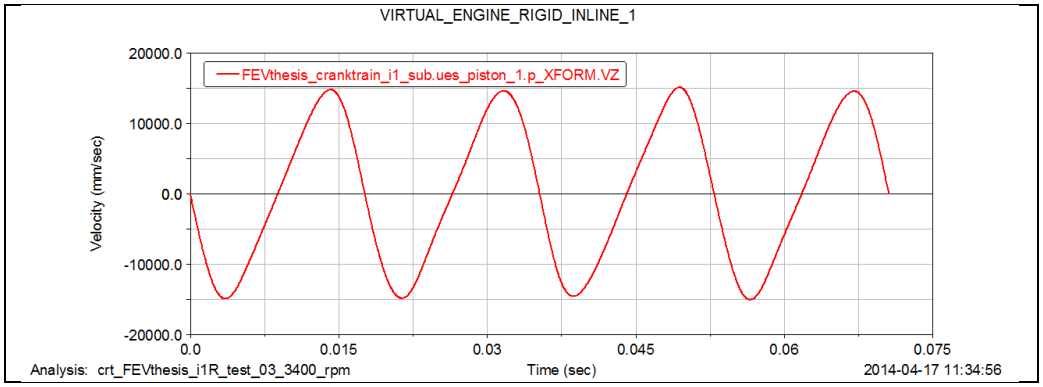

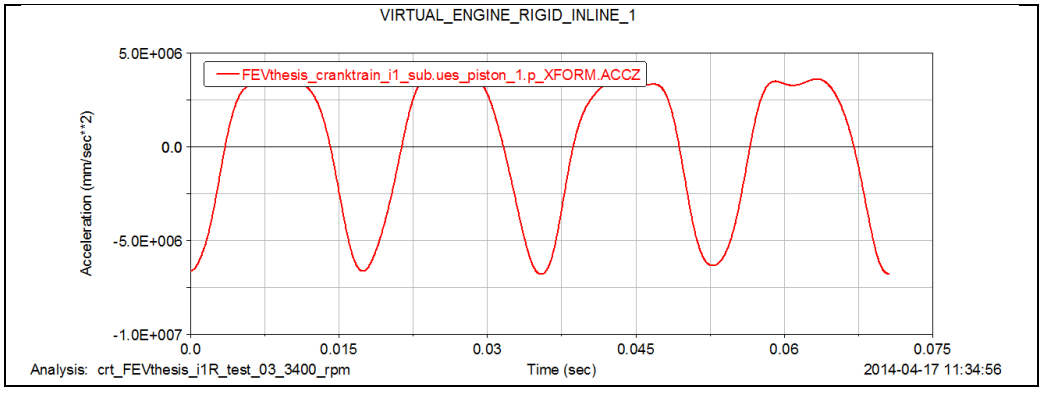

APPENDIX L (continued)

Piston Pin Joint Y Force Plot

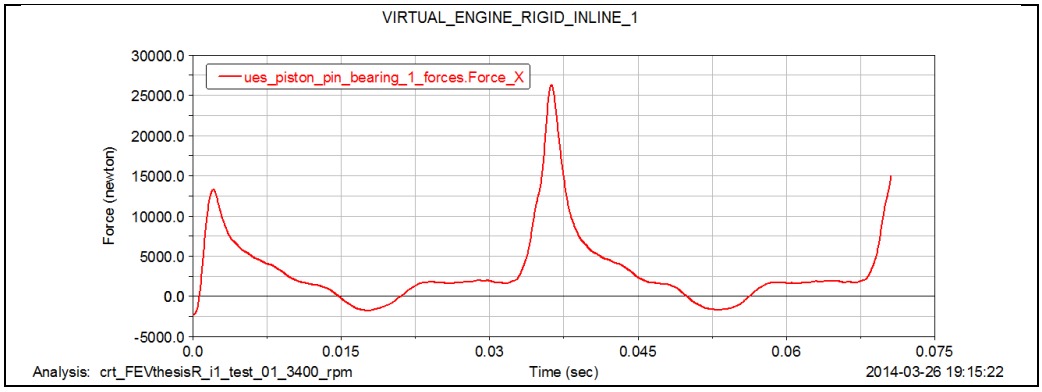

Piston Pin Joint Z Force Plot

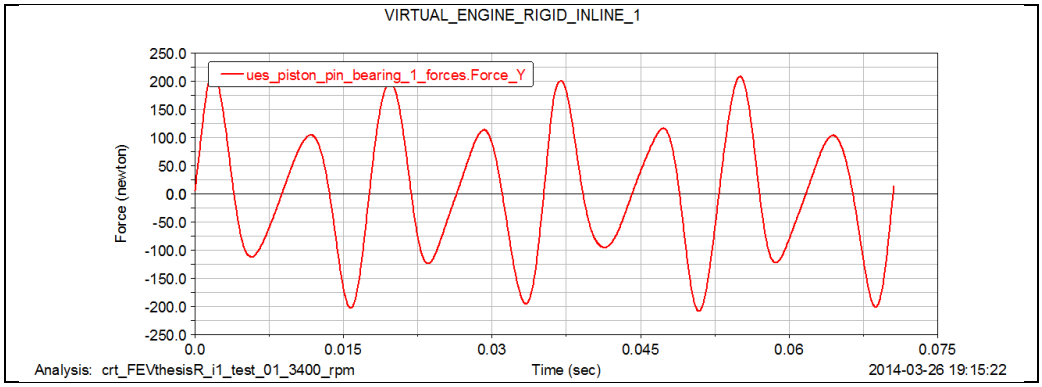

Piston Pin Joint Force Magnitude Plot

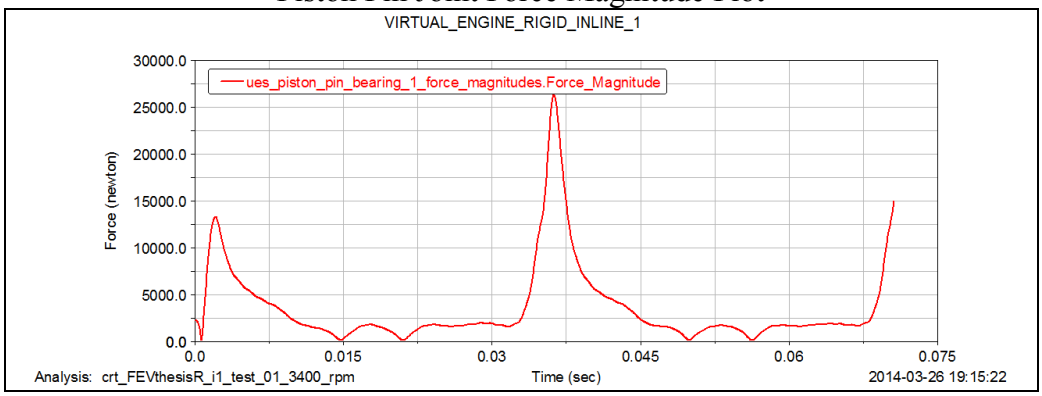

APPENDIX L (continued)

Piston Pin Joint Angular Velocity about X Plot

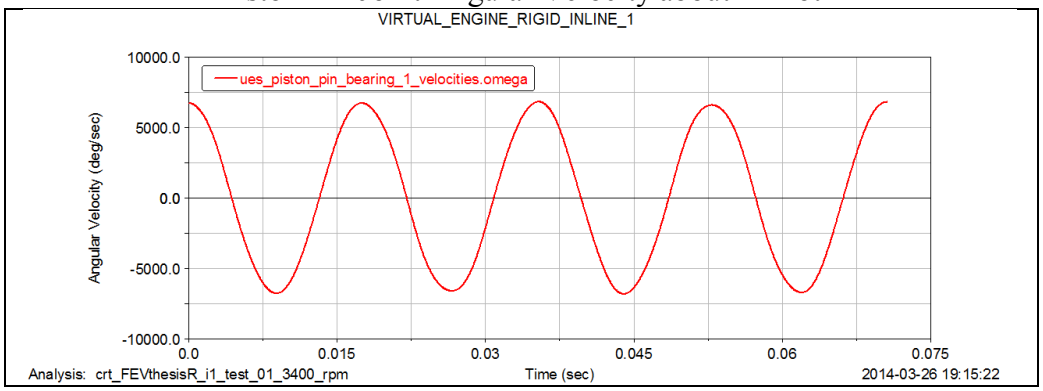

Crank Pin Joint Y Force Plot

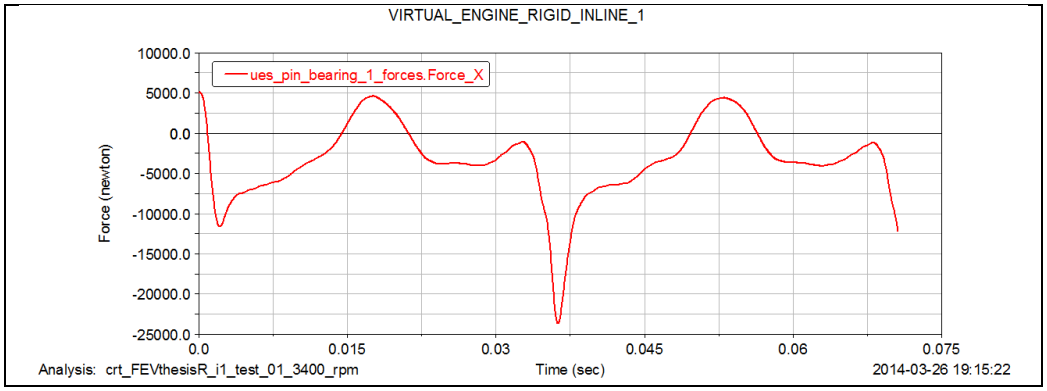

Crank Pin Joint Z Force Plot

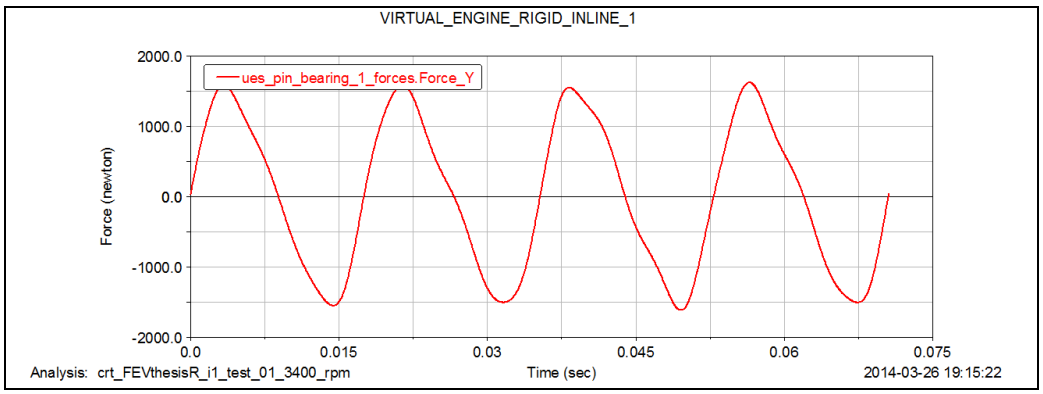

APPENDIX L (continued)

Crank Pin Joint X Force Plot

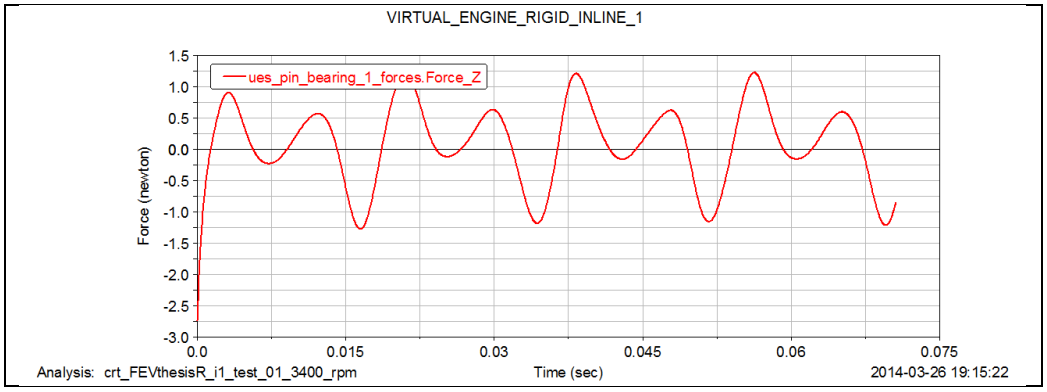

Crank Pin Joint Force Magnitude Plot

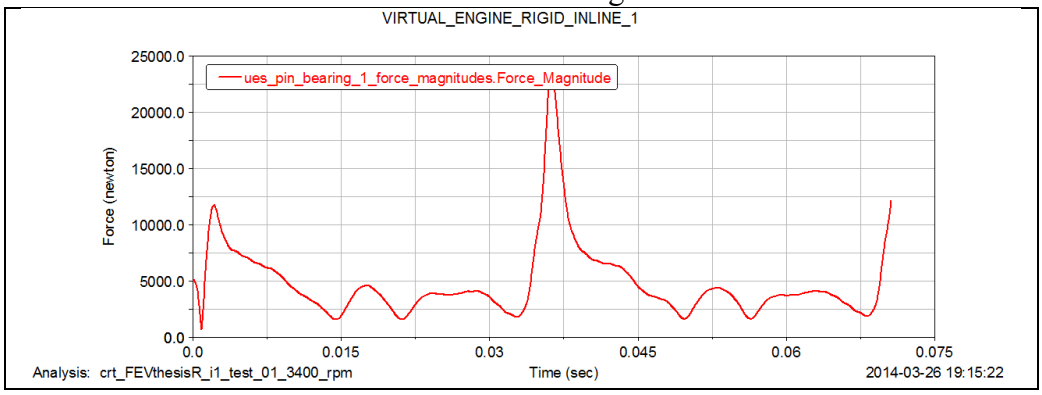

Crank Pin Joint Angular Velocity Magnitude Plot

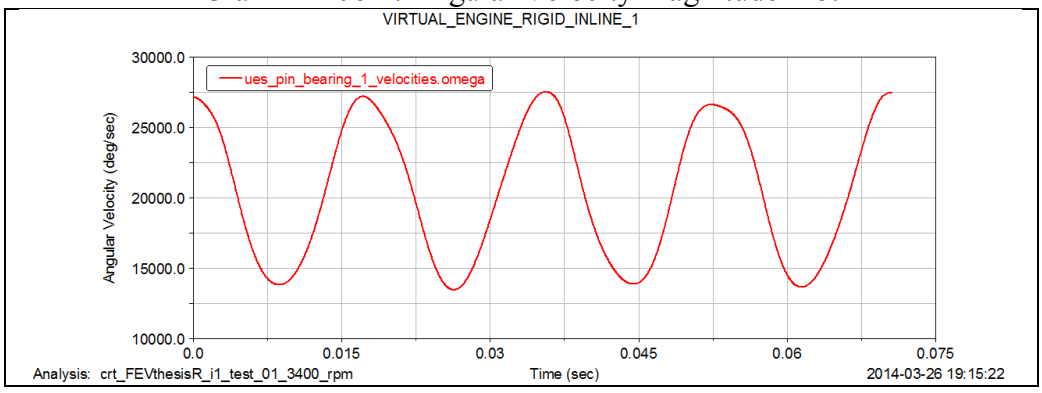

APPENDIX M

FEV VIRTUAL ENGINE FLEX INLINE-1 RESULTS

Piston Position, Velocity and Acceleration Plots

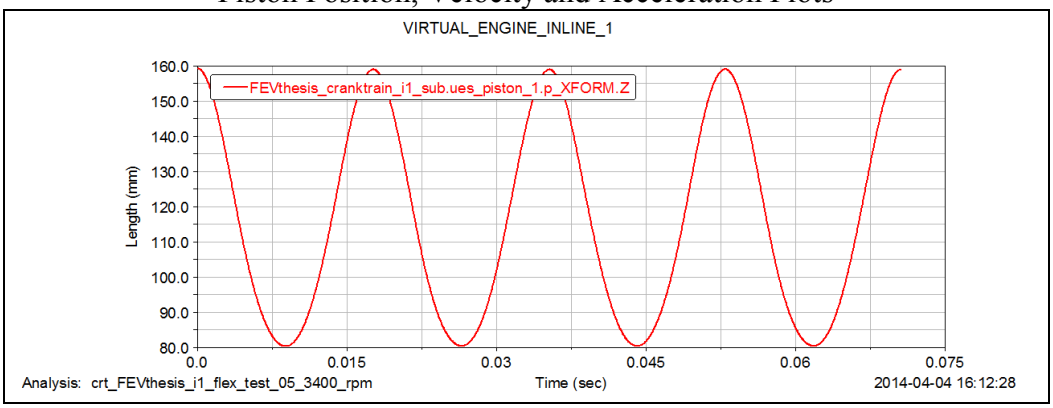

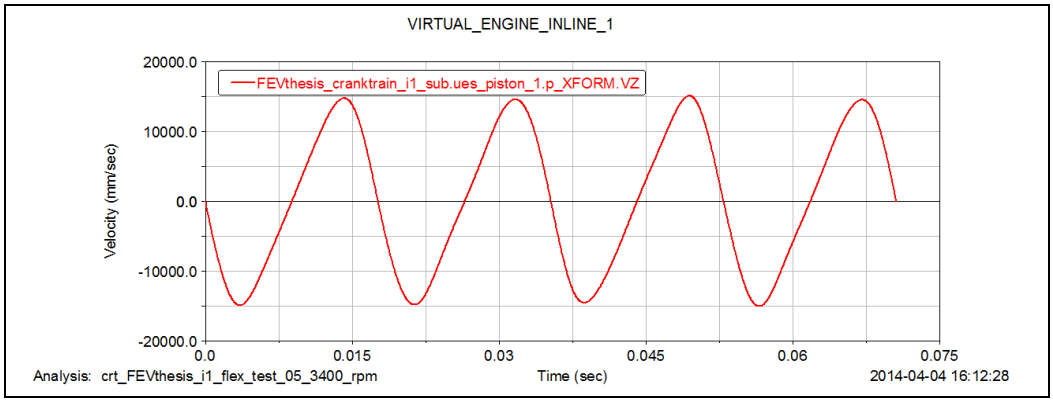

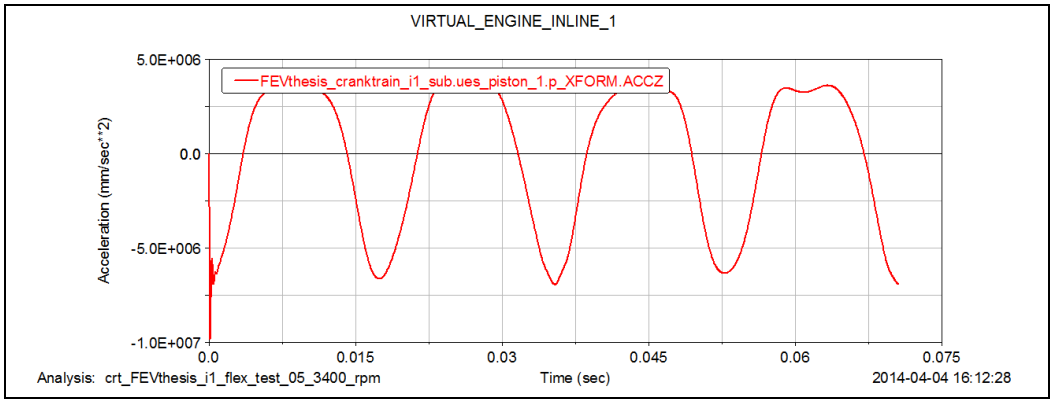

APPENDIX M (continued)

Piston Pin Joint Y Force Plot

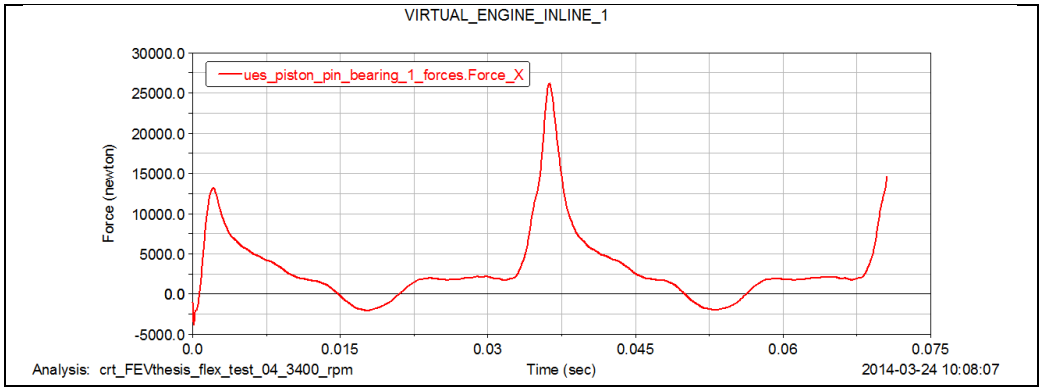

Piston Pin Joint Z Force Plot

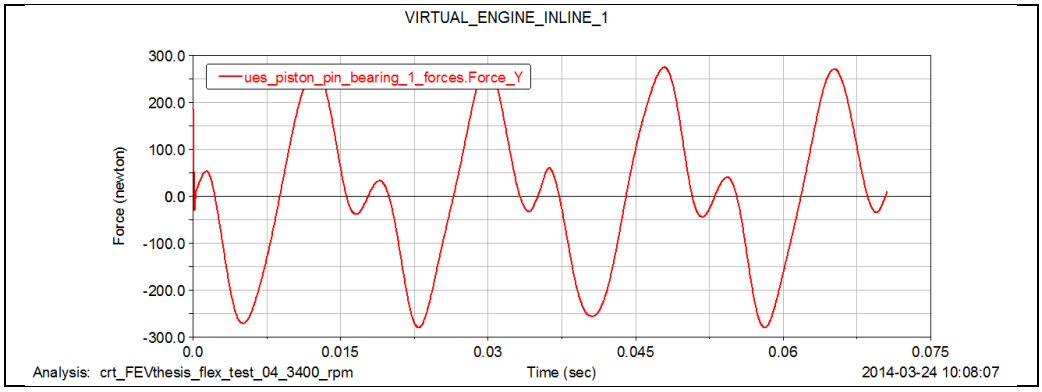

Piston Pin Joint Force Magnitude Plot

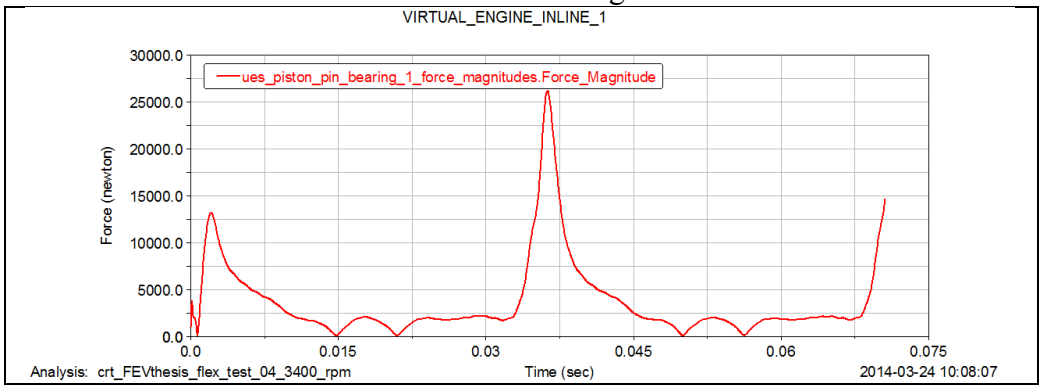

APPENDIX M (continued)

Piston Pin Joint Angular Velocity about X Plot

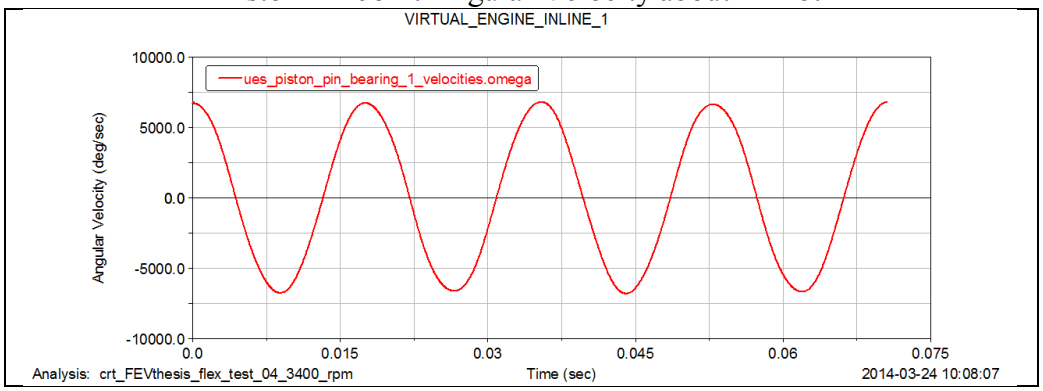

Crank Pin Joint Y Force Plot

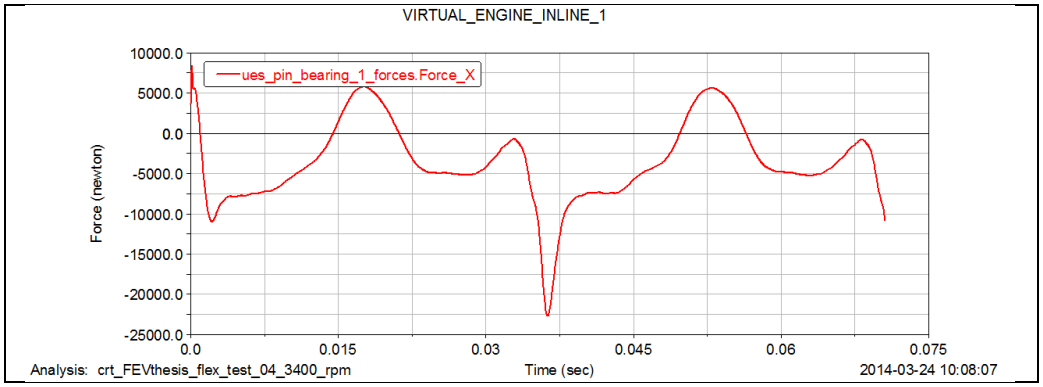

Crank Pin Joint Z Force Plot

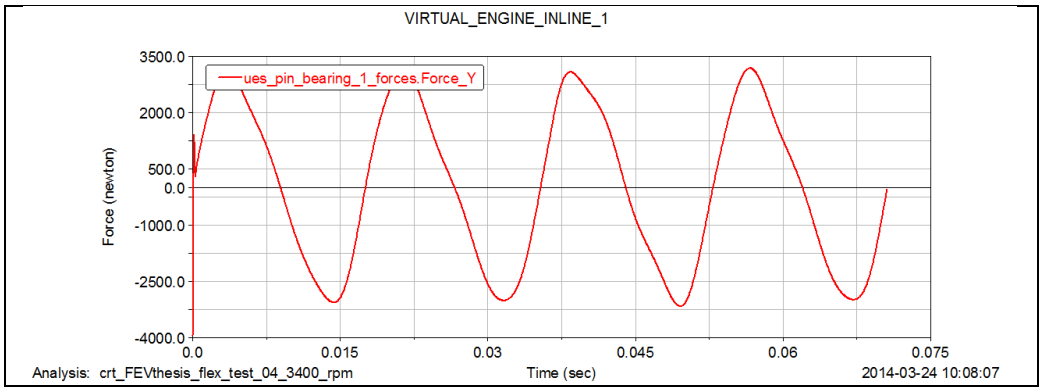

APPENDIX M (continued)

Crank Pin Joint X Force Plot

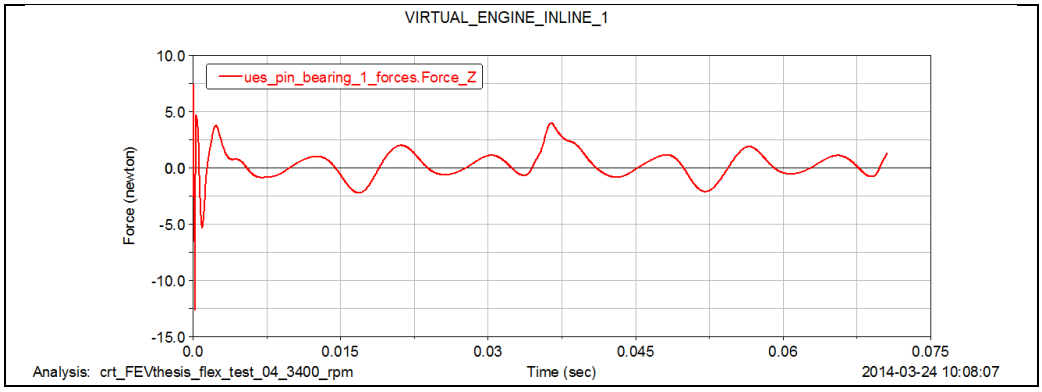

Crank Pin Joint Force Magnitude Plot

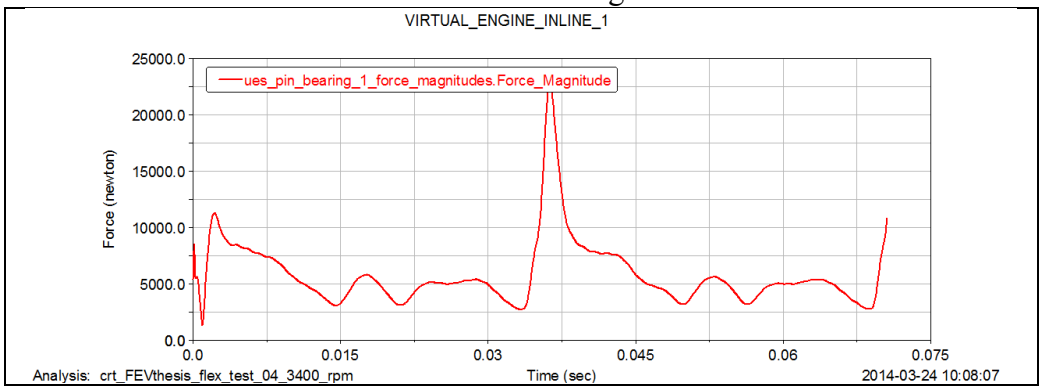

Crank Pin Joint Angular Velocity Magnitude Plot

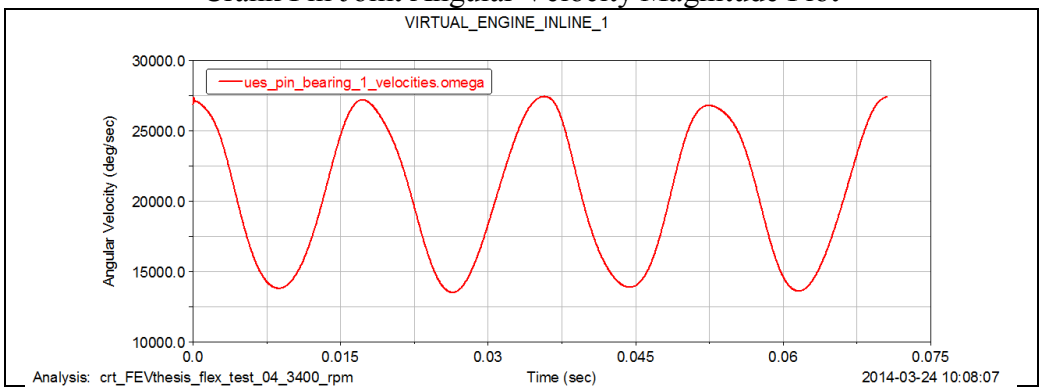

APPENDIX N

FEV VIRTUAL ENGINE RIGID VEE-6 RESULTS

Piston Position, Velocity and Acceleration Plots

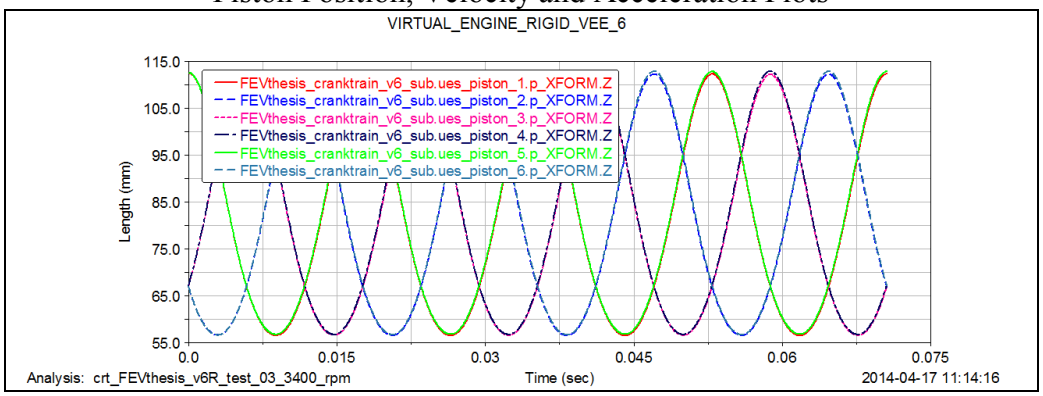

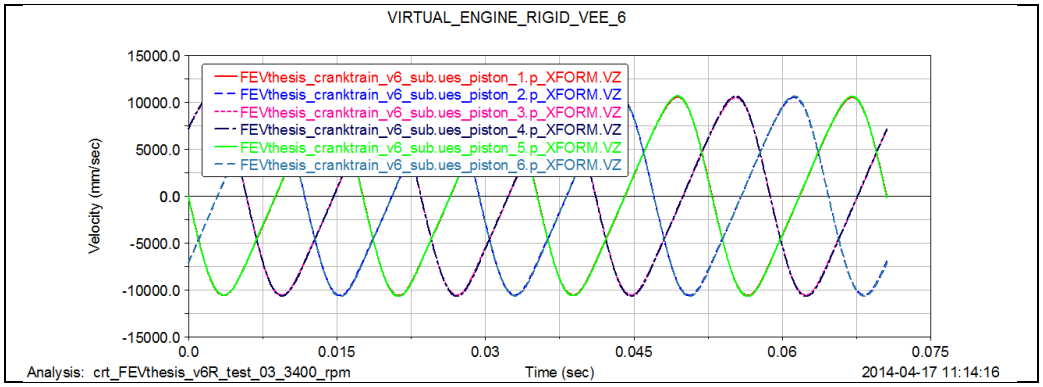

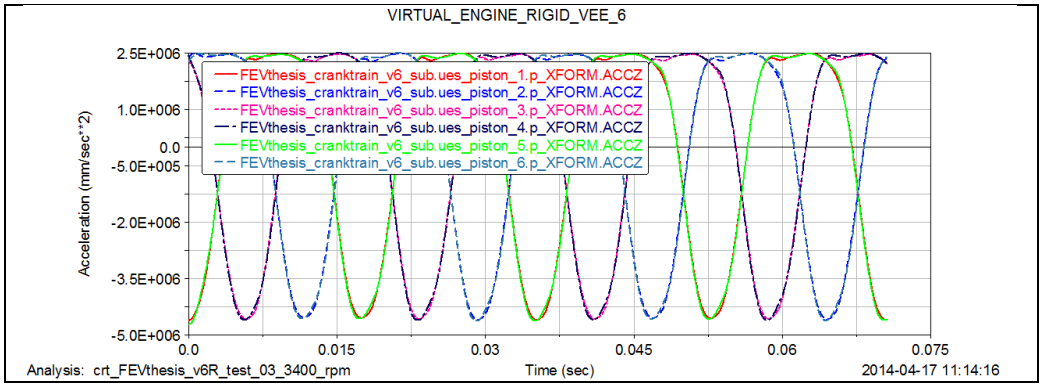

APPENDIX N (continued)

Piston Pin Joint Y Force Plots

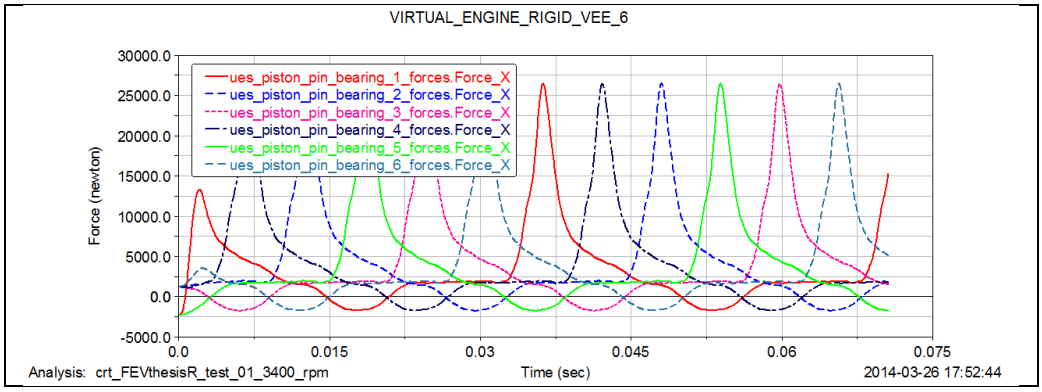

Piston Pin Joint Z Force Plots

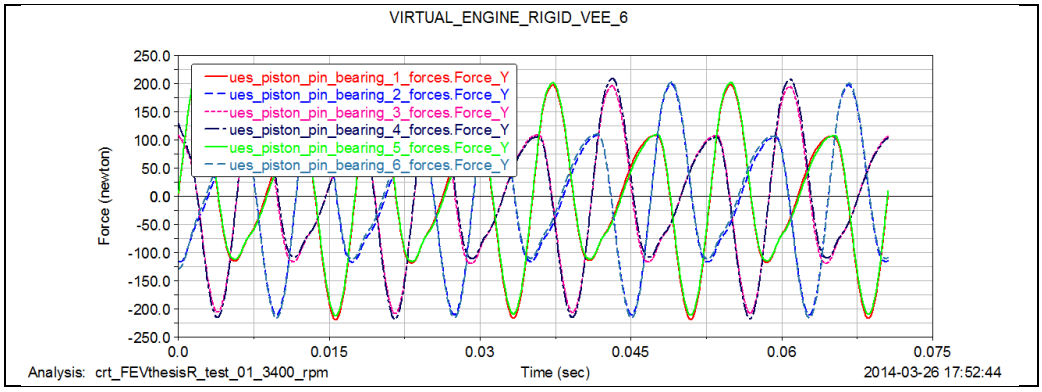

Piston Pin Joint Force Magnitude Plots

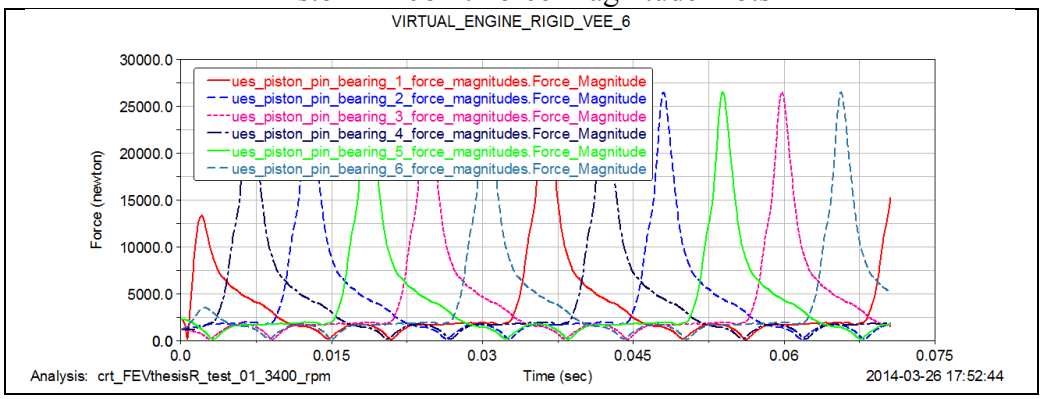

APPENDIX N (continued)

Piston Pin Joint Angular Velocity about X Plots

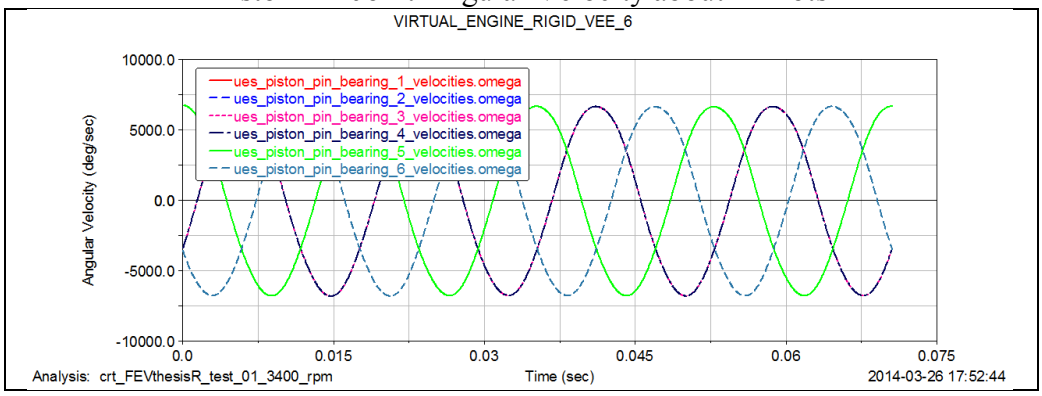

Crank Pin Joint Y Force Plots

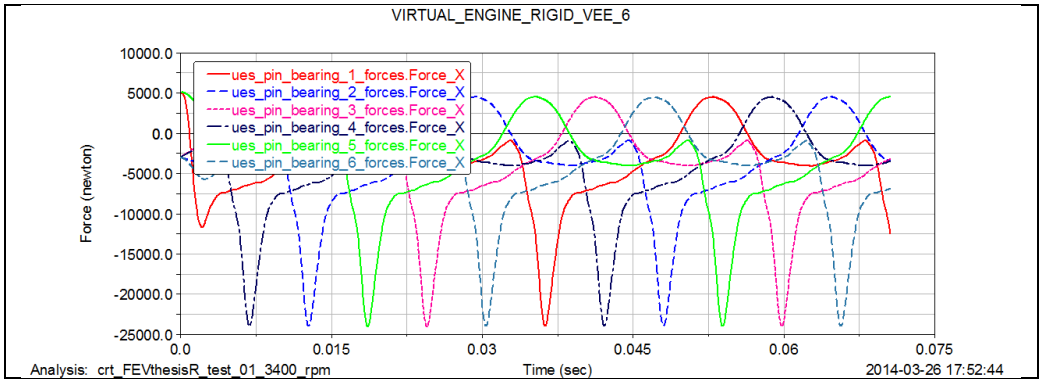

Crank Pin Joint Z Force Plots

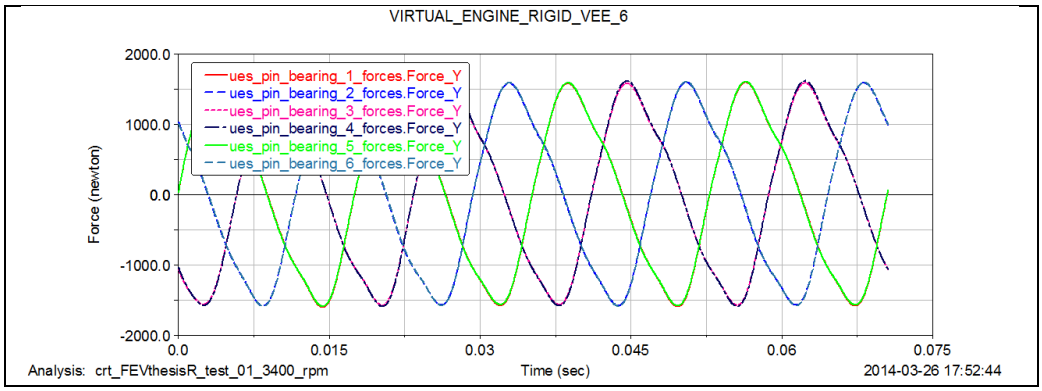

APPENDIX N (continued)

Crank Pin Joint X Force Plots

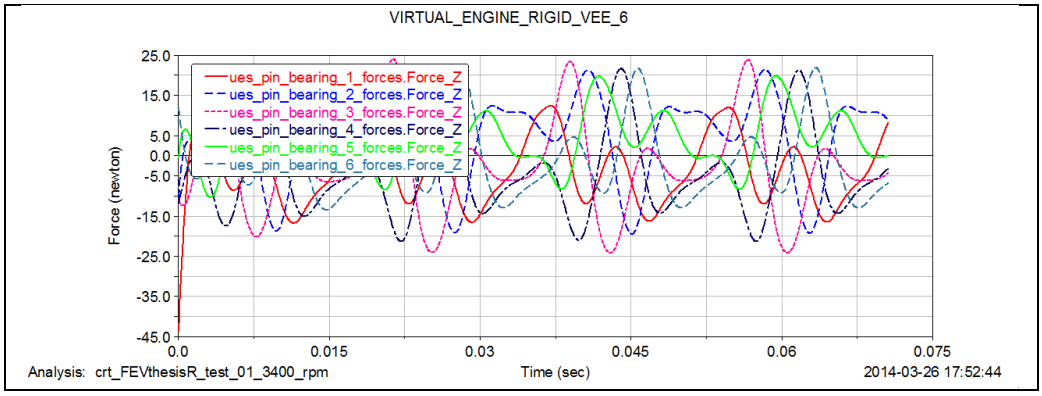

Crank Pin Joint Force Magnitude Plots

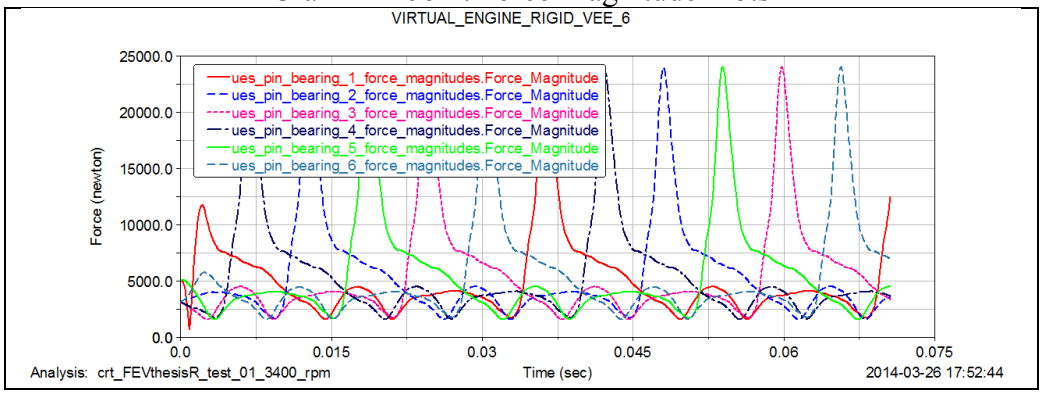

Crank Pin Joint Angular Velocity Magnitude Plots

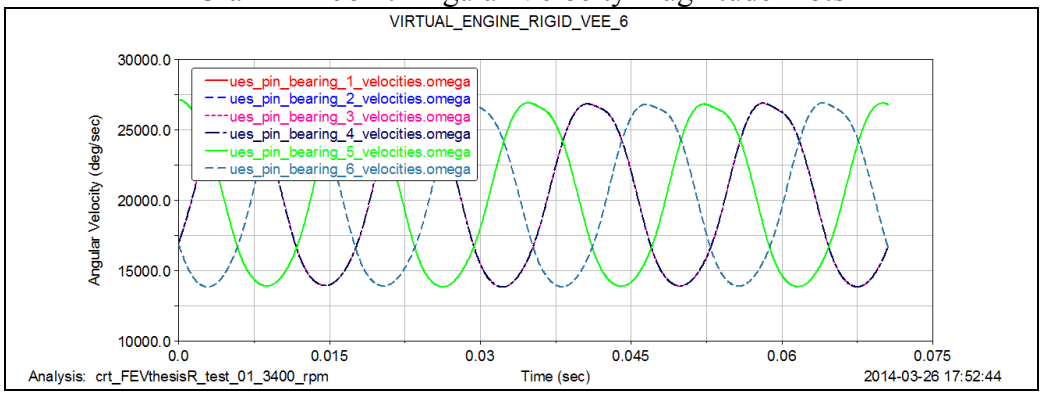

APPENDIX O

FEV VIRTUAL ENGINE FLEX VEE-6 RESULTS

Piston Position, Velocity and Acceleration Plots

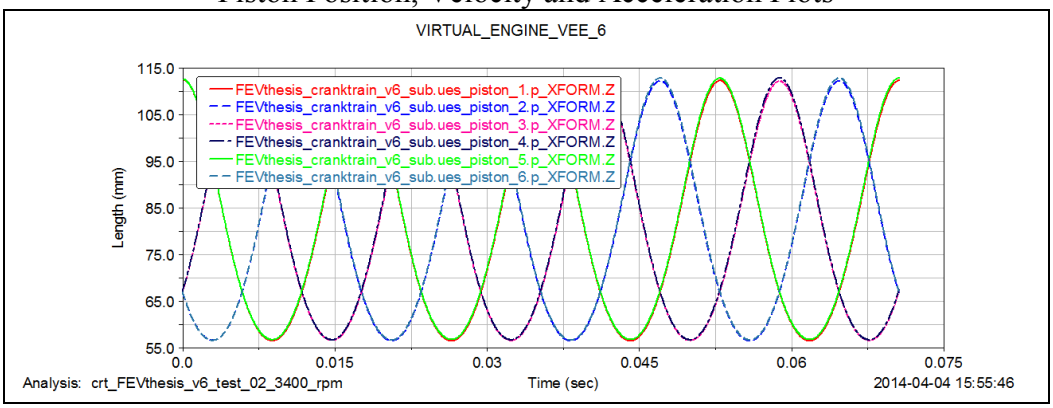

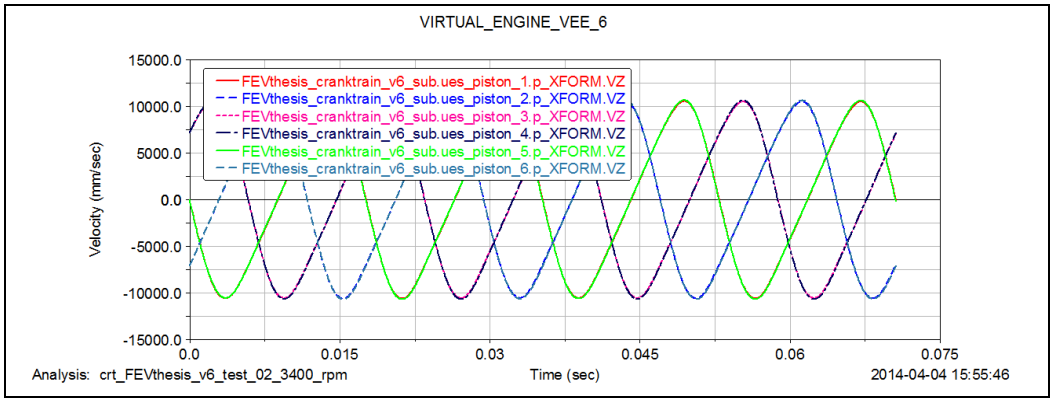

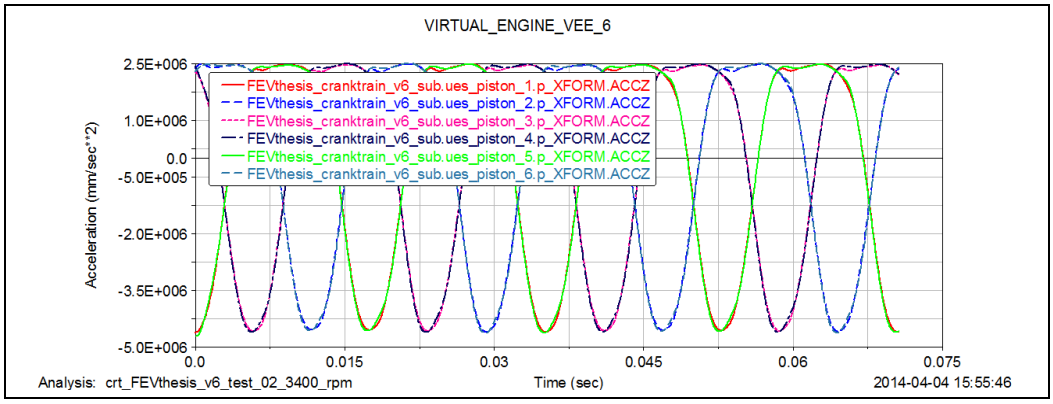

APPENDIX O (continued)

Piston Pin Joint Y Forces Plots

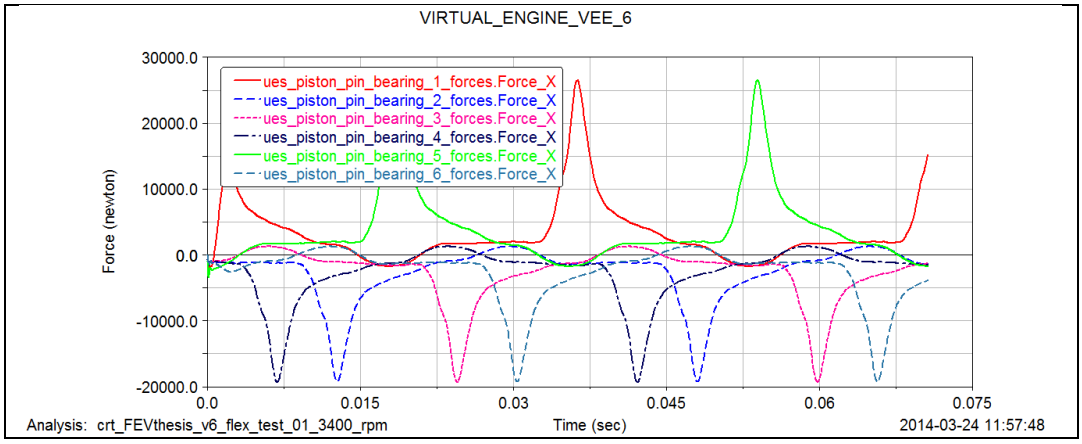

Piston Pin Joint Z Forces Plots

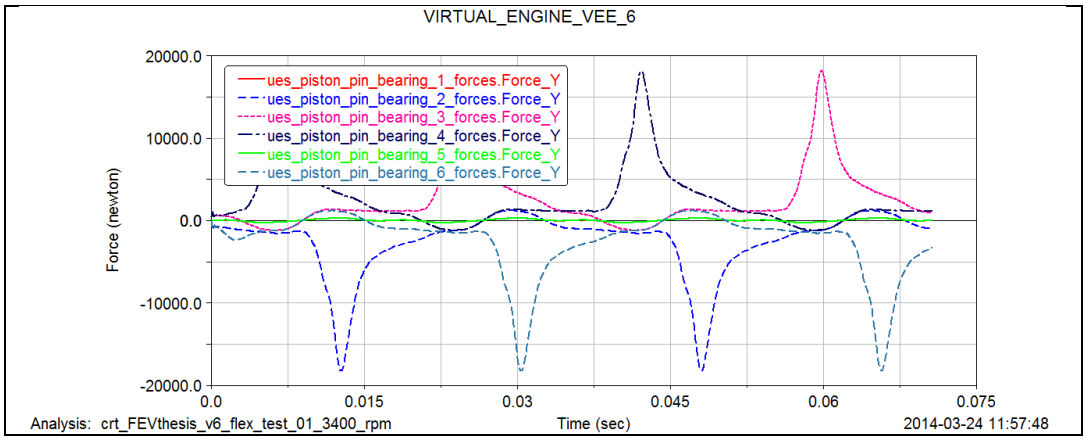

Piston Pin Joint Force Magnitudes Plots

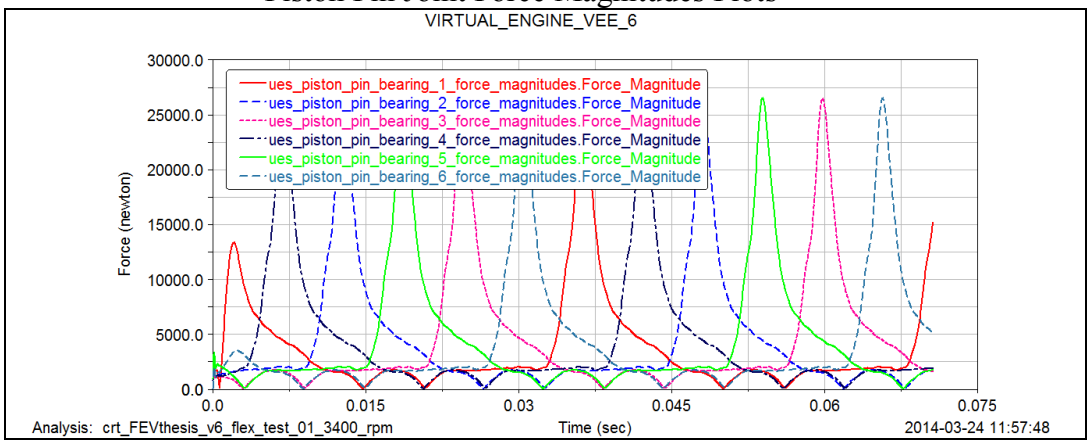

APPENDIX O (continued)

Piston Pin Joint Angular Velocity about X Plots

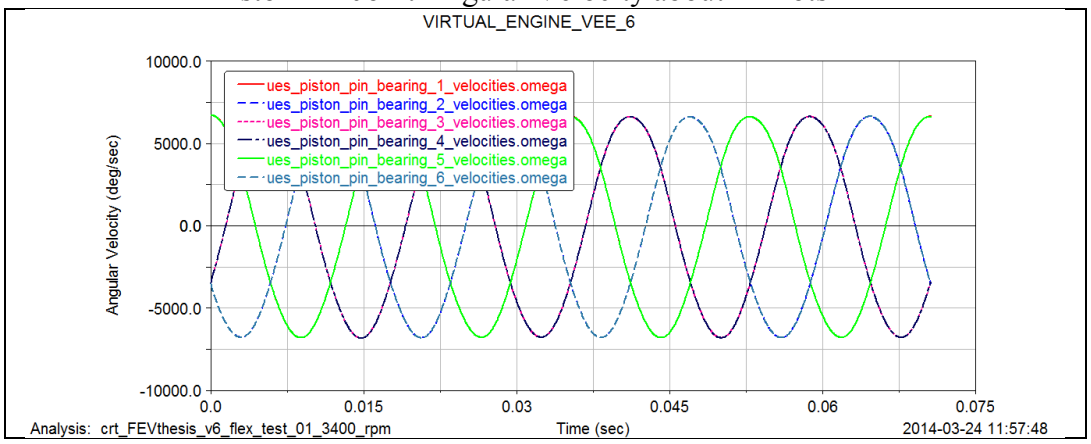

Crank Pin Joint Y Force Plots

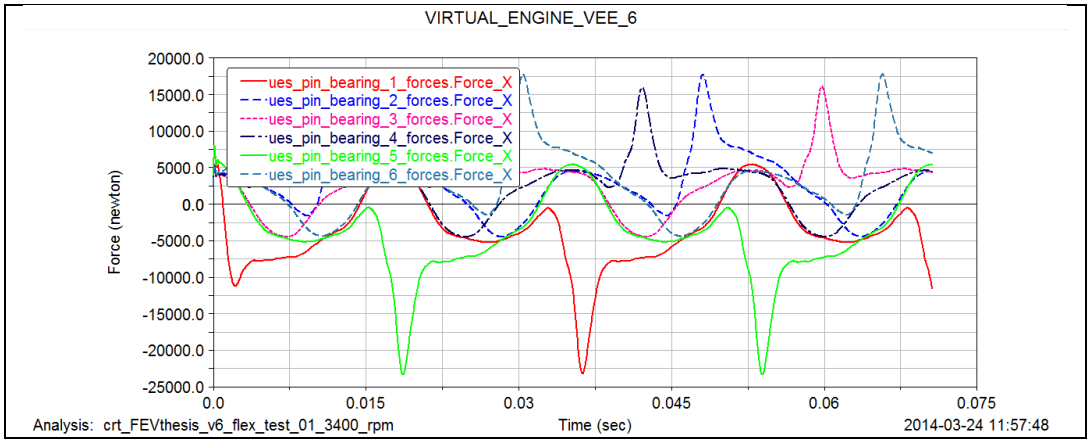

Crank Pin Joint Z Force Plots

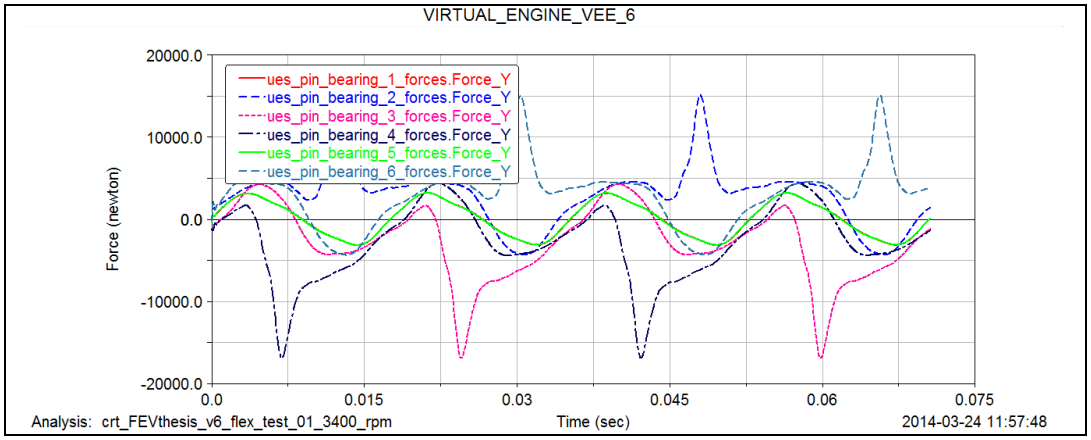

APPENDIX O (continued)

Crank Pin Joint X Force Plots

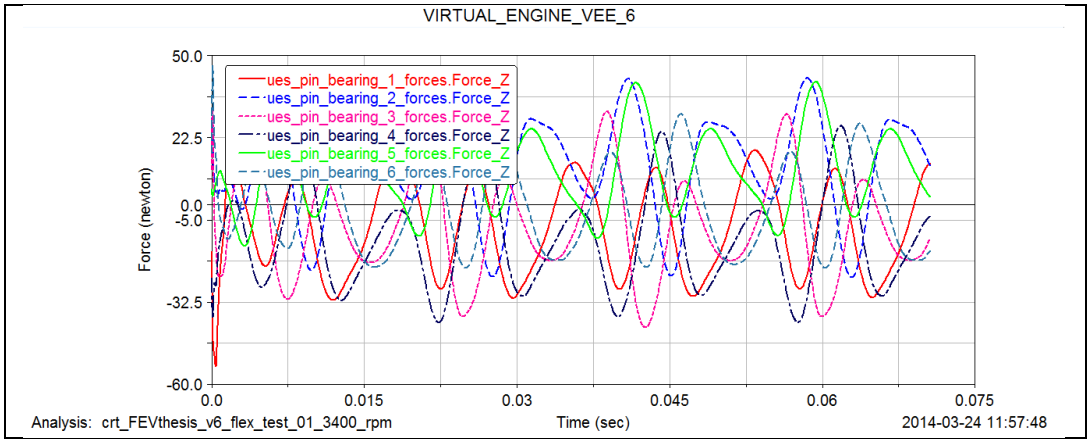

Crank Pin Force Joint Magnitude Plots

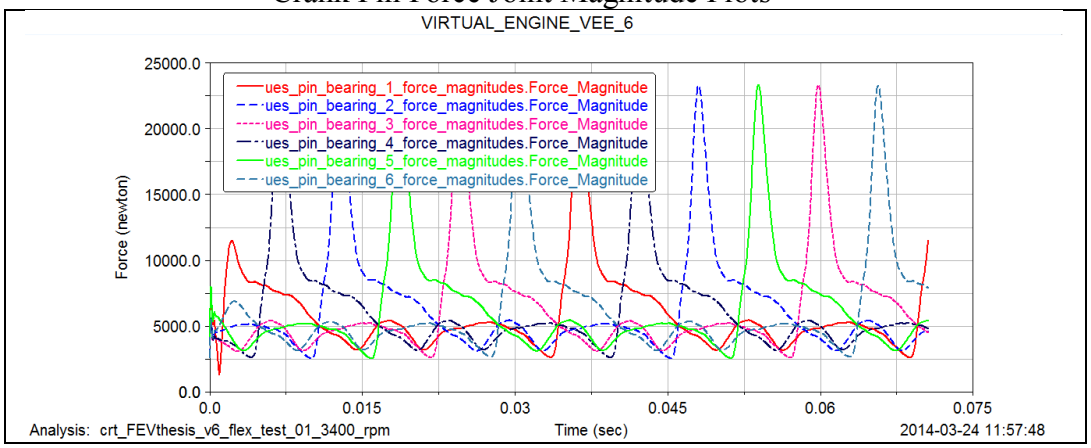

Crank Pin Joint Angular Velocity Magnitude Plots